Ultrasonography of the Hand in Rheumatology

Peter Vince Balint
Peter Mandl
Editors

Springer

Ultrasonography of the Hand in Rheumatology

Peter Vince Balint • Peter Mandl
Editors

Ultrasonography of the Hand in Rheumatology

Springer

Editors
Peter Vince Balint
3rd Rheumatology Department
National Institute of Rheumatology and Physiotherapy
Budapest, Hungary

Peter Mandl
Division of Rheumatology, Department of Internal Medicine III
Medical University of Vienna
Vienna, Austria

ISBN 978-3-319-74206-9 ISBN 978-3-319-74207-6 (eBook)
https://doi.org/10.1007/978-3-319-74207-6

Library of Congress Control Number: 2018939901

Printed on acid-free paper

This Springer imprint is published by the registered company Springer International Publishing AG part of Springer Nature
The registered company address is: Gewerbestrasse 11, 6330 Cham, Switzerland

In loving memory of my mother Elvira
and my mother-in-law Klára
Peter Vince Balint
To Klara, Sara, Robert and Simon for
their support, patience and love
Peter Mandl

Preface

"An ultrasonic voyage around the hand and wrist"

In the era of William Shakespeare, one of the greatest masters of the English language, the five human senses, namely vision, audition, gustation, olfaction and somatosensation, were termed outward wits, while inward wits included common wit, imagination, fantasy, estimation (more recently referred to as instinct) and memory.

It seems as though many rheumatologists have found their sixth sense in ultrasonography: using sound to permeate the skin through the surrounding soft tissue into synovial joints. Ultrasound developed in the animal kingdom as a means to facilitate hunting and movement through echolocation. In more modern times physicians adopted ultrasound from the field of engineering where it was first utilized for non-destructive testing. However, the sixth sense does not replace the other five senses during the clinical examination of a rheumatic patient. Ultrasound is a *complementary sense* which should only be used if new information can be gained. Thus, it may aid clinical examination, screening, disease classification, pathology monitoring, therapeutic decision-making, guided interventions, recognition of complications and can also be used as a research or educational tool. However, it rarely provides a diagnosis on its own without other diagnostic methods. For this reason, we strongly believe that ultrasonography should be incorporated into clinical examination. On the other hand, as an imaging tool, ultrasound should always be used in conjunction with normal human anatomy, X-ray, CT and MRI. This book is structured in a way that follows this chain of thought.

Why focus on the hand and wrist? Put simply, the hand of a rheumatic patient serves as a kind of 'visiting card', informing the rheumatologist about their disease. Furthermore, with high-frequency transducers, we can achieve the highest resolution when examining hands (and to a similar extent, feet), especially the five digits (thumb, index, middle, ring and little finger) that are examined with ultrasound by holding the transducer with all five fingers.

With this parting thought, we would like to thank all co-writers for using their respective five fingers to create this book. We ask our distinguished readers to use their senses and wits to the best of their ability while examining patients during their rheumatology carrier.

Bon voyage

Budapest, Hungary
Vienna, Austria
November 8, 2017

Peter Vince Balint, MD., PhD., FRCP.
Peter Mandl, MD., PhD.

About the Editors

Peter Vince Balint is Head of the 3rd Department of Rheumatology at the National Institute of Rheumatology and Physiotherapy in Budapest, a EULAR Centre of Excellence in Imaging, and Professor Honoris Causa at Semmelweis University in Budapest. Prof. Balint began working at the National Institute of Rheumatology and Physiotherapy and obtained board certification in rheumatology and physiotherapy in 1991. After completing his doctorate at the University of Glasgow, he defended his PhD thesis (*Ultrasound Imaging in Joint and Soft Tissue Inflammation*) in 2002 under the supervision of Prof. Roger D. Sturrock. He defended his habilitation thesis *"The Role of Ultrasonography in Assessing Synovitis, Tendon Damage and Cartilage Destruction in Rheumatoid Arthritis"* in 2014 at the University of Debrecen. The Senate of Semmelweis University awarded him the title of Professor Honoris Causa in 2015. Prof. Balint is a fellow of the Royal College of Physicians and Surgeons (Glasgow). He has held a particular interest in musculoskeletal ultrasonography since 1991. He has published more than 150 papers, several books and book chapters, has been an invited speaker at numerous international meetings, and organized and convened several musculoskeletal ultrasound courses. He was co-chairman of the ACR Ultrasound Study Group between 2011 and 2016. He is a member of the EULAR Standing Committee on Musculoskeletal Imaging, EULAR/OMERACT Ultrasound Special Interest Group, USSONAR-MSSK, EFSUMB, GRAPPA and the Association of Hungarian Rheumatologists. He is a reviewer for several international rheumatology journals in the field of sonography and is the editor of the imaging section of Hungarian Rheumatology.

Peter Mandl is Privatdozent and consultant at the Division of Rheumatology, Medical University of Vienna, Austria, and a member of the EULAR Network of Imaging Research Centres. After graduating with honours from Semmelweis University, Budapest, he completed his doctorate in functional neuroscience with honours at the Nathan Kline Institute in Orangeburg, New York, and at the Institute of Experimental Medicine, Budapest, and defended his PhD thesis (*The Effects of Antidepressants on Nicotinic Acetylcholine Receptors of the Central and Peripheral Nervous System)* at Semmelweis University, Budapest in 2007. He received his Habilitation in Internal Medicine (*Role of Ultrasound in Assessing Inflammation and Structural Damage in Rheumatoid Arthritis*) from the Medical University of Vienna in 2017. His major research interests include the use of imaging for diagnosing, monitoring and predicting rheumatic and musculoskeletal diseases, in particular the utility of ultrasound for the monitoring of inflammation and structural changes. He served as chairman of EMEUNET, the Emerging EULAR Network, is a prior OMERACT Fellow of the Ultrasound Taskforce, member of the EULAR Standing Committee of Musculoskeletal Imaging, convenor of the OMERACT Working Group on Cartilage Change in Rheumatoid Arthritis and has coordinated or was involved in several EULAR Taskforces (EULAR Recommendations for the use of imaging in spondyloarthritis, EULAR points to consider on the use of ultrasound for health professionals, etc.). Peter Mandl is associate editor of *BMC Medical Imaging* and *Frontiers in Medicine: Rheumatology* and has authored more than 50 peer-reviewed publications and several book chapters. He has organized and served on the faculty of numerous national and international musculoskeletal ultrasound courses and workshops, including the EULAR and ACR Musculoskeletal Ultrasound Courses. He is a member of the imaging section of the Austrian Society of Rheumatology.

Contents

Contributors

Gabor Baksa, MD Laboratory of Applied and Clinical Anatomy, Department of Anatomy, Histology and Embryology, Semmelweis University, Budapest, Hungary

Geza P. Balint, MD, FRCP, DSc Ambulatory Care Clinic, National Institute of Rheumatology and Physiotherapy, Budapest, Hungary

Peter Vince Balint, MD, PhD, FRCP 3rd Rheumatology Department, National Institute of Rheumatology and Physiotherapy, Budapest, Hungary

Szabolcs Benis, MD Department of Orthopaedics and Traumatology, Ghent University Hospital, Ghent, Belgium

Emilio Filippucci, MD, PhD Clinica Reumatologica, Università Politecnica delle Marche, Ospedale "C. Urbani", Ancona, Italy

Irina Gessl, MD Division of Rheumatology, Department of Internal Medicine III, Medical University of Vienna, Vienna, Austria

Walter Grassi, MD Clinica Reumatologica, Università Politecnica delle Marche, Ospedale "C. Urbani", Ancona, Italy

Gyorgy Gulacsi, MD Semmelweis University, Doctoral School of Clinical Medicine, Budapest, Hungary

Janos Gyebnar, MD Radiology Department, National Institute of Rheumatology and Physiotherapy, Budapest, Hungary

Lena Hirtler, MA, MD, PhD Division of Anatomy, Center for Anatomy and Cell Biology, Medical University of Vienna, Vienna, Austria

Florian Huber, MD Division of Neuro- and Musculoskeletal Radiology, Department of Biomedical Imaging and Image-Guided Therapy, Medical University of Vienna, Vienna, Austria

Franz Kainberger, MD Division of Neuro- and Musculoskeletal Radiology, Department of Biomedical Imaging and Image-Guided Therapy, Medical University of Vienna, Vienna, Austria

Eszter Kovari, MD Semmelweis University, Doctoral School of Clinical Medicine, Budapest, Hungary

Reka Kurucz, MD 3rd Rheumatology Department, National Institute of Rheumatology and Physiotherapy, Budapest, Hungary

Peter Mandl, MD, PhD Division of Rheumatology, Department of Internal Medicine III, Medical University of Vienna, Vienna, Austria

Lajos Patonay, MD, DDS Laboratory of Applied and Clinical Anatomy, Department of Anatomy, Histology and Embryology, Semmelweis University, Budapest, Hungary

Janina Patsch, MD, PhD Division of Neuro- and Musculoskeletal Radiology, Department of Biomedical Imaging and Image-Guided Therapy, Medical University of Vienna, Vienna, Austria

Hannes Platzgummer, MD Division of Neuro- and Musculoskeletal Radiology, Department of Biomedical Imaging and Image-Guided Therapy, Medical University of Vienna, Vienna, Austria

Gabriela M. Supp, MA Division of Rheumatology, Department of Internal Medicine III, Medical University of Vienna, Vienna, Austria

Claudia Weidekamm, MD, MBA Division of Neuro- and Musculoskeletal Radiology, Department of Biomedical Imaging and Image-Guided Therapy, Medical University of Vienna, Vienna, Austria

Clinical Examination of the Hand and Wrist in Rheumatology

1

Eszter Kovari, Reka Kurucz, Peter Mandl, Geza P. Balint, and Peter Vince Balint

Inspection

Visual inspection is the first step of any physical examination (Fig. 1.1). Table 1.1 lists the most common findings, which may occur in a rheumatological setting. Involved joints may be counted and mapped. This may provide important information for classifying arthritis, i.e. as mono-/oligo- and polyarthritis, ray pattern typical in psoriatic arthritis, etc.

Palpation

Temperature of the skin may be decreased in diffuse fashion seen in Raynaud's phenomenon; however, localized hyperthermia over a joint or area is more common and may be commonly found in septic arthritis and cellulitis/panniculitis, respectively (Fig. 1.2). The skin itself may be elevated in cutis laxa, i.e. Ehlers-Danlos syndrome, or thickened as in systemic sclerosis (diffused or localized). Localized thickening of the palmar aponeurosis may also be seen in Dupuytren's contracture

E. Kovari, MD (✉)
Semmelweis University, Doctoral School of Clinical Medicine, Budapest, Hungary

R. Kurucz, MD · P. V. Balint, MD, PhD, FRCP
3rd Rheumatology Department, National Institute of Rheumatology and Physiotherapy, Budapest, Hungary

P. Mandl, MD, PhD
Division of Rheumatology, Department of Internal Medicine III, Medical University of Vienna, Vienna, Austria

G. P. Balint, MD, FRCP, DSc
Ambulatory Care Clinic, National Institute of Rheumatology and Physiotherapy, Budapest, Hungary

P. V. Balint, P. Mandl (eds.), *Ultrasonography of the Hand in Rheumatology*,
https://doi.org/10.1007/978-3-319-74207-6_1

Fig. 1.1 Inspection of the dorsal aspect of the hands and wrists

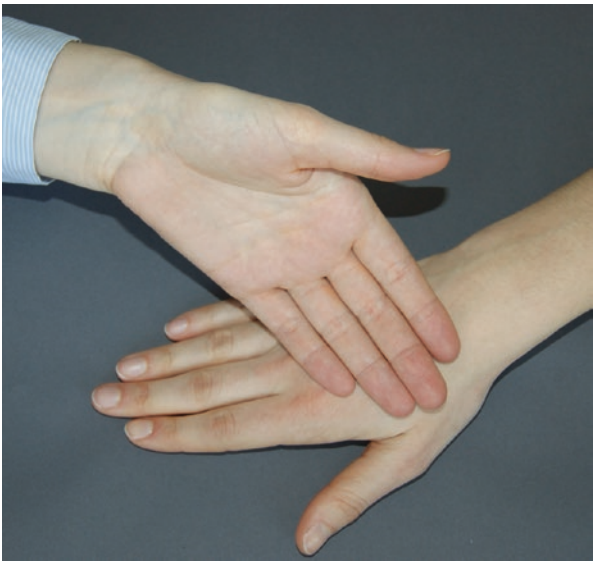

Fig. 1. 2 Testing skin temperature

(particularly affecting the fourth digit) and in diabetic cheiroarthropathy (Fig. 1.3). Diffuse thinning of the skin may be age-related; however, localized atrophy is a common side-effect of glucocorticoid injections. Swelling may be articular as commonly seen in arthritides (Fig. 1.4) and periarticular as in the case of rheumatoid nodules or ganglion cysts, both of which commonly occur on the dorsal side of the hand. The tuck sign denotes a bulging of the dorsal aspect of the wrist during active wrist/finger extension seen in extensor tenosynovitis. Patients with septic tenosynovitis of the flexor tendons of the hand may exhibit Kanavel's cardinal signs consisting of slight flexion of the affected finger, swelling and tenderness along the affected tendon and pain on passive extension of the affected finger. Swelling may also be

Table 1.1 Common signs on visual inspection in rheumatic and musculoskeletal diseases

Sign	Localization
Erythema	Single/multiple joint (e.g. septic arthritis)
	Region (e.g. palmar erythema in SLE: systemic lupus erythematosus with hepatic involvement)
	Diffuse (e.g. cellulitis, erysipelas)
Pallor	Single or multiple digits (e.g. Raynaud's phenomenon)
Cyanosis	Fingertip, nail bed (e.g. acrocyanosis)
	Diffuse (e.g. Raynaud's phenomenon)
Cutis reticularis/marmorata	Diffuse (e.g. antiphospholipid syndrome)
Mottled skin	Varied (e.g. vitiligo)
Stained skin	Fingertips (nicotine)
	Diffuse (e.g. diffuse yellow in carotenemia)
Suffusion	Dorsal surface of the hand (e.g. glucocorticoid use)
Scars, wounds and keloids	Palmar (e.g. median nerve release scars)
	Dorsal (e.g. common injuries, scars, ulcerated gouty tophi, Gottron's sign)
Subcutaneous calcinosis	Diffuse (e.g. CREST syndrome)
Cracks and fissures	Diffuse (e.g. mechanic's hand, dermatomyositis)
Atrophy	Diffuse (e.g. systemic sclerosis, glucocorticoid use)
Slacking skin	Dorsal (e.g. anetoderma in systemic lupus erythematosus)
	Diffuse (e.g. cutis laxa—Ehlers-Danlos syndrome)
Nail bed lesions	Localized (e.g. nailfold vasculitis, splinter haemorrhage)
Swelling	Diffuse (e.g. puffy hands in remitting seronegative symmetrical synovitis with pitting edema, algodystrophy, palindromic rheumatism, paraneoplastic syndrome)
	Single/multiple finger (e.g. dactylitis, spina ventosa)
	Single/multiple joint/tendon (e.g. rheumatoid arthritis)
Deformity	Diffuse nail (e.g. hourglass deformity)
	Single nail (e.g. pitting subungual hyperkeratosis, Beau's lines, oil drop patches, onycholysis in psoriatic arthritis, mycosis)
	Diffuse finger (e.g. clubbing)
	DIP: distal interphalangeal joint (e.g. Heberden's node)
	PIP: proximal interphalangeal joint (e.g. Bouchard's node)
	CMC joint (e.g. squaring in rhizarthrosis)
	Ulnar head (e.g. piano key sign in rheumatoid arthritis, Bayonet deformity or Madelung's deformity)
	Palmar aponeurosis (e.g. Dupuytren's syndrome, cheiroarthropathy)
	Diffuse (e.g. Volkmann's contracture)
Gangrene, ulcer	Fingertip (e.g. systemic sclerosis)
Malalignment	Swan-neck deformity (proximal interphalangeal joint hyperextension and distal interphalangeal joint flexion)
	Boutonniere (or buttonhole) deformity (proximal interphalangeal joint flexion and distal interphalangeal joint extension)
	Radial deviation of the wrist (e.g. juvenile idiopathic arthritis)
	Ulnar deviation and subluxation of the metacarpophalangeal joints (e.g. rheumatoid arthritis)
	Z or zigzag deformity of the thumb (e.g. rheumatoid arthritis)

(continued)

Table 1.1 (continued)

Sign	Localization
Muscle atrophy	Thenar (e.g. carpal tunnel syndrome)
	Hypothenar (e.g. Guyon's tunnel syndrome)
	Interossei (e.g. rheumatoid arthritis)
	Claw hand (e.g. syringomyelia)
Non-voluntary movement	Single muscle/diffuse (e.g. fasciculation, tremor)

Fig. 1.3 Placing palms together to test for diabetic cheiroarthropathy

Fig. 1.4 Palpation of joint swelling

diffuse, e.g. occurring in gout or pseudogout. Puffy hands are seen in remitting seronegative symmetrical synovitis with pitting oedema (RS3PE). Localized swelling of the nailbed or fingertip may indicate a glomus tumor. Swelling of an entire finger seen in dactylitis can also be measured using a dactylometer (Fig. 1.5) [1].

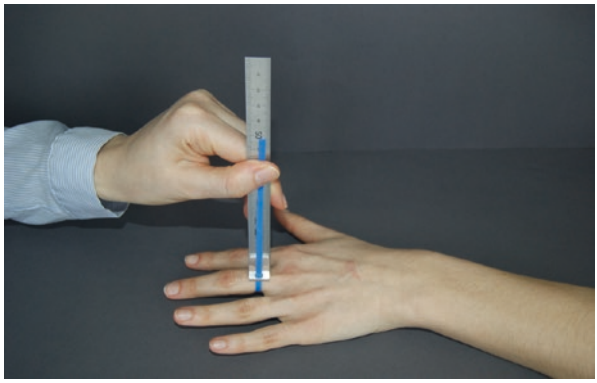

Fig. 1.5 Use of the Leeds dactylometer

Fig. 1.6 Radial pulse palpation

Pulsating swelling localized over an artery can be encountered in aneurysm or pseudoaneurysm of the radial artery. Lack or weakness of the radial pulse may indicate Takayasu's arteritis (Fig. 1.6). Capillary refill can be prolonged in Raynaud's phenomenon (Fig. 1.7). Deformities may either be localized when occurring after trauma or affect multiple localizations, such as those occurring in rheumatoid arthritis (ulnar deviation, swan-neck deformity, etc.). Palpation can also be used to elicit pain over single joints or regions, such as Tinel's sign elicited by light tapping over the nerve (e.g. over the median nerve in carpal tunnel syndrome or over the ulnar nerve in Guyon's canal syndrome) (Fig. 1.8). Crepitation may be detected over the tendon sheath of finger flexor tendons in chronic flexor tenosynovitis and de Quervain's tenosynovitis.

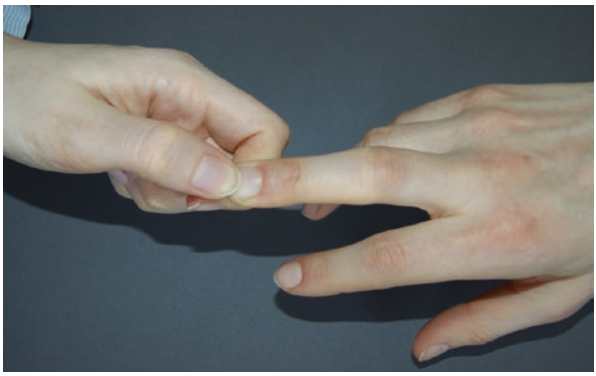

Fig. 1.7 Capillary refill test

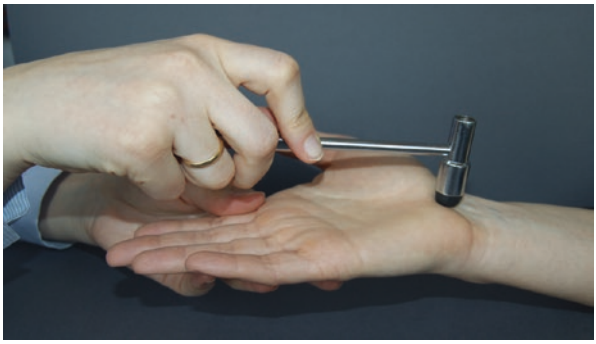

Fig. 1.8 Testing for Tinel's sign

Movement

Testing of passive motion and observation of active motion of the wrists and hands may reveal limited range of motion (ROM), seen in a wide range of pathological conditions from arthritides to osteoarthritis (Fig. 1.9). Limited ROM may be seen also in tendon pathology, including tendon tears or the limitation of smooth movement coupled with the sensation of sudden release during extension of the tendon seen in trigger finger. Movement beyond the normal range of motion may be seen in hypermobility syndrome, which may also be a feature of rare inherited diseases such as Ehlers-Danlos syndrome, Marfan syndrome or Down syndrome. Hypermobility is commonly assessed among others by the Beighton score or the Brighton or Bulbena criteria (Fig. 1.10) [2–4]. Passive range of motion may be limited by excess synovial fluid/synovitis, joint dislocation or subluxation, intra-articular chondromatosis, intra-articular loose bodies, extra-articular masses blocking motion, muscle spasms and contractures (myogenic, desmogenic or arthrogenic), among others. All of the above may of course interfere also with active motion (Figs. 1.11 and 1.12). Normal range of active motion for the hand and fingers is listed in Table 1.2. Observation of motion may in addition reveal muscle rupture, muscle weakness/paresis or paralysis, tendon rupture/damage as well as malingering.

Fig. 1.9 Dorsiflexion of the wrist

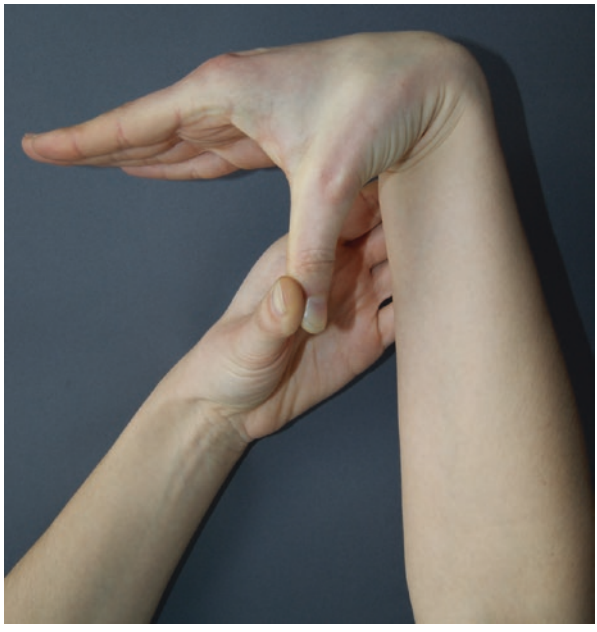

Fig. 1.10 Hypermobility test

Table 1.2 Normal ranges of motion for hand and finger joints

Movement	Range
Wrist	
Volar (palmar) flexion	0–80°
Dorsal flexion (extension)	0–70°
Radial deviation	0–20°
Ulnar deviation	0–30°
Thumb; carpometacarpal joint	
Abduction	0–50°
Flexion	0–15°
Extension	0–20°
Thumb; metacarpophalangeal joint	
Flexion	0–50°
Extension	0–10°
Thumb; interphalangeal joint	
Flexion	0–80°
Extension	0–20°
Finger; metacarpophalangeal joint	
Flexion	0–90°
Extension	0–45°
Finger; proximal interphalangeal joint	
Flexion	0–100°
Extension	0–5°
Finger; distal interphalangeal joint	
Flexion	0–90°
Extension	0–10°

Fig. 1.11 Active hyperextension of the finger

Neutral position of the wrist: hand with palm facing down in the axis and plane of the underarm.

Neutral position of the thumb: thumb resting at the side of the index finger which is in the plane of the radius. Opposition and circumduction are complex movements composed of basic motions.

Neutral position of the fingers: fingers are positioned side by side in the plane of the underarm. Muscle strength can be assessed by quantitative methods using a

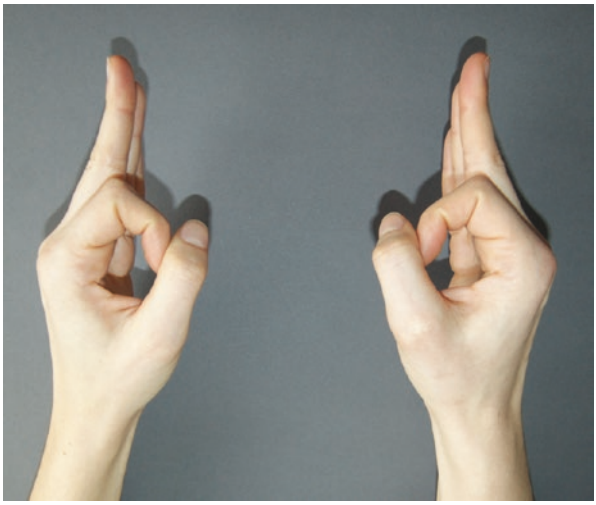

Fig. 1.12 Active flexion of the fingers

Fig. 1.13 Testing of grip strength using a dynamometer

dynamometer (Fig. 1.13) [5] and qualitative methods such as manual muscle testing (MMT) [6] or the widely accepted and used scale proposed by the Medical Research Council [7], both of which have been modified by various authors.

Specific Tests

A number of tests have been developed to test hand function, innervation and circulation as well various hand injuries and joint stability. The following specific tests designed to evaluate motion as well as signs relevant to the field of rheumatology are commonly performed during a rheumatological examination:

- Turning hands over: testing pronation-supination.
- Balling of fists: testing multiple joint flexion.
- Gripping the middle and index finger: testing of power grip (Fig. 1.14).
- Opposing thumb with individual fingers: testing of precision grip (Fig. 1.15).
- Everyday activities: opening a jar or picking up small objects (Figs. 1.16, 1.17).

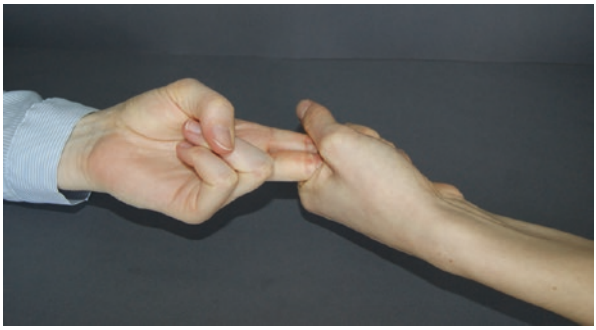

Fig. 1.14 Testing of the power grip

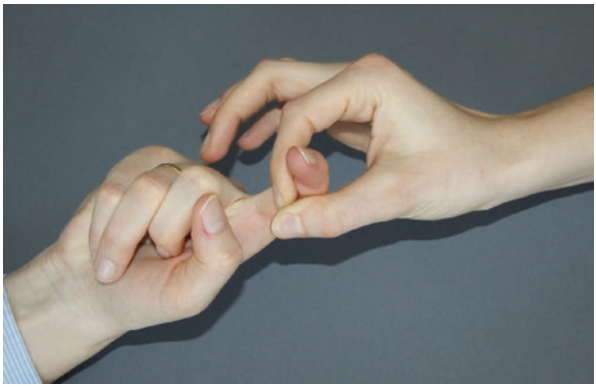

Fig. 1.15 Testing of the precision grip

Fig. 1.16 Everyday activity: opening a jar

Fig. 1.17 Everyday activity: picking up small objects

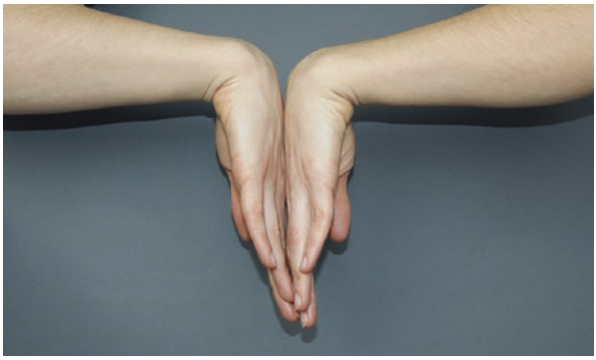

Fig. 1.18 Testing for Phalen's sign

Fig. 1.19 Finkelstein's test

- Phalen's sign test: the wrists are pressed together in forced flexion for at least 60 seconds; tingling, numbness or pain may indicate carpal tunnel syndrome (Fig. 1.18).
- Finkelstein's test: the examining physician or therapist grasps thumb and ulnar deviates the hand sharply. Sharp pain occurring along the distal radius may indicate de Quervain's tenosynovitis (Fig. 1.19). Alternatively a modified Eichhoff's test may be performed in which the patient is asked to flex their thumb and clench their fist over the thumb followed by ulnar deviation performed by the practitioner.
- Watson's test: the examining physician grasps the wrist with their thumb over the scaphoid tubercle on the volar aspect of the palm with the wrist held in slight extension. The patient's wrist is then moved from ulnar to radial deviation. The feeling of a "clunk" or the indication of pain upon the manoeuver may indicate a tear of the scapholunate ligament or scapholunate instability.
- Gaenslen's squeeze test: lateral compression (squeezing) of the metacarpophalangeal (or metatarsophalangeal) joints (Fig. 1.20). Tenderness indicates arthritis.

Information from all of the above-mentioned domains may be graded on a scale, e.g. 0–4, and summarized into a uniform scoring system, such as the STWL (swelling, tenderness, warmth and limitation of movement) system. Using the above-mentioned system, the right fifth PIP S3T4W1 L3 would denote moderate swelling, severe tenderness, trace warmth and 75% loss of normal range of motion of the right fifth PIP joint [8].

Fig. 1.20 Gaenslen's squeeze test

References

1. Helliwell PS, Firth J, Ibrahim GH, Melsom RD, Shah I, Turner DE. Development of an assessment tool for dactylitis in patients with psoriatic arthritis. J Rheumatol. 2005;32:1745–50.
2. Beighton P, Solomon L, Soskolne CL. Articular mobility in an African population. Ann Rheum Dis. 1973;32:413–8.
3. Bulbena A, Duro JC, Porta M, Faus S, Vallescar R, Martin-Santos R. Clinical assessment of hypermobility of joints: assembling criteria. J Rheumatol. 1992;19:115–22.
4. Grahame R, Bird HA, Child A. The revised (Brighton 1998) criteria for the diagnosis of benign joint hypermobility syndrome (BJHS). J Rheumatol. 2000;27:1777–9.
5. Beasley WC. Instrumentation and equipment for quantitative clinical muscle testing. Arch Phys Med Rehabil. 1956;37:604–21.
6. Wright W. Muscle training in the treatment of infantile paralysis. Boston Med Surg J. 1912;167:567.
7. Medical Research Council. Aids to examination of the peripheral nervous system. Memorandum no. 45. London: Her Majesty's Stationary Office; 1976.
8. Meehan RT. History and physical examination. In: West SG, editor. Rheumatology secrets. 3rd ed. Philadelphia: Elsevier; 2015. p. 41–8.

Gross Anatomy of the Human Hand

2

Gabor Baksa, Peter Mandl, Szabolcs Benis, Lajos Patonay, Geza P. Balint, and Peter Vince Balint

Layer-by-Layer Anatomy of the Hand

Skin, Subcutis and Nail

The first anatomical layer that both the rheumatologist and the ultrasonographer encounter is the surface of the skin. Despite a lot of anatomical variants, there are constant lines of the skin, which can serve as markers, e.g. for joint spaces. Several sets of anatomical skin lines (e.g. Langer's, Kreissl's, Blaschko's, etc.) have been defined either in cadavers or live subjects. On the dorsal surface, the superficial venous network of the hand feeds into the cephalic vein on the radial side and the basilic vein on the ulnar side. The dorsal metacarpal veins run over the knuckles as a venous arch. Skin creases over the proximal interphalangeal joints (PIP) and distal interphalangeal joints (DIP) are also well visualized (Fig. 2.1). The surface of the palm is broken by hills and valleys. Lumbrical muscles and neurovascular bundles produce hills, while valleys contain flexor tendons. Distinction of creases on the

G. Baksa, MD (✉) · L. Patonay, MD, DDS
Laboratory of Applied and Clinical Anatomy, Department of Anatomy, Histology and Embryology, Semmelweis University, Budapest, Hungary

P. Mandl, MD, PhD
Division of Rheumatology, Department of Internal Medicine III, Medical University of Vienna, Vienna, Austria

S. Benis, MD
Department of Orthopaedics and Traumatology, Ghent University Hospital, Ghent, Belgium

G. P. Balint, MD, FRCP, DSc
Ambulatory Care Clinic, National Institute of Rheumatology and Physiotherapy, Budapest, Hungary

P. V. Balint, MD, PhD, FRCP
3rd Rheumatology Department, National Institute of Rheumatology and Physiotherapy, Budapest, Hungary

P. V. Balint, P. Mandl (eds.), *Ultrasonography of the Hand in Rheumatology*,
https://doi.org/10.1007/978-3-319-74207-6_2

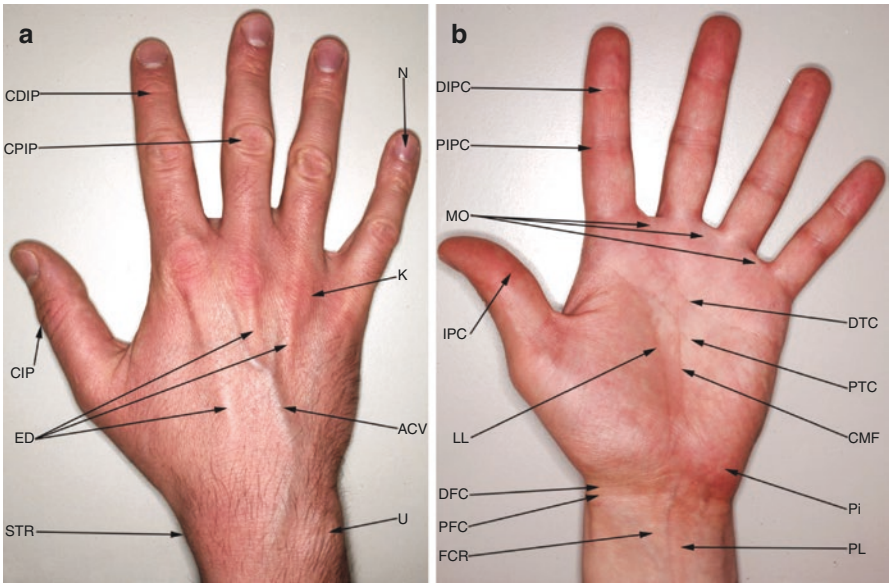

Fig. 2.1 Surface anatomy of the hand. (**a**) Dorsal surface; (**b**) palmar surface. *ACV* accessory cephalic vein, *CDIP* crease over the distal interphalangeal joint, *CIP* crease over the interphalangeal joint, *CMF* crease of middle finger, *CPIP* crease over the proximal interphalangeal joint, *DFC* distal flexure crease, *DIPC* distal interphalangeal crease, *DTC* distal transverse crease, *ED* extensor digitorum tendons, *FCR* flexor carpi radialis tendon, *IPC* interphalangeal crease, *K* knuckle, *LL* life line, *MO* monticuli, *N* nail, *PFC* proximal flexure crease, *Pi* pisiform, *PIPC* proximal interphalangeal crease, *PL* palmaris longus tendon, *PTC* proximal transverse crease, *STR* styloid process of radius, *U* ulna

palmar hand are generally easy (Fig. 2.1). Friction ridges on the fingertips and the palm are important not only for forensic medicine and identification (fingerprint) but help with gripping function as well.

The palmar side of the hand is divided into the regions of the thenar, mesothenar and hypothenar by the palmar aponeurosis and the medial and lateral intermuscular septa. The intermuscular septae originate on both margins of the aponeurosis, anchoring it to the second and fifth metacarpals. The palmar aponeurosis originates either from the palmar ligament or in most cases is continuous with the tendon of the palmaris longus muscle. However, it always inserts with longitudinal fibres on the fibrous tendon sheets sheaths of the second to fifth fingers as well as sending fibres into their subcutaneous tissue, respectively. At certain points proximally, it adheres tightly to the palmar skin, while distally its fibres are looser. There are also some transverse fibres traversing between the longitudinal fibres. These fibres form three windows between the second and fifth fingers, where the common digital arteries bifurcate into their proper digital branches. The nerves pass under the superficial transverse metacarpal ligament, also called natatory ligament, more proximally, just under the transversal fibres. The nerves and vessels are covered only by thick subcutaneous fat pads (monticuli), which are best visible when the palmar skin is stretched by forced extension of the fingers (Fig. 2.2).

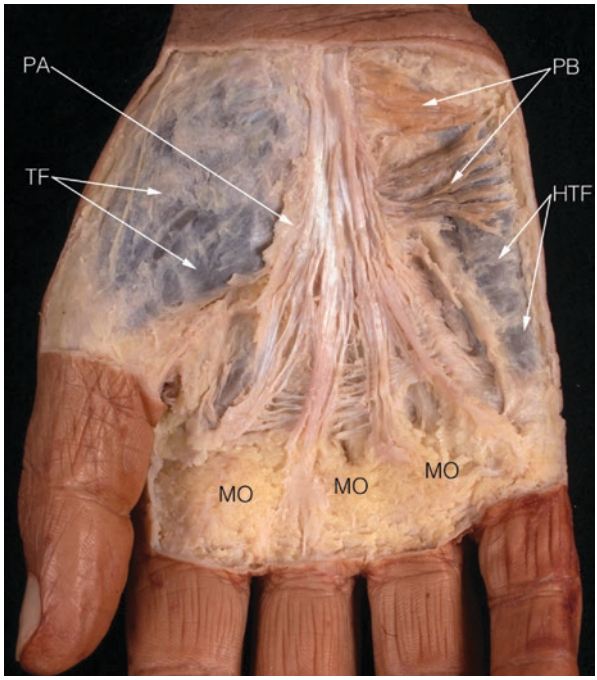

Fig. 2.2 First palmar layer under the skin and subcutaneous tissue. *HTF* hypothenar fascia, *MO* monticuli, *PA* palmar aponeurosis, *PB* palmaris brevis muscle, *TF* thenar fascia

Palmaris brevis is a tiny muscle originating from the flexor retinaculum and the palmar aponeurosis and inserting onto the skin of the hypothenar. It is the only hand muscle innervated by the superficial branch of the ulnar nerve.

On the palmar side of the hand on the palm the skin is fixed to the palmar aponeurosis by perpendicular septae; similar septae fix the skin on the fingers at the level of the metacarpophalangeal (MCP), PIP and DIP joints. At the fingers, digital cutaneous ligaments called Cleland's ligaments run dorsal to the digital nerves, while on the volar aspect, we find Grayson's ligament, superficial to the digital nerves, attached to the skin fixing deep layers of fascia. A major advantage of this type of tethering is that it limits the mobility of the skin during active movement, and these structures also stabilize the digital neurovascular bundle.The distal dorsal end of the finger is covered by a slightly convex nail. The nail plate has several folds, namely two lateral (paronychium) and one proximal fold covered by the cuticle at the eponychium. Altogether this is defined as the perionychium. The fourth free margin is called the distal edge. On the opposite, proximal side we find the lunula, which is the named after its resemblance to the shape and color of a waxing or waning gibbous moon. The nail matrix (sterile (or hyponychium) and germinal) lies deeply at the proximal folds. The proximal edge (or root) of the nail lies under the skin and is called the occult margin. The nail bed has a very rich capillary network and appears pink in healthy subjects. The nail itself has a hard keratin structure attached to the germinal and sterile matrix with two plates (dorsal and a ventral). Not too far from the distal interphalangeal joint the ventral floor is attached firmly to the periosteum next to the insertion of the extensor tendon.

Bones

Like the middle layer of a "sandwich", bones divide the hand into the dorsal and palmar aspect. Hand bones lay closer to the dorsal surface than to the palmar surface, with the latter containing relatively more soft tissue and muscles. This leads to the palmar part of the hand being thicker than the dorsal, which in turn results in better acoustic resolution when examining the dorsal aspect of the hand. The hand is joined to the two bones of the forearm (radius and ulna) and consists of the carpus, metacarpus and fingers. The distal ends of the radius and the ulna form a pivot joint with the radial distal edge rotating in the ulnar notch. The proximal transverse arch is formed by the two rows of carpal bones. Metacarpal heads form the distal transverse palmar arch of the palm. The major longitudinal arch (third digital ray) runs from the dorsal tubercle of the radius (Lister's tubercle), through one of the largest and strongest carpal bones, the capitate to the base of the third metacarpal. Longitudinal hand arches fan out on both sides of the major longitudinal arch reaching the second, fourth and fifth metacarpal bases, respectively. Along with the thumb which opposes the other fingers, these arches form a ball-catcher's hand. We can also visualize four diagonal arches between the thumb and other fingers. All these arches contribute to a semi-spherical basket hilt of the hand ideal for catching and holding objects (Fig. 2.3).

The carpus is formed by four proximal and four distal carpal bones. The proximal row of the carpal bones (from radial to ulnar: scaphoid, lunate, triquetrum, pisiform) forms the radiocarpal joint proximally with the radial bone and the midcarpal joint distally with the second row of carpal bones (from radial to ulnar: trapezium, trapezoid, capitate and hamate) (Fig. 2.4). The most medially located

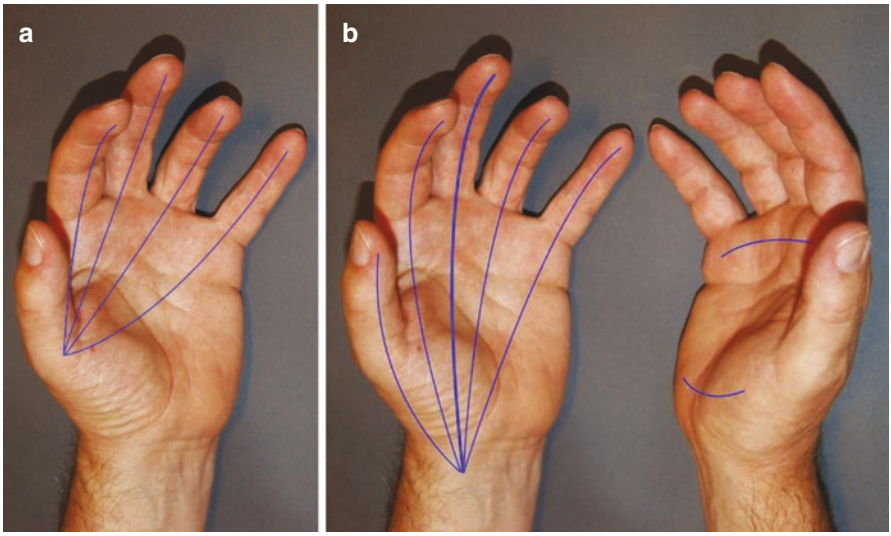

Fig. 2.3 Hand arches. (**a**) Diagonal arches; (**b**) digital rays of the left hand and proximal and distal transverse palmar arches of the right hand

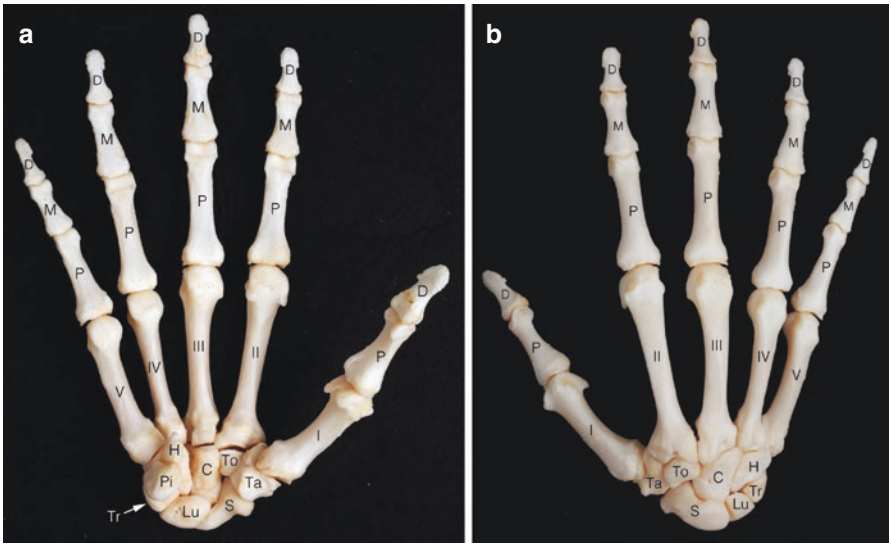

Fig. 2.4 Bones of the hand. (**a**) Palmar aspect; (**b**) dorsal aspect. *C* capitate, *D* distal phalanx, *H* hamate, *I–V* first to fifth metacarpals, *Lu* lunate, *M* middle phalanx, *P* proximal phalanx, *Pi* pisiform, *S* scaphoid, *Ta* trapezium, *To* trapezoid, *Tr* triquetrum

pisiform and hamate bones and the laterally positioned scaphoid (with its tubercle) and trapezium form the medial and lateral carpal eminences, respectively. The distal end of the ulna and ulnar styloid process form a joint with the proximal carpal bones and with the triangular fibrocartilage complex. The pisiform, a sesamoid bone on which the flexor carpi ulnaris muscle inserts, is not an actual part of the radiocarpal joint because it has a joint articulation surface only dorsally towards the triquetrum.

The pisiform is the ulnar bony landmark of the proximal entry of the carpal tunnel. The tubercle of the scaphoid is the radial landmark of the proximal entry of the carpal tunnel and also an identification point to localize the ulnar artery, situated laterally from the pea-shaped bone. The distal bony pillars of the carpal tunnel are the hook of the hamate (hamulus ossis hamatum) and the trapezium at the ulnar and radial sides, respectively.

Sesamoid bones occur commonly on the palmar aspect of the hand and are considered normal variants. The numbers of carpal bones are frequently and variably increased, with a large number of accessory ossicles described, the detailed review of which is beyond the scope of this book.

The metacarpus consists of the five metacarpals, which can be divided into base, shaft, neck and head. The head of the metacarpal bone is oblong and slightly elongated in the dorso-palmar axis; although it may be irregular, the head has a smooth convex area that is the intraarticular part. The extrasynovial areas of the head are rough and contain a medial and lateral tubercle for the attachment of the collateral ligaments, as well as an elevated ridge surrounding the intraarticular smooth area. This ridge forms a dorsal depression which is smooth and well-demarcated and has

reflective bone at its base. It occurs at the site of the fused growth plate and is a site of entry for nutritional/feeding vessels. In an ultrasound study on cadavers, this depression was visualized in 37% of examined MCP joints (highest frequency found in the second MCP joint) and appeared as a well-defined bony groove on both longitudinal and transverse ultrasound scans, with no cortical break [1].

The fingers are built up by the proximal, middle and distal phalanges, respectively. The thumb has no middle phalanx. The distal phalanges have a so-called tuberosity on their head portion.

Extrinsic and Intrinsic Ligament of the Wrists

Extrinsic ligaments connect the carpal bones proximally to the radius and ulna and distally to the metacarpals. Intrinsic ligaments originate from and insert into different carpal bones. Ligaments form a dorsal radiocarpal "V" ligament and proximal and distal palmar "V" ligament complexes. For rheumatologists, perhaps the most important ligaments are the scapholunate and the lunotriquetral ligament (Fig. 2.5). Both ligaments have three parts: palmar, dorsal and intermediate. Both intrinsic

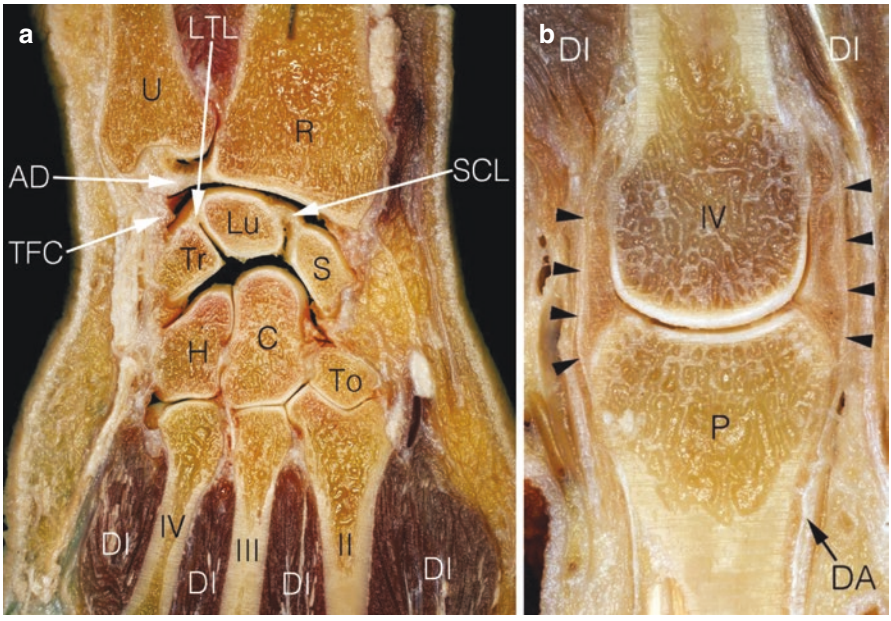

Fig. 2.5 Coronal sections of hand joints. (**a**) Coronal section across the wrist, carpal and carpometacarpal joints, (**b**) coronal section across the fourth metacarpal joint. *AD* articular disc, *C* capitate, *DA* dorsal aponeurosis, *DI* dorsal interosseous, *H* hamate, *II–IV* second to fourth metacarpals, *LTL* lunotriquetral ligament, *Lu* lunate, *P* proximal phalanx, *R* radius, *S* scaphoid, *SCL* scapholunate ligament, *TFC* triangular fibrocartilage complex, *To* trapezoid, *Tr* triquetrum, *U* ulna, *arrowheads* metacarpal joint capsule and collateral ligament

interosseous and intrinsic capsular ligaments are important to maintain carpal arches, mobility and stability; however ultrasound cannot depict interosseous ligaments. Scaphoid and lunate are the most mobile bones, and the second and third metacarpal bases are the most fixed parts of the wrist.

Ligaments of the MCPs, PIPs, DIPs and IPs

Despite their different size and type of joint MCP joints are condyloid while the others are hinge joints, ligaments are arranged similarly around MCPs, PIPs, DIPs and interphalangeal joints (IPs) (Fig. 2.5). A major exception is the deep transverse metacarpal ligament connecting the second, third, fourth and fifth metacarpal heads and their respective palmar plates to avoid any unexpected separation of the metacarpals during the individual movement of the fingers. All joints have radial (more horizontal) and ulnar (more oblique) collateral ligaments. Collateral ligaments have two parts: the cord-like proper ligaments, which are located more dorsally, and fan-shaped accessory ligaments, which are more palmar and at the proximal phalanx are attached to the palmar plate and to the transverse metacarpal ligament. They act differently based on their location of origin and insertion. Both stabilize the joint, with the proper ligament tightening during flexion and relaxing during extension. Accessory ligaments are tight during extension and relaxed during flexion. The interosseous muscles pass dorsally to the transverse metacarpal ligament, while the lumbrical muscles pass palmar to the same ligament and insert onto the collateral ligaments, stabilizing the joints from lateral. Retinacular ligaments (both transverse and oblique retinacular ligaments of Landsmeer) aid in flexion and extension of the PIP and DIP joints. Oblique ligaments originate on the palmar part of the proximal phalanx, cross the collateral ligament and insert more dorsally on the distal phalanx. Transverse bands originating from the border of the flexor tendon sheath and insert onto the lateral bands of the extensor hood.

Muscles in the Mid-layer

Lumbrical muscles originate from the deep flexor tendons and run towards and insert onto the expansion of the extensor tendon functioning as flexors of the MCP joints and extensors of the PIP joints. Interosseous muscles have two groups. The palmar interossei originate on the side of the shaft of the second, fourth and fifth metacarpal and insert onto the bases of the proximal phalanges of the second, fourth and fifth fingers as well as onto the expansion of the extensor tendons (Fig. 2.6). Their main action is adduction, but they also contribute to flexion and extension of the fingers. The dorsal interossei also originate on the side of the shaft of the second to fifth metacarpal and attach to the proximal phalanges of the second to fourth fingers as well as onto the dorsal aponeurosis of the extensor tendons. Their main action is abduction of the fingers.

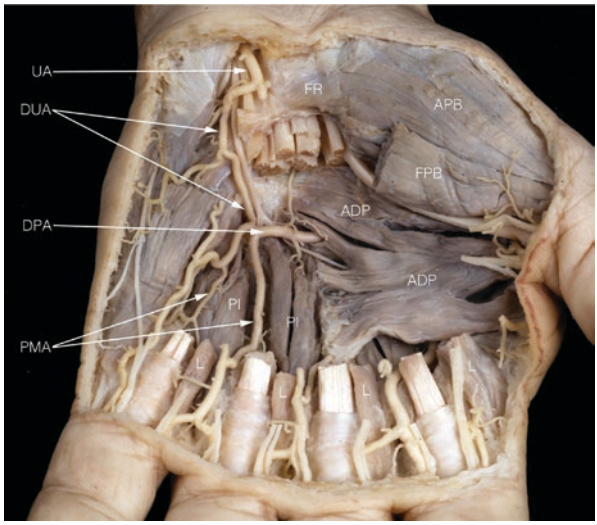

Fig. 2.6 Deep layer of the hand muscles. Note, the first palmar interosseous muscle is covered by the adductor pollicis muscle. *ADP* adductor pollicis muscle (oblique and transverse head), *APB* abductor pollicis brevis muscle, *DPA* deep palmar arch, *DUA* deep branch of ulnar artery, *FPB* flexor pollicis brevis muscle, *FR* flexor retinaculum, *L* lumbricals, *PI* palmar interosseous muscle, *PMA* palmar metacarpal arteries, *UA* ulnar artery

Vascular Arches, Blood Supply and Lymphatic Vessels

Due to their complexity and clinical importance, we provide a brief overview of the arterial supply of the hand. The vessels originate from the two main branches of the brachial artery: the radial and ulnar artery. The radial artery is located on the dorsal side of the hand, where it runs above the wrist through the radial foveola ("fossa tabatiere"), then cruises under the tendon of extensor pollicis longus and perforates the first dorsal interosseous muscle. This perforator branch is the main input of the deep palmar arch, which takes its other origin from the deep branch of the ulnar artery. The latter enters the hypothenar between the flexor digiti minimi brevis and abductor digiti minimi muscles. The deep arch gives off the four palmar metacarpal arteries, which then supply the interosseous muscles and partially also some carpal structures. Running then distally forward, they usually anastomose with the common digital palmar arteries from the superficial arch. The digital arteries originate from the superficial arch, and even small arteries enter into the joint cavity and also supply tendons via the mesotenon. Under the joint capsule, the central slip and the dorsal depression of the metacarpal head are rich in small vessels and capillaries (Figs. 2.7 and 2.8). Outside the joints, muscles and especially nailbeds are characterized by rich capillary networks. Deoxygenated blood is collected first by the palmar digital veins, flowing into the superficial and deep palmar arches before finally reaching the medial antebrachial vein, ulnar vein and radial vein and ultimately the basilic and cephalic veins into the upper arm. Lymphatic vessels follow the veins, and the first major lymph nodes are located in the cubital region. No lymph node exists in the hand and wrist.

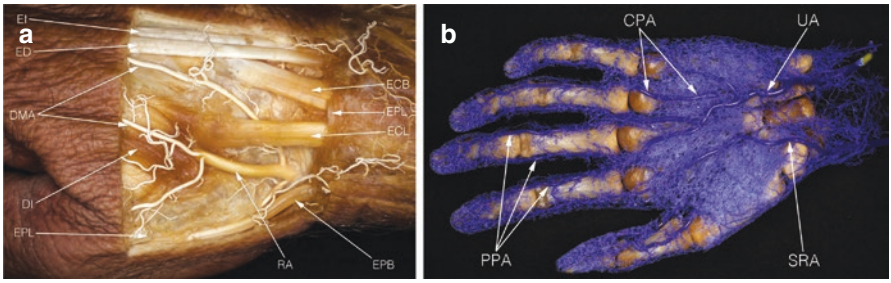

Fig. 2.7 (**a**) Anatomical snuff box with injected radial artery (tendon of extensor pollicis longus muscle are cut). (**b**) Vascular corrosion cast of hand arteries. Arteries injected with blue-coloured resin. *CPA* common palmar digital artery, *DI* first dorsal interosseous muscle, *DMA* dorsal metacarpal arteries, *ECB* extensor carpi radialis brevis tendon, *ECL* extensor carpi radialis longus tendon, *ED* extensor digitorum tendon, *EI* extensor indicis tendon, *EPB* extensor pollicis brevis tendon, *EPL* extensor pollicis longus tendon, *PPA* proper palmar digital artery, *RA* radial artery, *SRA* superficial branch of radial artery, *UA* ulnar artery

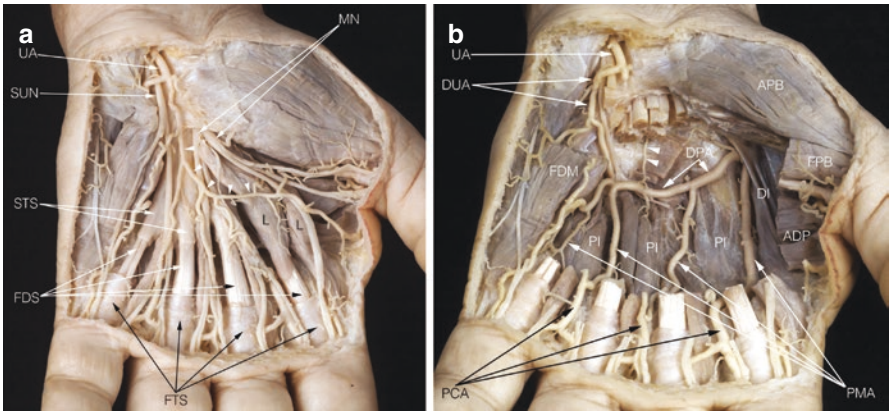

Fig. 2.8 Arterial arches of the hand. (**a**) Superficial palmar arch; (**b**) deep palmar arch. *ADP* adductor pollicis muscle, *APB* abductor pollicis brevis muscle, *DI* second dorsal interosseous muscle, *DPA* deep palmar arch, *DUA* deep branch of the ulnar artery, *FDM* flexor digiti minimi brevis, *FDS* flexor digitorum superficialis tendons, *FPB* flexor pollicis brevis muscle, *FTS* fibrous tendon sheath, *L* lumbricals, *MN* median nerve, *PCA* common palmar digital arteries, *PI* palmar interosseous muscle, *PMA* palmar metacarpal arteries, *STS* synovial tendon sheath, *SUN* superficial branch of ulnar nerve, *UA* ulnar artery, *arrowheads* superficial palmar arch, *double arrowheads* volar carpal artery

Neural Network

The median nerve divides into three main branches, the recurrent branch and the digital cutaneous branches (separating further to common palmar digital and proper palmar digital branches) before the nerve enters the carpal tunnel, but the branches remain strictly together and diverge only after exiting the tunnel. The lateral

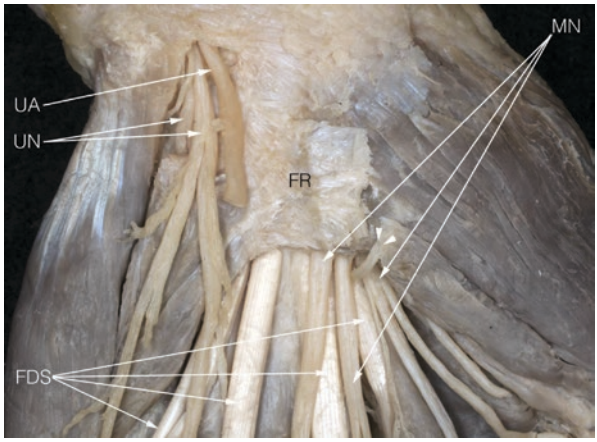

Fig. 2.9 Guyon's canal and carpal tunnel. Note, the median nerve divided in three branches and the thenar motoric branch exiting from the carpal tunnel. *FDS* superficial flexor digitorum tendons, *FR* flexor retinaculum, *MN* median nerve, *UA* ulnar artery, *UN* deep and superficial branches of the ulnar nerve, *arrowheads* motor branch to thenar muscles

recurrent branch, also called "the million-dollar nerve", perforates the lateral intermuscular septum and runs to the thumb and to the radial side of the index. Just after exiting from the tunnel, it gives off a short branch to the thenar musculature. The further two branches remain in the mesothenar running towards the second to fourth fingers. A well-known variation is the so-called "bifid" median nerve, where the nerve enters the carpal tunnel as two strong nerve stems. The prevalence of a bifid median nerve is less than 10% with a high likelihood of a bilateral condition and is sometimes but not always accompanied by a persistent median artery. The median nerve provides sensory innervation for the skin of the palmar aspect of the thumb, index and middle fingers and the palmar-radial side of the ring finger. The median nerve also innervates the dorsal aspect of the first three fingertips. The ulnar nerve enters Guyon's canal (Fig. 2.9). During ramification, it gives off two branches called the superficial and deep branches of the ulnar nerve. A number of anastomoses between the median and ulnar nerve have been described, as anatomical variations [2]. The ulnar nerve provides sensory innervation to the palmar side of the fifth digit as well as the palmar-ulnar aspect of the fourth digit. Radial nerve: the main trunk of the nerve does not enter the hand. It divides into a deep branch, which becomes the posterior interosseous nerve and a superficial branch, which goes on to innervate the back of the hand. Branches of the radial nerve innervate the dorsal surface of the lateral side of the palm as well as the lateral three and half digits. Finally, common palmar digital nerves and proper palmar (digital) nerves run on both sides of the fingers along the arteries until the finger tips. Motor innervation of extrinsic and intrinsic hand muscles and their origin, insertion and function are shown in Tables 2.1 and 2.2.

Table 2.1 Extrinsic hand muscles

Muscle	Origin	Insertion	Function	Innervation
Flexor carpi radialis	Medial epicondyle, fascia antebrachii	Base of the second metacarpal bone	Elbow: flexion, pronation Wrist: radial abduction, palmar flexion	Median nerve
Flexor carpi ulnaris	Medial epicondyle, medial part of the olecranon	Hamate, the tendon also includes the pisiform as a sesamoid bone, basis of the fifth metacarpal bone	Elbow: flexion Wrist: ulnar abduction, palmar flexion	Muscular branches of the ulnar nerve
Palmaris longus	Medial epicondyle	Palmar aponeurosis	Ensure firm hand grip	Median nerve
Flexor digitorum superficialis	Medial epicondyle, tendinous arc between coronoid process of ulna and radius	Second to fifth middle phalanx	Second to fifth fingers: flexion	Median nerve
Flexor pollicis longus	Palmar part of the radius	Thumb distal phalanx	Thumb flexion	Median nerve
Flexor digitorum profundus	Ulnar tuberosity and interosseous membrane	Distal phalanx of the second to fifth fingers	Second to fifth fingers: flexion	Median (second and third fingers) and ulnar nerve (fourth and fifth fingers)
Pronator quadratus	Medial part of the distal ulna	Lateral and palmar part of the distal radius	Lower arm pronation	Median nerve
Brachioradialis	Above the lateral epicondyle of the humerus	Styloid process of radius	Elbow: flexion Lower arm: pronation Joint stabilizator	Radial nerve
Extensor carpi radialis longus	Above the lateral epicondyle of the humerus	Dorsal part of the base of the second metacarpal	Wrist: dorsal flexion, radial abduction	Radial nerve
Extensor carpi radialis brevis	Lateral epicondyle of the humerus	Dorsal part of the base of the third metacarpal	Wrist: dorsal flexion	Radial nerve

(continued)

Table 2.1 (continued)

Muscle	Origin	Insertion	Function	Innervation
Extensor digitorum	Lateral epicondyle of the humerus and dorsal forearm fascia	Second to fifth middle and distal phalanx	Finger extensor	Radial nerve
Extensor digitorum minimi	Lateral epicondyle of the humerus	Fifth extensor tendon	Fifth finger extensor	Radial nerve
Extensor carpi ulnaris	Lateral epicondyle of humerus, superficial forearm fascia	Dorsal part of the base of the fifth metacarpal	Wrist: dorsal flexion, ulnar abduction	Radial nerve
Abductor pollicis longus	Middle part of the ulna, radius and interosseous membrane	Base of the first metacarpal	Abduction of the thumb	Radial nerve
Extensor pollicis brevis	Ulna, interosseous membrane and dorsal part of the radius	Base of the proximal phalanx of the thumb	Thumb extensor and abductor	Radial nerve
Extensor pollicis longus	Middle part of the ulna and interosseous membrane	Base of the distal phalanx of the thumb	Thumb extensor and abductor	Radial nerve
Extensor indicis	Distal part of the ulna	Second extensor tendon	Second finger extensor	Radial nerve

Table 2.2 Intrinsic hand muscles

Muscle	Origin	Insertion	Function	Innervation
Palmaris brevis	Flexor retinaculum and from the palmar aponeurosis	Skin of the hypothenar	Keeping skin stretched out, improving grip	Superficial branch of the ulnar nerve
Abductor pollicis brevis	Transverse carpal ligament/tubercle of the scaphoid and tubercle of the trapezium	Lateral side of the base of the proximal phalanx of the thumb and the capsule of the metacarpophalangeal joint	Abduction of the thumb and assists in opposition and extension of the thumb	Recurrent branch of the median nerve
Opponens pollicis	Transverse carpal ligament and trapezium	Radial side of the first metacarpal bone	Opposition of the thumb and flexion of the thumb	Median nerve

Table 2.2 (continued)

Muscle	Origin	Insertion	Function	Innervation
Flexor pollicis brevis	Flexor retinaculum, trapezium	Proximal phalanx of the thumb	Flexion of the thumb	Superficial head of the muscle: recurrent branch of the median nerve Deep head of the muscle: deep branch of the ulnar nerve
Adductor pollicis	Anterior part of the third metacarpal bone (transverse head of the muscle) Bases of the second and the third metacarpal bones, trapezoid and capitate (oblique head of the muscle)	Medial part of the proximal phalanx of the thumb and the ulnar sesamoid	Adductor of thumb	Deep branch of the ulnar nerve
Abductor digiti minimi	Flexor retinaculum, pisiform and pisohamate ligament	Base of the proximal phalanx of the fifth finger	Abduction of fifth finger	Deep branch of the ulnar nerve
Flexor digiti minimi	Hamate	The base of the proximal phalanx of the fifth finger	Flexor of the fifth finger	Deep branch of the ulnar nerve
Opponens digiti minimi	Flexor retinaculum and hook of the hamate	Medial part of the fifth metacarpal bone	Opposition of fifth finger, fifth finger rotator	Deep branch of the ulnar nerve
Lumbricals	Deep flexor digitorum tendon	Extensor expansion	Flexion of MCP joints and extension of PIP joints	Third and fourth: deep branch of the ulnar nerve First and second: median nerve
Volar interossei	Side part of second, fourth and fifth metacarpal shaft	Bases of proximal phalanges of the second, fourth and fifth fingers and extensor expansions	Adduction, flexion and extension of fingers	Deep branch of the ulnar nerve
Dorsal interossei	Side part of the second to fifth metacarpal shaft	Proximal phalanges of the second to fourth fingers and extensor expansions	Abduction of fingers	Deep branch of the ulnar nerve

Cross-Sectional Anatomy

In order to better understand the topography of the anatomical structures, the hand can be examined from the three standard anatomical planes: coronal (Fig. 2.5), transverse (Figs. 2.10 through 2.18) and sagittal (Figs. 2.19 and 2.20).

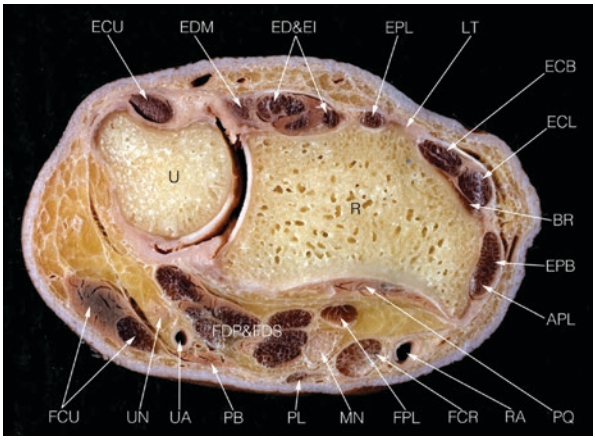

Fig. 2.10 Transverse section of wrist at the level of radius and ulna. Proximal view, left hand. *APL* abductor pollicis longus tendon, *BR* brachioradialis tendon, *ECB* extensor carpi radialis brevis tendon, *ECL* extensor carpi radialis longus tendon, *ECU* extensor carpi ulnaris tendon, *ED&EI* extensor digitorum and extensor indicis tendons, *EDM* extensor digiti minimi tendon, *EPB* extensor pollicis brevis tendon, *EPL* extensor pollicis longus tendon, *FCR* flexor carpi radialis tendon, *FCU* flexor carpi ulnaris muscle and tendon, *FDS&FDP* flexor digitorum superficialis tendons and flexor digitorum profundus tendons, *FPL* flexor pollicis longus tendon, *LT* Lister's tubercle, *MN* median nerve, *PB* palmaris brevis tendon, *PL* palmaris longus tendon, *PQ* pronator quadratus, *R* radius, *RA* radial artery, *U* ulna, *UA* ulnar artery, *UN* ulnar nerve

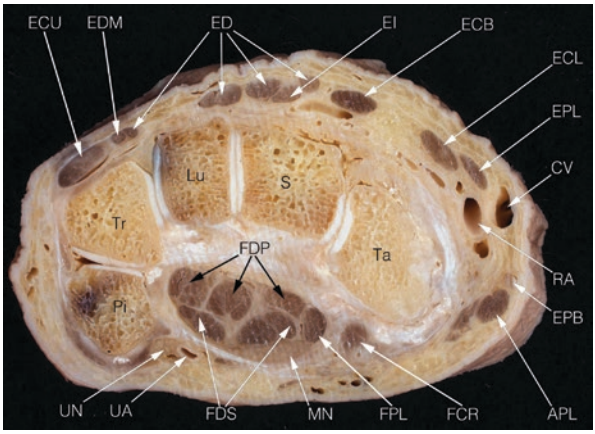

Fig. 2.11 Transverse section across the proximal carpal bones. Proximal view, left hand. *APL* abductor pollicis longus tendon, *CV* cephalic vein, *ECB* extensor carpi radialis brevis tendon, *ECL* extensor carpi radialis longus tendon, *ECU* extensor carpi ulnaris tendon, *ED* extensor digitorum tendons, *EDM* extensor digiti minimi tendon, *EI* extensor indicis tendon, *EPB* extensor pollicis brevis tendon, *EPL* extensor pollicis longus tendon, *FCR* flexor carpi radialis tendon, *FDP* flexor digitorum profundus tendons, *FDS* flexor digitorum superficialis tendons, *FPL* flexor pollicis longus tendon, *Lu* lunate, *MN* median nerve, *Pi* pisiform, *RA* radial artery, *S* scaphoid, *Ta* trapezium, *Tr* triquetrum, *UA* ulnar artery, *UN* ulnar nerve

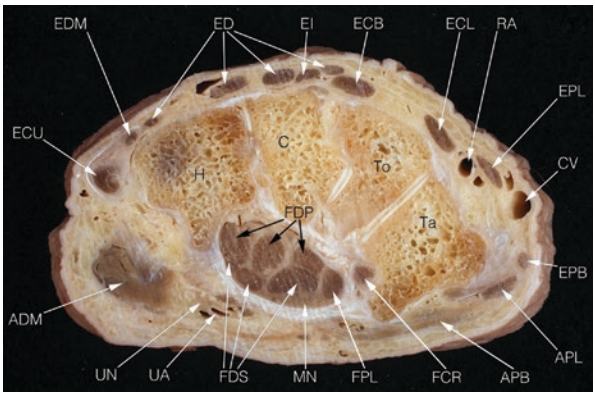

Fig. 2.12 Transverse section across the distal carpal bones. Proximal view, left hand. *ADM* abductor digiti minimi muscle, *APB* abductor pollicis brevis muscle, *APL* abductor pollicis longus tendon, *C* capitate, *CV* cephalic vein, *ECB* extensor carpi radialis brevis tendon, *ECL* extensor carpi radialis longus tendon, *ECU* extensor carpi ulnaris tendon, *ED* extensor digitorum tendons, *EDM* extensor digiti minimi tendon, *EI* extensor indicis tendon, *EPB* extensor pollicis brevis tendon, *EPL* extensor pollicis longus tendon, *FCR* flexor carpi radialis tendon, *FDP* flexor digitorum profundus tendons, *FDS* flexor digitorum superficialis tendons, *FPL* flexor pollicis longus tendon, *H* hamate, *MN* median nerve, *RA* radial artery, *Ta* trapezium, *To* trapezoid, *UA* ulnar artery, *UN* ulnar nerve

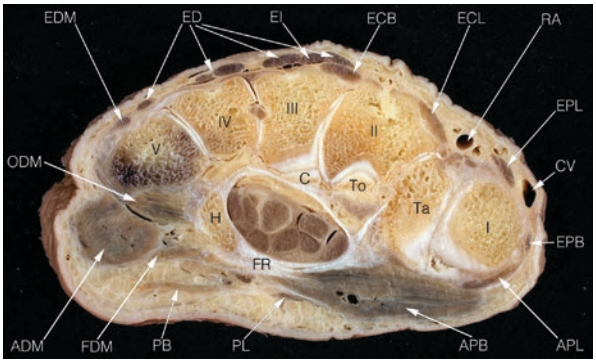

Fig. 2.13 Transverse section across the metacarpal bases. Proximal view, left hand. *ADM* abductor digiti minimi muscle, *APB* abductor pollicis brevis muscle, *APL* abductor pollicis longus tendon, *C* capitate, *CV* cephalic vein, *ECB* extensor carpi radialis brevis tendon, *ECL* extensor carpi radialis longus tendon, *ED* extensor digitorum tendons, *EDM* extensor digiti minimi tendon, *EI* extensor indicis tendon, *EPB* extensor pollicis brevis tendon, *EPL* extensor pollicis longus tendon, *FDM* flexor digiti minimi muscle, *FR* flexor retinaculum, *H* hamate, *I–V* first to fifth metacarpals, *ODM* opponens digiti minimi muscle, *PB* palmaris brevis muscle, *PL* palmaris longus tendon, *RA* radial artery, *Ta* trapezium, *To* trapezoid

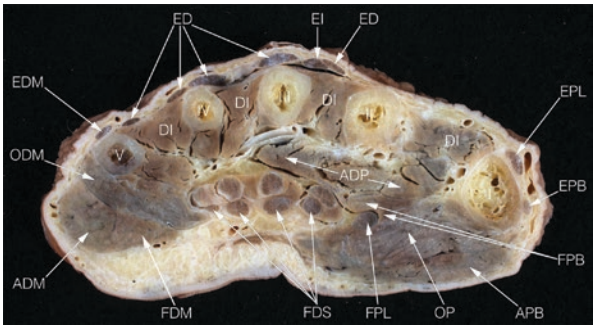

Fig. 2.14 Transverse section across the metacarpal bones. Proximal view, left hand. *ADM* abductor digiti minimi muscle, *ADP* adductor pollicis muscle, *APB* abductor pollicis brevis muscle, *DI* dorsal interosseous muscle, *ED* extensor digitorum tendons, *EDM* extensor digiti minimi tendon, *EI* extensor indicis tendon, *EPB* extensor pollicis brevis tendon, *EPL* extensor pollicis longus tendon, *FDM* flexor digiti minimi muscle, *FDS* flexor digitorum superficialis muscle, *FPB* flexor pollicis brevis muscle, *FPL* flexor pollicis longus muscle, *I–V* first to fifth metacarpals, *ODM* opponens digiti minimi muscle, *OP* opponens pollicis muscle

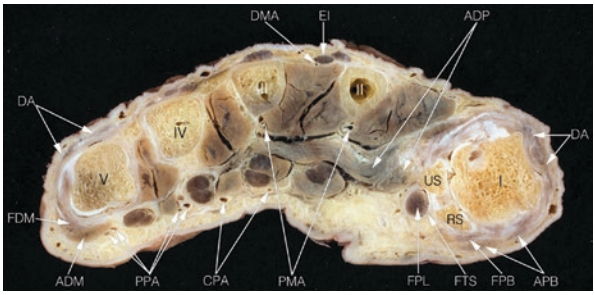

Fig. 2.15 Transverse section proximal to the metacarpal heads. Proximal view, left hand. *ADM* abductor digiti minimi muscle, *ADP* adductor pollicis muscle, *APB* abductor pollicis brevis muscle, *CPA* common palmar digital arteries, *DA* dorsal aponeurosis, *DMA* dorsal metacarpal artery, *EI* extensor indicis tendon, *FDM* flexor digiti minimi muscle, *FPB* flexor pollicis brevis muscle, *FPL* flexor pollicis longus muscle, *FTS* fibrous tendon sheath, *I–V* first to fifth metacarpals, *PMA* palmar metacarpal arteries, *PPA* proper palmar digital arteries, *RS* radial sesamoid of pollex, *US* ulnar sesamoid of the thumb

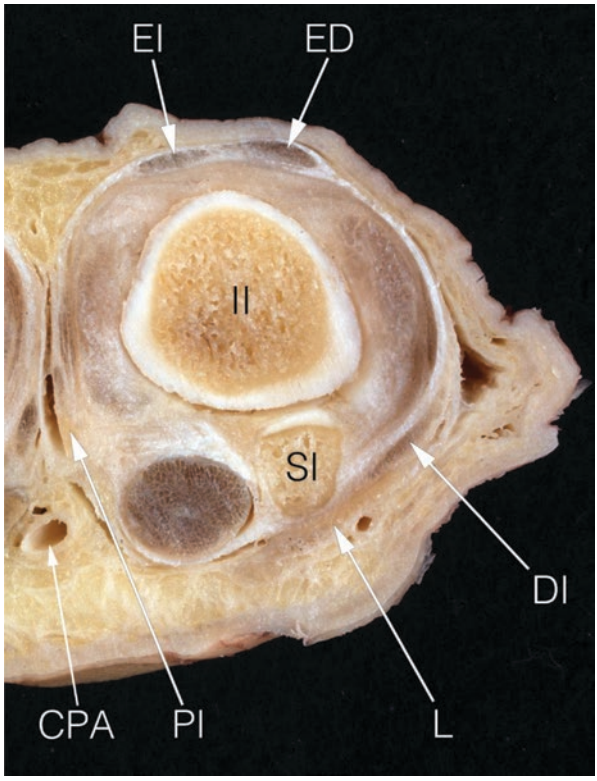

Fig. 2.16 Transverse section of the second finger (index) across the metacarpal head. *CPA* common palmar digital artery, *DI* dorsal interosseous tendon, *ED* extensor digitorum tendon, *EI* extensor indicis tendon, *II* second metacarpal bone (head), *L* lumbrical, *PI* palmar interosseous tendon, *SI* sesamoid bone of index

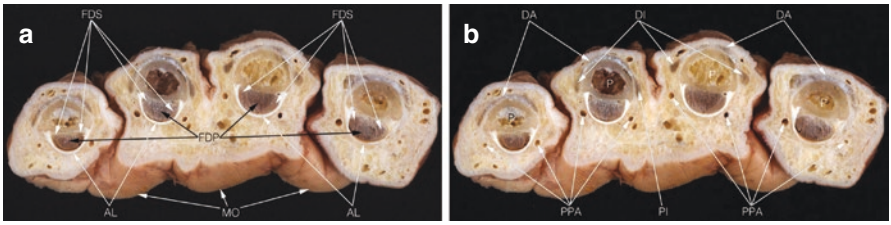

Fig. 2.17 Transverse section across the proximal phalanges at the level of crossing of the flexor digitorum tendons. (**a** and **b**) Same section; different structures indicated. *AL* annular ligament, *DA* dorsal aponeurosis, *DI* dorsal interosseous tendons, *FDP* flexor digitorum profundus tendons, *FDS* flexor digitorum superficialis tendons, *MO* monticuli, *P* proximal phalanges, *PI* palmar interosseous tendons, *PPA* proper palmar digital arteries

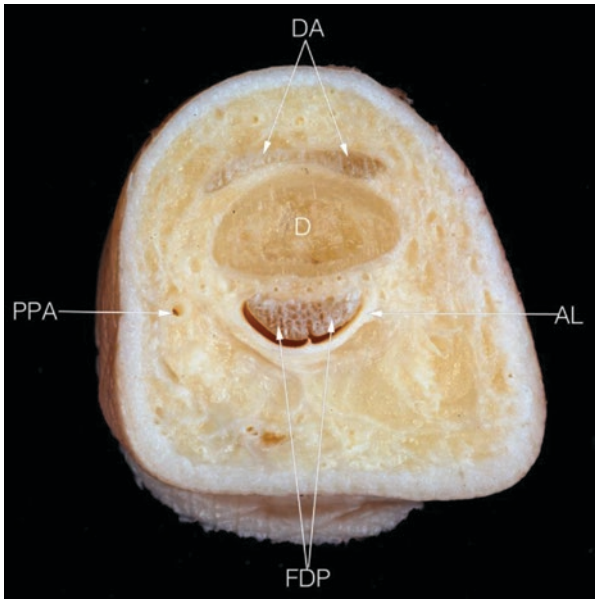

Fig. 2.18 Transverse section across the distal phalanx of the middle finger. *AL* annular ligament, *D* distal phalanx, *DA* dorsal aponeurosis, *FDP* flexor digitorum profundus tendon, *PPA* proper palmar digital artery

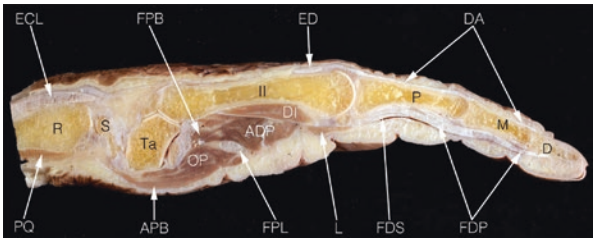

Fig. 2.19 Sagittal section across the second digital ray. *ADP* adductor pollicis muscle, *APB* abductor pollicis brevis muscle, *D* distal phalanx, *DA* dorsal aponeurosis, *ECL* extensor carpi radialis longus tendon, *ED* extensor digitorum tendon, *FDP* flexor digitorum profundus tendon, *FDS* flexor digitorum superficialis tendon, *FPB* flexor pollicis brevis muscle, *FPL* flexor pollicis longus tendon, *DI* dorsal interosseous muscle, *II* second metacarpal, *L* lumbrical, *M* middle phalanx, *OP* opponens pollicis muscle, *P* proximal phalanx, *PQ* pronator quadratus, *R* radius, *S* scaphoid, *Ta* trapezium

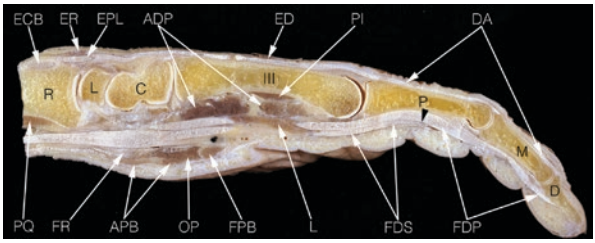

Fig. 2.20 Sagittal section across the third digital ray. *ADP* adductor pollicis brevis muscle, *APB* abductor pollicis brevis muscle, *C* capitate, *D* distal phalanx, *DA* dorsal aponeurosis, *ECB* extensor carpi radialis brevis tendon, *ED* extensor digitorum tendon, *EPL* extensor pollicis longus tendon, *ER* extensor retinaculum, *FDP* flexor digitorum profundus tendon, *FDS* flexor digitorum superficialis tendon, *FPB* flexor pollicis brevis muscle, *FR* flexor retinaculum, *III* third metacarpal, *L* lumbrical, *L* lunate, *M* middle phalanx, *OP* opponens pollicis muscle, *P* proximal phalanx, *PI* palmar interosseous muscle, *PQ* pronator quadratus, *R* radius, *arrowhead* crossing of the flexor digitorum tendons (chiasma)

Regional and Subregional Anatomy

Compartments, Canals, Channels, Cavities, Capsules and Connections

The "six Cs", namely, compartments, canals, channels, cavities, capsules and connections, are very important structures for rheumatologists. Commonly affected by pathological changes and lesions, they are essential landmarks for orientation for any imaging method and are key sites for anatomical variants.

Compartments

Compartments have two, different meanings in medicine, namely, fascial compartments and pharmacokinetic compartments. Examples of pharmacokinetic compartments include blood plasma, interstitial fluid, fatty tissue, intracellular fluid and transcellular fluid. Intraarticular joint fluid is a good example for what we call a transcellular fluid compartment.

Fascial compartments are anatomical structures surrounded by fascicules (connective tissue septa, intermuscular septa) that contain muscles, their blood supply and nerves. Bones can serve as the basis of a compartment, but they are not part of the compartment.

The hand is divided into five major fascial compartments: from radial to ulnar on the palmar side thenar, mesothenar (or central compartment) and hypothenar and on the dorsal side the interosseous compartments and the adductor compartment between the thenar and interosseous compartments (Table 2.3).

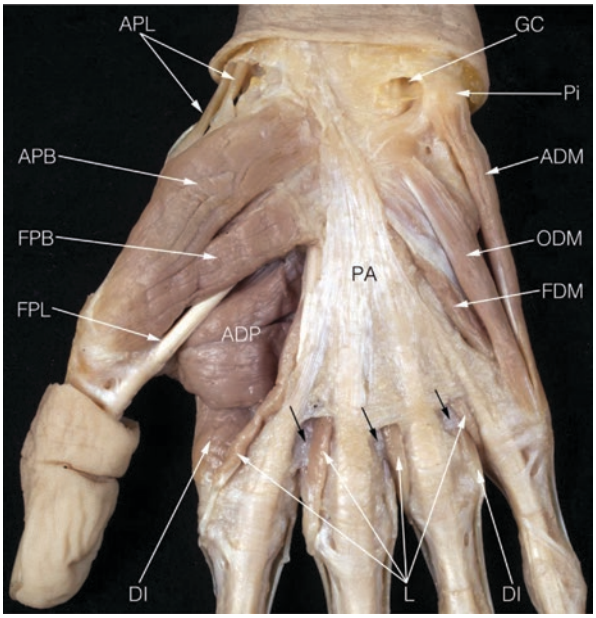

Fig. 2.21 Compartments of the hand. Muscles of thenar and hypothenar. Structures of mesothenar are covered by the palmar aponeurosis. *ADM* abductor digiti minimi muscle, *ADP* adductor pollicis muscle, *APB* abductor pollicis brevis muscle, *APL* abductor pollicis longus tendon, *DI* dorsal interosseous muscle, *FDM* flexor digiti minimi muscle, *FPB* flexor pollicis brevis muscle, *FPL* flexor pollicis longus tendon, *GC* Guyon's canal, *L* lumbricals, *ODM* opponens digiti minimi muscle, *PA* palmar aponeurosis, *Pi* pisiform, *black arrows* deep transverse metacarpal ligament

Table 2.3 Muscle contents of the fascial compartments

1. Thenar compartment: abductor pollicis brevis, flexor pollicis brevis and opponens pollicis muscles
2. Mesothenar (or central) compartment: lumbrical muscles and three palmar interossei (all unipennate)
3. Hypothenar compartment: abductor digiti minimi, opponens digiti minimi and flexor digiti minimi brevis muscles over the fascia of the palmaris brevis muscle (Fig. 2.21)
4. Interosseous compartment: four dorsal interossei (all of them bipennate)
5. Adductor compartment: adductor pollicis (caput obliquum and transversum)

Anatomical Snuffbox

Anatomical snuffbox (foveola radialis/fossa tabatiere) is not a compartment but a very important subregion of the hand. The radial border of the anatomical snuffbox is formed by the tendon sheath of the extensor pollicis brevis and the abductor pollicis longus muscles, while on its ulnar side, we find the extensor pollicis longus muscle. This causes the appearance of a radial and an ulnar cord-like eminence of the skin which is visible especially when the thumb is abducted and extended. Between these cords, we find a pit known as the snuffbox (where people put tobacco for snuffing). The radial artery runs through the floor of the snuffbox, then passes under the tendon of extensor pollicis longus and perforates the first dorsal interosseous muscle (Figs 2.7 and 2.22).

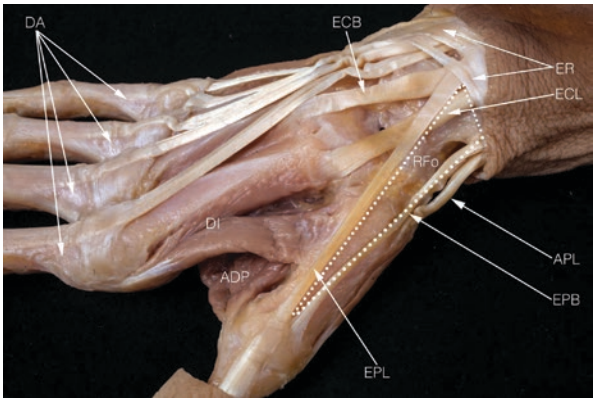

Fig. 2.22 Anatomical snuff box. *ADP* adductor pollicis muscle, *APL* abductor pollicis longus tendon, *DA* dorsal aponeurosis, *DI* dorsal interosseous muscle, *ECB* extensor carpi radialis brevis tendon, *ECL* extensor carpi radialis longus tendon, *EPB* extensor pollicis brevis tendon, *EPL* extensor pollicis longus tendon, *ER* extensor retinaculum, *RFo* anatomical snuff box (radial foveola)

Canals

The two most important canals of the hand are the carpal tunnel (canalis carpi) and Guyon's tunnel (canalis ulnaris). They are also called osteofibrous canals, which highlights the fact that the bottom and the sides are often paved by fibrocartilage and bony tissue easing the gliding of the sheathed flexor tendons in the canals.

Carpal Tunnel

This canal is situated on the palmar side of the wrist. Because it narrows from proximal to distal, its spatial shape resembles that of a truncated gullet. The bottom of the tunnel is formed by the carpal bones. The medial and lateral sides of the tunnel rest on four pillars: we find the pisiform on the medial side proximally and distally the hook of the hamate and laterally the tubercles of the scaphoid (proximally) and the trapezium (distally). The palmar side of the tunnel is covered by the slightly convex transverse carpal ligament, which is attached medially to the scaphoid and laterally to the pisiform. Outside of the tunnel, most laterally we find the tendon of the flexor carpi radialis muscle in its sheath lying in the bony sulcus of the scaphoid and the trapezium. Within the tunnel, in the most lateral position, we can identify the tendon of the flexor pollicis longus muscle which possesses its own tendon sheath. The median nerve is situated just directly under the retinaculum over the second and third superficial flexor tendons. Usually the median nerve is ellipsoid, but in some cases, it may be more rounded or triangular. There is one more common tendon sheath in the tunnel, that of the superficial and the deep common flexors of the fingers. The superficial tendons run superficial in the tunnel and form two rows. In the first row, we find the third and fourth tendons, while the second and the fifth tendons constitute the second row. At the entry of the carpal tunnel, the deep tendons envelop their respective superficial tendons (forming a U). Finally, as we exit the tunnel, the superficial and the deep tendons rearrange themselves, forming two rows, respectively, located in close proximity to the appropriate digits (Fig. 2.23).

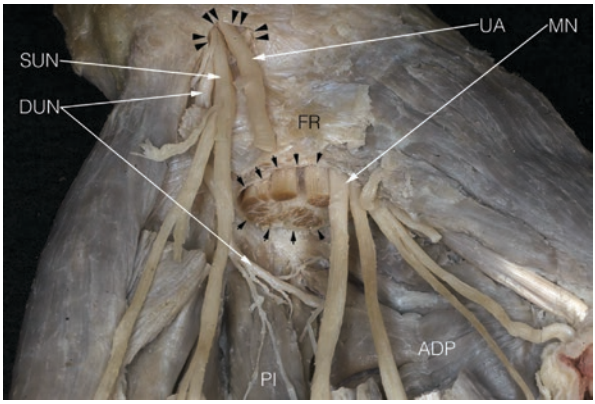

Fig. 2.23 Guyon's canal and carpal tunnel. Superficial and deep flexor digitorum tendons are cut. *ADP* adductor pollicis muscle, *DUN* deep branch of ulnar nerve, *FR* flexor retinaculum, *MN* median nerve, *PI* palmar interosseous muscle, *SUN* superficial branch of ulnar nerve, *UA* ulnar artery, *arrowheads* carpal tunnel, *doubled arrowheads* Guyon's canal

Guyon's Tunnel

The triangular Guyon canal is situated medially and more superficially than the carpal tunnel. A small ligament runs between the pisiform and the hamate (pisohamate ligament) bridging over the ulnar nerve. The medial border of the tunnel is the pisiform, the roof is the transverse carpal ligament, and the lateral border is formed by the hook of the hamate. The ulnar artery is positioned lateral to the ulnar nerve (Fig. 2.23).

The sensory and motor branches are usually divided into three zones. Zone 1 is situated before the ulnar nerve bifurcation (holding mixed motor and sensory branches), Zone 2 includes the deep motor branch, and Zone 3 includes the superficial sensory branch of the ulnar nerve.

Channels

Channels contain tendons with tendon sheaths or paratenon or tendons which are simply covered with loose connective tissue. The terms channels and compartments are used interchangeably.

Extensor Tendon Channels of the Wrist

The extensor tendons of the hand can be found under the extensor retinaculum on the dorsal surface of the wrist. The extensor retinaculum attaches medially to the distal part of the ulna and the medial carpal bones and laterally to distal part of the radius and the lateral carpal bones. The foundation of the channels is formed by the dorsal surface of the distal part of the radius and the ulna and the dorsal surface of the carpal bones. The six extensor channels are separated by septae, which originate from the extensor retinaculum. Starting radially, the first channel contains the tendons of the abductor pollicis longus and extensor pollicis brevis muscles sharing a single tendon sheath. In the second channel, we find the tendons of the extensor

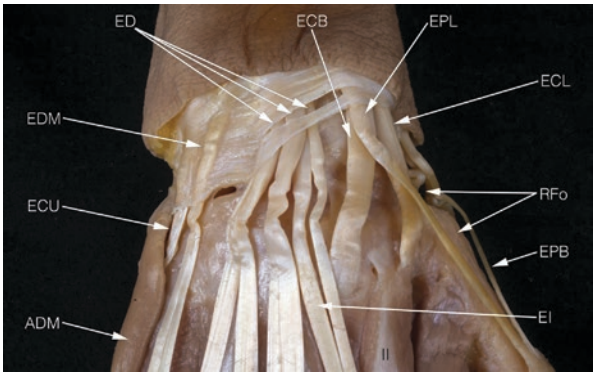

Fig. 2.24 Extensor tendon channels. *ADM* abductor digiti minimi muscle, *ECB* extensor carpi radialis brevis tendon, *ECL* extensor carpi radialis longus tendon, *ECU* extensor carpi ulnaris tendon, *ED* extensor digitorum tendons, *EDM* extensor digiti minimi tendon, *EI* extensor indicis tendon, *EPB* extensor pollicis brevis tendon, *EPL* extensor pollicis longus tendon, *II* second metacarpal, *RFo* anatomical snuff box (radial foveola)

carpi radialis longus and brevis muscles, situated in their common tendon sheath, while in the third channel, the tendon of the extensor pollicis longus muscle can be found in its own sheath. In the fourth channel, the tendons of extensor digitorum and of the indicis muscles run in a common tendon sheath. In the fifth channel, the tendon of the extensor digiti minimi muscle and in the sixth the tendon of the extensor carpi ulnaris muscle are situated in their respective tendon sheaths (Fig. 2.24). It helps to count the different tendons by starting medially (or radially) from the first channel or by remembering that Lister's tubercle separates the second from the third channel. Also, a simple mnemonic (longus, brevis, longus, brevis) starting from radial until the fourth channel may help in memorizing the muscles.

Finger Flexor Channels

The common tendon sheaths for the deep and superficial flexor tendons of the second, third, and fourth fingers run in separate channels beginning from the middle of the palm (Figs. 2.11, 2.12, and 2.13). Proximally of the carpal tunnel, the flexor tendon sheath of the thumb and of the fifth finger is usually continuous with the forearm. At the level of the proximal phalanx, the superficial flexor tendons split into two parts, and between them the deep flexor tendon emerges to become superficial (chiasma tendinum). The superficial flexor tendons insert onto the shaft of the middle phalanx and the deep flexor tendons attach to the distal phalanx.

On the outside the sheaths are fibrous, while on the inside they are similar to the synovial membrane of joints and also produce synovial fluid, partly ensuring smooth movement of the tendons and partly contributing to the nutrition of the tendons via the mesotenon (Fig. 2.25). The two parts of the tendon sheath may also be called the visceral (close to the tendon) and parietal (far from the tendon separated from the visceral layer by a layer of synovial fluid) part. Unlike the joint cavity or the hyaline cartilage found on bone endings, tendons also get their blood supply from the longitudinal artery on the dorsal surface of the tendon, which segmentally gives

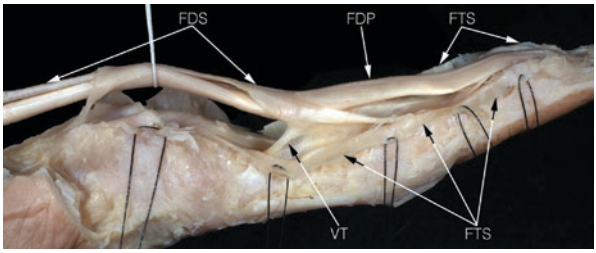

Fig. 2.25 Crossing and insertion of flexor digitorum tendons. *FDP* flexor digitorum profundus tendon, *FDS* flexor digitorum superficialis tendon, *FTS* fibrous tendon sheath, *VT* vinculum

branches to the tendon. Arising from the tendon sheath some small arteries also supply the tendon itself.

Connections

It is clear that on a microstructural level, all structures are connected to adjacent structures. Here we use the term connection to implicate soft-tissue structures whose main function is to connect (or surround) structures. Ligaments which connect bones were covered previously in the chapter.

Extensor Retinaculum

The main function of the extensor retinaculum is to keep the extensor tendons in place during the movement of the wrist and tendons and to ease the gliding of the tendons during extension. The extensor retinaculum attaches to the lateral margin of the radius and to the triquetrum and pisiform.

Connexus Intertendinei

Between the third and fourth and also between the fourth and fifth extensor digitorum tendons, connexus intertendinei can be seen proximally from the MCP joints. These connexi help harmonize the movement of extensor digitorum tendons and help to avoid the medial drift or slipping of the extensor tendon over the MCP joints (Fig. 2.26).

Extensor Hood

The extensor hood, also known as dorsal aponeurosis extends over the dorsal surface from the base of the proximal phalangeal bone until the distal phalangeal bone and conveys the traction of the tendons of the lumbricals, the interossei and the extensor digitorum and indicis tendons, thereby facilitating the extension of the PIP and the DIP joint. The central slip component of the extensor hood acts primarily on the PIPs, while the lateral bands act primarily on DIPs (Fig. 2.27).

Flexor Retinaculum

The flexor retinaculum forms the roof of the carpal tunnel as well as the floor of Guyon's tunnel. Located on the palmar side of the wrist, it attaches to the pisiform bone and to the hook of the hamate and on the radial side to the tubercle of scaphoid and to the trapezium. Palmaris longus and brevis are very superficial muscles lying

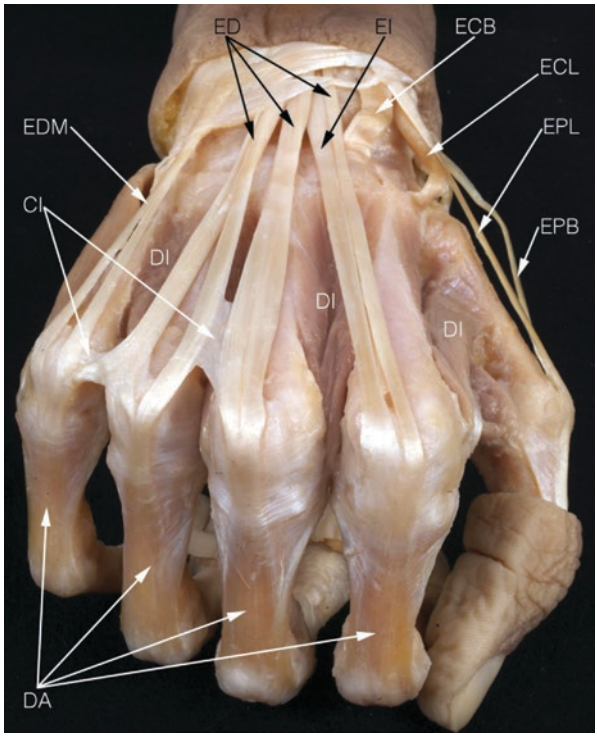

Fig. 2.26 Dorsal tendinous structures of the hand. *CI* connexus intertendinei, *DA* dorsal aponeurosis, *DI* dorsal interossei, *ECB* extensor carpi radialis brevis tendon, *ECL* extensor carpi radialis longus tendon, *ED* extensor digitorum tendons, *EDM* extensor digiti minimi tendon, *EI* extensor indicis tendon, *EPB* extensor pollicis brevis tendon, *EPL* extensor pollicis longus tendon

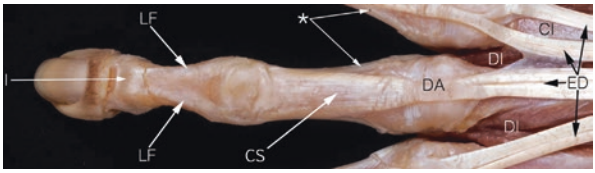

Fig. 2.27 Extensor hood of middle finger. *CI* connexus intertendinei, *DA* dorsal aponeurosis, *DI* dorsal interosseous muscles, *ED* extensor digitorum tendons, *I* insertion of the extensor hood, *LF* lateral fibres, *MF* medial fibres, *asterisks* insertion of dorsal interosseous muscle tendons

over this retinaculum. Many hand muscles originate from the flexor retinaculum and the transverse carpal ligament (Tables 2.1 and 2.2).

Pulleys

The pulley is a cuff-like, fibrous structure embracing the tendon sheath of flexor tendons. Annular pulleys are fixed to the palmar plates of the metacarpals (A1 pulley) or to the palmar plate of proximal interphalangeal joints (A3 pulley). Between them we find the A2 pulley located around the tendon over the proximal phalangeal shaft. The A5 pulley is located over the DIP joint, while the A4 is located between the A3 and the A5 pulleys over the midphalangeal shaft. Over other parts of the tendon sheath, we find the cross-like structures of the cruciate pulleys (C1-3) which are located between the annular pulleys (Fig. 2.28). When the finger is flexed, the

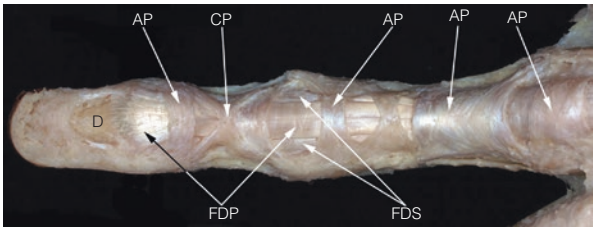

Fig. 2.28 Pulleys of the third finger. *AP* annular pulley, *CP* cruciate pulley, *D* distal phalanx, *FDP* flexor digitorum profundus tendon, *FDS* flexor digitorum superficialis tendon

rigid annular pulleys move closer to each other, while the softer parts of the fibrous sheath bunch up as we can see when flexing the finger. Annular pulleys prevent the bowstringing of the flexor tendons while cruciate pulleys prevent the sheath from collapsing and expanding during the movement of the fingers. The thumb also has an oblique pulley between the A1 and A2 annular pulleys. The flexor tendon sheaths contain both the deep and superficial flexor tendon.

Cavities and Capsules

Wrist (Distal Radioulnar, Radiocarpal, Ulnocarpal and Midcarpal Joint)

The wrist is a relatively loose, mobile, instable joint, with a system of strong stabilizing ligaments. The joint cavities of the wrist are surrounded by the joint capsule, that is strengthened by ligaments. The wrist consists of four different joints: the distal radioulnar joint, the radiocarpal joint, the ulnocarpal joint – with the articular disc located between the ulnar styloid and the lunate and triquetrum – and the midcarpal joint. These joint frequently communicate with each other and furthermore may communicate with the pisiform-triquetral cavity, the common carpometacarpal cavity, the first carpometacarpal cavity and with the intermetacarpal cavities as well. In the distal radioulnar joint the main synovial recess is the sacciform recess. The ulnocarpal joint has a recess known as the prestyloid recess which sometimes communicates with the pisotriquetral joint and its recess. The radiocarpal joint has a palmar and a more relaxed dorsal joint recess and may communicate with the space of Poirier, a central weak area of the wrist in the floor of the carpal tunnel. Between the proximal and distal row of carpal bones, there lies the well-defined but nearly fully immobile intercarpal joint, which communicates with the carpometacarpal joints. Strong interosseal, palmar and dorsal ligaments are strengthening the carpus. The carpometacarpal joints are also nearly immobile joints. There are strong ligaments between the carpal bones and the bases of the metacarpals both on the palmar and dorsal side. The midcarpal joint has one dorsal recess over the capitate. Certain terms are used specifically within the clinical context, for example, the triscaphe joint which is a shared joint between the scaphoid, trapezium and trapezoid bones in the wrist. This joint is also known as the scaphotrapeziotrapezoid (STT) joint.

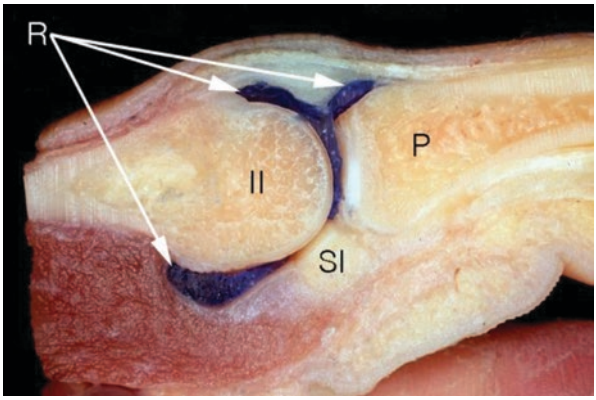

Fig. 2.29 Sagittal section of second metacarpophalangeal joint. *II* second metacarpal head, *P* proximal phalanx, *R* joint recesses, *SI* sesamoid bone of index finger

The first carpometacarpal joint is a very mobile saddle joint between the trapezium and the base of the first metacarpal bone. The capsule of this joint is ample; there are no strengthening ligaments which results in a relatively free range of movement required for gripping.

The second to fifth metacarpophalangeal joints are limited in their range of motion. The spherical head of the metacarpal bones is flattened on both sides. The joint capsules are ample, especially dorsally. Dorsal proximal, palmar proximal and phalangeal base recesses are the most important joint cavity enlargements (Fig. 2.29). The extensor tendon is fixed to the palmar plate by ligaments preventing the dislocation of the tendon. The palmar plate is a fibrocartilaginous plate for fixation of the flexor tendon sheath. Each plate is connected to the neighbouring plates by strong ligaments. This causes, for example, the passive flexion of the fourth digit upon active flexion of the third digit. The MCP joint can be slightly hyperextended, abducted and adducted; adjacent fingers can also be crossed. In the flexed position, both abduction and adduction are impossible due to the tightening of the collateral ligament. The interphalangeal joints are ginglymus joints allowing only flexion and extension. The collateral ligaments of the interphalangeal joints are also very tight.

References

1. Boutry N, Lardé A, Demondion X, Cortet B, Cotten H, Cotten A. Metacarpophalangeal joints at US in asymptomatic volunteers and cadaveric specimens. Radiology. 2004;232:716–24.
2. Roy J, Henry BM, PĘkala PA, Vikse J, Saganiak K, Walocha JA, Tomaszewski KA. Median and ulnar nerve anastomoses in the upper limb: a meta-analysis. Muscle Nerve. 2016;54:36–47.

Imaging Anatomy: Conventional Radiography

3

Janos Gyebnar, Gyorgy Gulacsi, Gabriela M. Supp, Peter Vince Balint, and Peter Mandl

Conventional Radiography: Diagnostic Imaging of the Skeletal System

If we irradiate the human body with X-rays and place an X-ray detector behind it, we acquire a shadow image corresponding to the location of different tissues, which make up the body and absorb X-rays to different degrees. The bone absorbs X-ray at a considerably higher degree as compared to cartilage or surrounding soft tissue because of its higher calcium content; thus, it appears as radiodense or radiopaque compared to its more radiolucent surroundings [1]. The two types of bone tissue compact or cortical bone and trabecular or cancellous bone are also characterized by different absorption properties, which is favorable for producing contrast images [2].

J. Gyebnar, MD (✉)
Radiology Department, National Institute of Rheumatology and Physiotherapy, Budapest, Hungary

G. Gulacsi, MD
Semmelweis University, Doctoral School of Clinical Medicine, Budapest, Hungary

G. M. Supp, MA · P. Mandl, MD, PhD
Division of Rheumatology, Department of Internal Medicine III, Medical University of Vienna, Vienna, Austria
e-mail: gabriela.supp@meduniwien.ac.at; peter.mandl@meduniwien.ac.at

P. V. Balint, MD, PhD, FRCP
3rd Rheumatology Department, National Institute of Rheumatology and Physiotherapy, Budapest, Hungary

P. V. Balint, P. Mandl (eds.), *Ultrasonography of the Hand in Rheumatology*,
https://doi.org/10.1007/978-3-319-74207-6_3

Bone on Conventional Radiography

Cortical bone appears as a homogenous, intensive band, which in long bones is thicker at the diaphysis and thinner at the metaphysis. Only a thin band of thick cortical bone covers the epiphysis. Cancellous or spongy bone is composed of the highly structured three-dimensional network of bone trabeculae. The bone is covered by a radiolucent periosteum, which, similarly to ligaments, capsule, and hyaline cartilage is not depicted on X-ray. As this also includes hyaline cartilage coating the epiphysis, the radiographic joint space always appears wider than its anatomical counterpart.

Under physiological conditions, the production of new bone and the resorption of old bone occur simultaneously in a series of complex metabolic interactions. In the first four decades of life, bone formation dominates, with bone resorption becoming dominant thereafter leading to an overall decrease in bone mass. This process affects cancellous bone to a greater degree, since its total area is much larger than that of cortical bone. Change in bone mass is a relatively slow process, with radiographic changes occurring only later in the disease – with the exception of traumatic abnormalities. The shape, size, and contour of bones as well as joint space width, along with pathological changes such as diffuse or focal bone loss can be readily assessed on conventional radiography [2].

Normal Variations

One of the most difficult things in radiology is ascertaining a normal finding [3]. There are countless anatomical variations that can have no or minimal pathological consequences. Differentiating such variations is important because they should not be mistaken for treating the patient's complaints. Often the combination of multiple pathological signs and individual anamnestic data can help establish the accurate diagnosis. Therefore, our most important task is the recognition of alterations and their value in the differential diagnostic process. In assessing pathological differences, it is often necessary to perform comparative radiographs. A standard radiograph is generally used to answer the following questions [2]:

- Can we identify an abnormality?
- Is the process acute or chronic?
- If it pertains to joints, is it mono-, oligo-, or polyarticular?
- Are both sides or both limbs affected?
- If both limbs are affected, are the abnormalities symmetrical?
- Are all joints affected or do the abnormalities occur in selected locations?

Radiographic Technique

When performing conventional radiography examination of the hand, several views may be acquired. During conventional radiography, a two-dimensional summation image is acquired from a three-dimensional object. This results in radially aligned

structures appearing superimposed on each other, which may therefore hinder the appropriate assessment and interpretation of morphological changes. Precise evaluation often requires different views, acquired from two or more directions. Typically, for long bones, two perpendicular projections are sufficient; however, in case of more complicated bony structures, it may be necessary to acquire a series of views from several directions [4].

Commonly Used Views

Posteroanterior (PA) View

The posteroanterior projection is the standard view in diagnostic imaging in rheumatology. They can be acquired from a single hand or from both hands to serve as comparison (Figs. 3.1 and 3.2). Whenever feasible, it is highly recommended to acquire images of each hand separately to ensure precision, in particular with regard to follow-up examinations.

Positioning: The patient places both or preferably a single hand on the detector, palm facing down, with the elbow flexed at 90°. The central beam is vertical; the X-ray tube is positioned over the examination table. Source to image-receptor distance (SID) is 100 cm. When projecting a single hand, the beam is centered on the head of the third metacarpal bone. The use of a grid is not necessary.

Requirements: One or both hands are positioned with no rotation. Metacarpophalangeal and interphalangeal joints are extended. The distal ends of the radius and the ulna are positioned with no rotation. The fifth digit is positioned with no rotation as evidenced by the symmetrical appearance of the concavities of the phalanges. Interphalangeal and metacarpophalangeal joint spaces

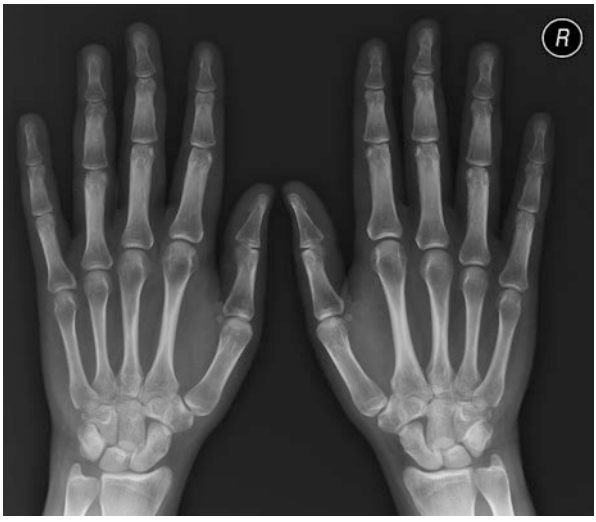

Fig. 3.1 Posteroanterior view of both hands

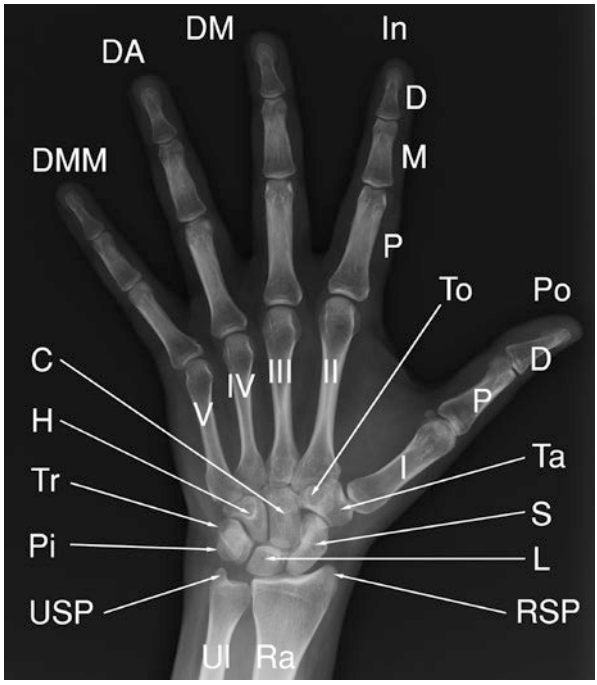

Fig. 3.2 Posteroanterior view of the left hand. *C* capitate, *D* distal phalanx, *DA* ring finger, *DM* middle finger, *DMM* little finger, *H* hamate, *In* index finger, *I–V* first to fifth metacarpals, *L* lunate, *M* middle phalanx, *P* proximal phalanx, *Pi* pisiform, *Po* thumb, *Ra* radius, *RSP* radial styloid process, *S* scaphoid, *Ta* trapezium, *To* trapezoid, *Tr* triquetrum, *Ul* ulna, *USP* ulnar styloid process

of the second to fifth digit appear open. The concavity of the metacarpal shafts is equal [5].

Nørgaard (Ball-Catcher) View

The ball catcher is a posterior oblique projection of both hands (Figs. 3.3 and 3.4). It is typically utilized together with the PA view in diagnostic imaging in rheumatology.

Positioning: Both hands are placed similarly as for the PA view, but in this case in supination, with the hands rotated 45° medial toward the patient. The central beam is vertical; the X-ray tube is positioned over the examination table. Source to image-receptor distance (SID) is 100 cm. The beam is centered on the MCP joints. The use of a grid is not necessary.

Requirements: There should be no superimposing of the midshafts of the metacarpals or of the phalangeal bases. The fingers are equal distance apart [5].

Fig. 3.3 Nørgaard view, both hands

Fig. 3.4 Nørgaard view, single hand, left. *C* capitate, *H* hamate, *L* lunate, *Pi* pisiform, *S* scaphoid, *Tr* triquetrum, *Ta* trapezium, *To* trapezoid, *Ra* radius, *Ul* ulna, *USP* ulnar styloid process, *RSP* radial styloid process, *Po* thumb, *In* index finger, *DM* middle finger, *DA* ring finger, *DMM* little finger, *I–V* first to fifth metacarpals, *P* proximal phalanx, *M* middle phalanx, *D* distal phalanx

Lateral View

This projection is typically acquired as a supplement to the PA view, to allow a more precise evaluation of the superimposed structures (Fig. 3.5). It is commonly used in traumatology but rarely in rheumatology.

Positioning: The entire upper extremity is positioned to be in plane with the film. The elbow is flexed at 90°. The hand is externally rotated by 90° and placed on its lateral edge; the second to fourth digits are closed lying on top of each other. The long axis of the hand and the lower arm are aligned to the long axis of the cassette. The thumb lies parallel to the detector. The direction of the beam is vertical; the X-ray tube is positioned over the examination table. The focus distance is 100 cm. The tube is aimed on the central area of the detector at the level of the MCP joints. The use of a grid is not necessary.

Requirements: The metacarpals and carpal bones as well as the distal ends of the radius and the ulna are superimposed [5].

Fig. 3.5 Lateral view of the hand. *C* capitate, *H* hamate, *I–V* first to fifth metacarpals, *L* lunate, *Pi* pisiform, *Ra* radius, *S* scaphoid, *Ta* trapezium, *Tr* triquetrum, *Ul* ulna, *USP* ulnar styloid process

Oblique Posteroanterior View

This view, also known as the zither-player projection, is also used as an additional view to the posteroanterior projection. The carpal and metacarpal bones, the phalanxes, and the distal radioulnar joint can be visualized from another direction but with less superimposition than the lateral view (Fig. 3.6).

Positioning: The patient puts his hand to the detector in a rotated position (45°). The lateral side of the fifht finger's lateral side should be in contact with the detector, with the fingers directed towards the detector. The fingers should be spread to avoid superimposing. The central beam is vertical; the X-ray tube is positioned over the examination table. SID is 100 cm. The beam is centered on the fifth MCP joint. The use of a grid is not necessary.

Requirements: There should be no superimposing of the midshafts of the third to fifth metacarpals or of the second to third metacarpal heads. The third to fifth metacarpal heads are slightly overlapped [5].

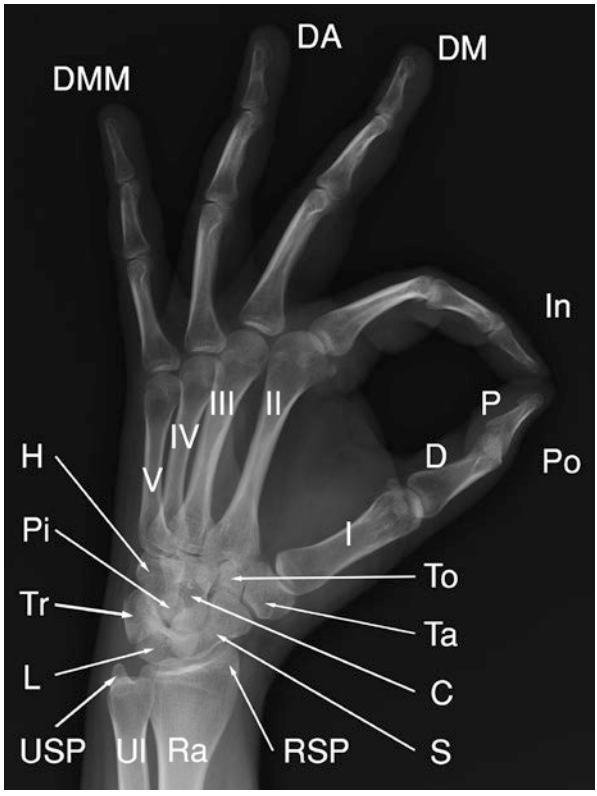

Fig. 3.6 Oblique posteroanterior view. *C* capitate, *D* distal phalanx, *DA* ring finger, *DM* middle finger, *DMM* little finger, *H* hamate, *In* index finger, *I–V* first to fifth metacarpals, *L* lunate, *M* middle phalanx, *P* proximal phalanx, *Pi* pisiform, *Po* thumb, *Ra* radius, *RSP* radial styloid process, *S* scaphoid, *Ta* trapezium, *To* trapezoid, *Tr* triquetrum, *Ul* ulna, *USP* ulnar styloid process

Carpal Tunnel View

On this view, the bony wall and shape of the tunnel can be evaluated, along with its relation to other structures and any morphological differences. It is a rarely used projection, with only a few indications.

Positioning: The cassette is placed level with the edge of the tabletop. The palm of the hand is pressed against the cassette, with the wrist joint dorsiflexed to approximately 135°. The fingers are curled around under the table to assist in immobilization. The vertical central ray is centered between the pisiform and the hook of the hamate medially and the tubercle of the scaphoid and the ridge of the trapezium laterally.

Requirements: The carpal bones must form an arc or tunnel. The pisiform is positioned with no or only minimal superimposing. The hook of the hamate, the scaphoid tuberosity, and the trapezium should form a palmar surface. The trapezium, capitate, and triquetrum should be well recognizable (Fig. 3.7) [5].

Two-View Series of the Wrist or Finger

In diagnostic imaging in rheumatology, the two-view series of the wrist is rarely used; the bones forming the wrist are commonly evaluated on hand views. Finger series are also rarely used for similar reasons. Targeted views of the fingers or wrist are acquired similar to the hand views, with the positioning modified to focus on the given region (Fig. 3.8).

Radiography in Rheumatic Diseases

Figures 3.9–3.14 demonstrate characteristic radiographic findings in common rheumatic diseases.

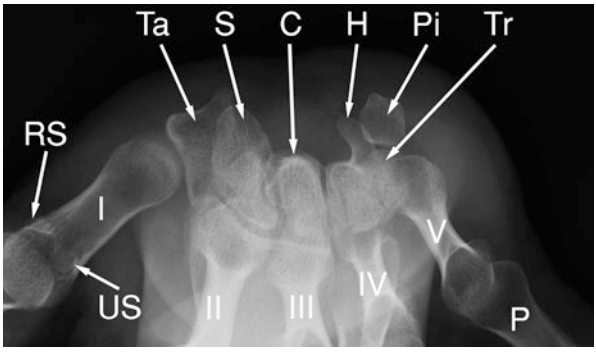

Fig. 3.7 Carpal tunnel view. *C* capitate, *H* hamate, *I–V* first to fifth metacarpals, *P* proximal phalanx, *Pi* pisiform, *RS* radial sesamoid of the thumb, *S* scaphoid, *Ta* trapezium, *Tr* triquetrum, *US* ulnar sesamoid of the thumb

Fig. 3.8 Two-view series of the II. *digit. II* second metacarpal bone, *D* distal phalanx, *M* middle phalanx, *P* proximal phalanx

Fig. 3.9 Early rheumatoid arthritis. Erosion on the base of the left third middle phalanx as well as the head of the right second to fourth proximal phalanges

Fig. 3.10 Psoriatic arthritis. Erosion of the head of the ulna, the scaphoid, and the hamate; pencil-in-cup deformity involving the distal interphalangeal joint of the third digit; joint space narrowing of the proximal interphalangeal joint of the third digit; subluxation of the distal interphalangeal joints of the second, fourth, and fifth digits; periosteal new bone formation evident in the fourth proximal interphalangeal joint

Fig. 3.11 Hand osteoarthritis. Bouchard and Heberden nodes of the proximal and distal interphalangeal joints, respectively, evident on the first to fifth digits bilaterally

Fig. 3.12 Osteoarthritis of the first carpometacarpal joint

Fig. 3.13 Chronic gout. Punched-out erosions of the third distal interphalangeal joint

Fig. 3.14 Chondrocalcinosis in calcium pyrophosphate deposition disease. Crystal deposits evident in both triangular fibrocartilage complexes as well as in the second to third right metacarpophalangeal joints bilaterally

Advantages and Disadvantages of Conventional Radiography as Compared to Sonography

As opposed to ultrasound, which allows the sonographer to assess the contours of bones which are more or less parallel to the transducer, conventional radiography allows the evaluation of the entire skeletal system, including cortical bone, joint surfaces, as well the internal structure of bones. The marked difference in acoustic impedance between bone and soft tissue leads to the almost complete reflection of

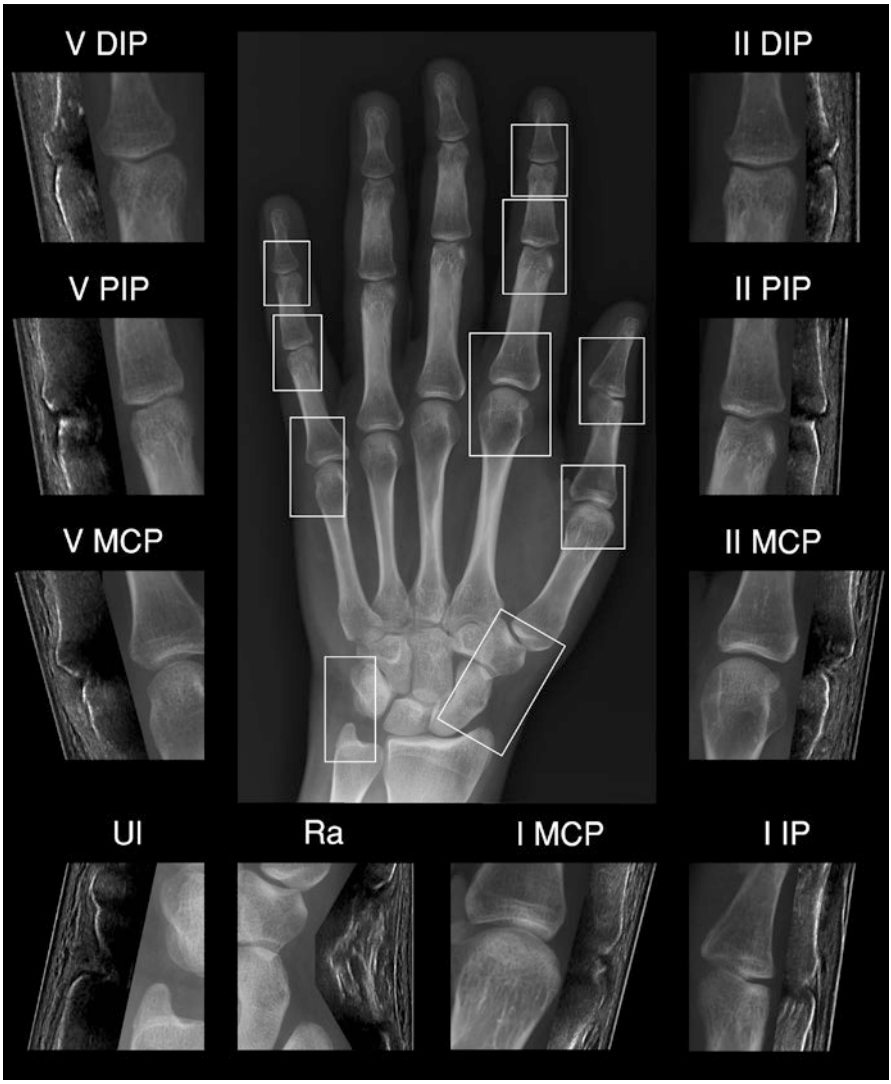

Fig. 3.15 Imaging of ultrasound and conventional radiography: comparing the anatomy. *I-V* first to fifth digit, *DIP* distal interphalangeal joint, *MCP* metacarpophalangeal joint, *IP* interphalangeal joint, *PIP* proximal interphalangeal joint, *Ra* radial, *Ul* ulnar

the ultrasound wave from the soft tissue-bone border, preventing the evaluation of the inner structure of bone. Furthermore, while providing a very detailed image of a limited area, the application of ultrasound as a tool for an overall evaluation remains limited [6].

The most important disadvantage of conventional radiography is exposure to radiation. While this radiation is relatively low for extremity imaging, care must

nevertheless taken to follow the ALARA (As Low As Reasonably Achievable) principle and perform X-ray examinations only when indicated [7]. The number of views should be restricted to the minimum required to form the appropriate diagnosis.

Additional disadvantages include the limited assessment and differentiation of depicted soft tissue structures. Soft tissue abnormalities can be evaluated solely as increases in the width of the respective structures. The targeted view of soft tissues is used solely for the localization of metallic foreign bodies. This is in stark contrast with the high diagnostic performance of ultrasound with regard to depicting abnormalities of superficial soft tissue structures, including tendons, ligaments, vessels, nerves, entheses, and muscles [6].

Comparison of Radiographic and Ultrasound Anatomy of the Hands

Comparative imaging enables the supplementation of ultrasound images with previously acquired CT, MRI, or PET/CT datasets. Similar to other already existing fusion techniques [8], such methods combine the "best of both worlds," i.e., detailed radiographic information on bone structure and margins with ultrasound's extraordinary capacity to image soft tissue changes (Figs. 3.15–3.29) [6, 9, 10].

Fig. 3.16 Fifth DIP joint. *M* middle phalanx, *D* distal phalanx

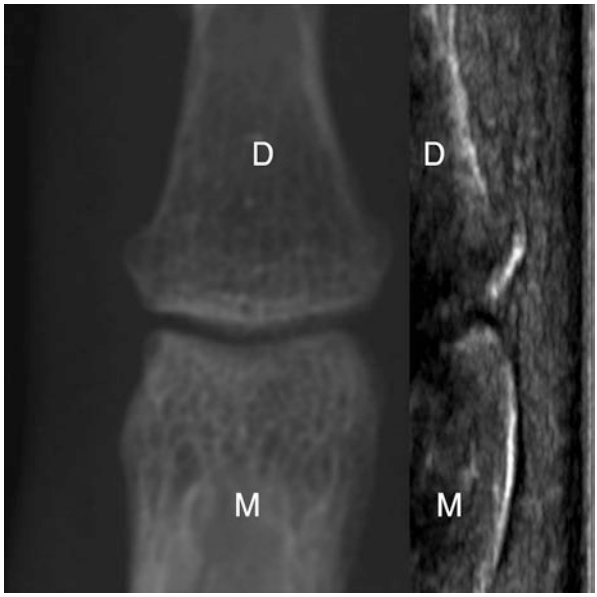

Fig. 3.17 Second DIP joint. *M* middle phalanx, *D* distal phalanx

Fig. 3.18 Fifth PIP joint. *P* proximal phalanx, *M* middle phalanx

Fig. 3.19 Second PIP joint. *P* proximal phalanx, *M* middle phalanx

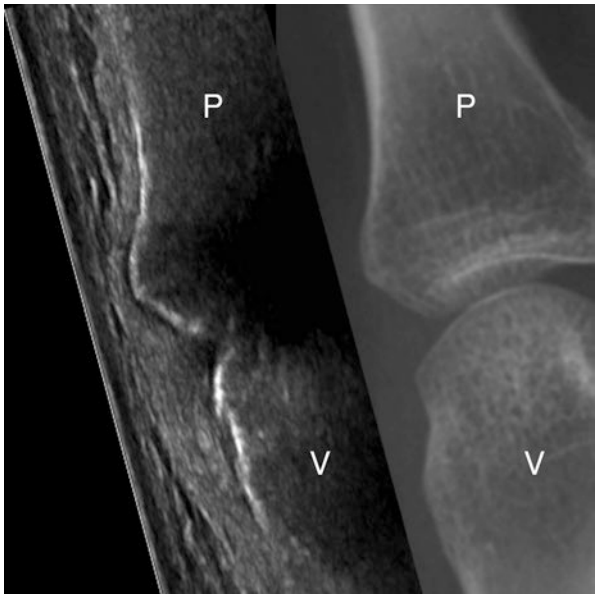

Fig. 3.20 Fifth MCP joint. *V* Fifth metacarpal bone, *P* proximal phalanx

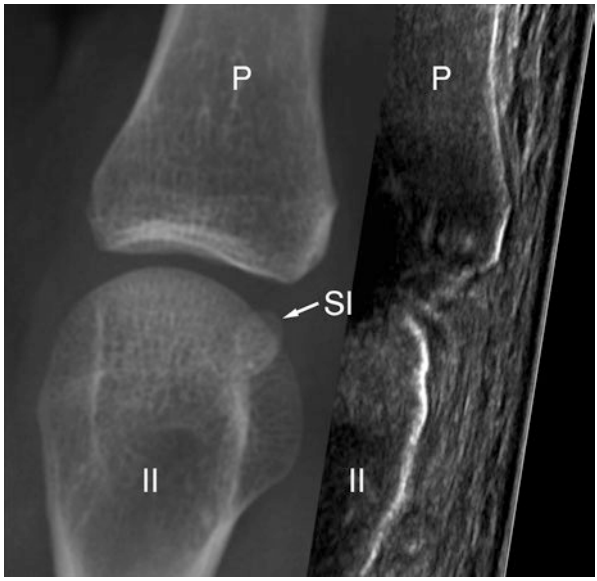

Fig. 3.21 Second MCP joint. *II* Second metacarpal bone, *SI* sesamoid bone of index finger, *P* proximal phalanx

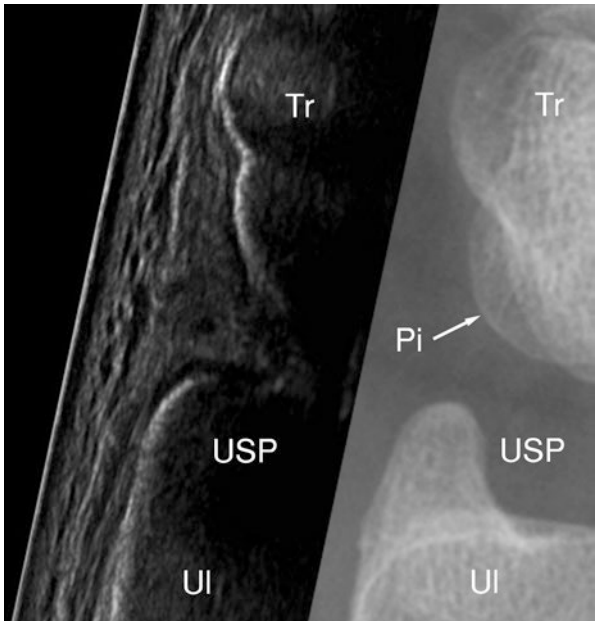

Fig. 3.22 Ulnar styloid process. *Ul* ulna, *USP* ulnar styloid process, *Pi* pisiform, *Tr* triquetrum

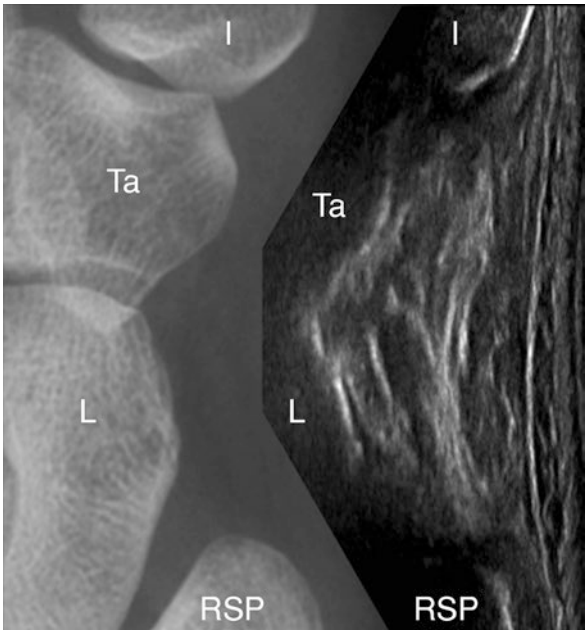

Fig. 3.23 Radial styloid process. *RSP* radial styloid process, *L* lunate, *Ta* trapezium, *I* first metacarpal bone

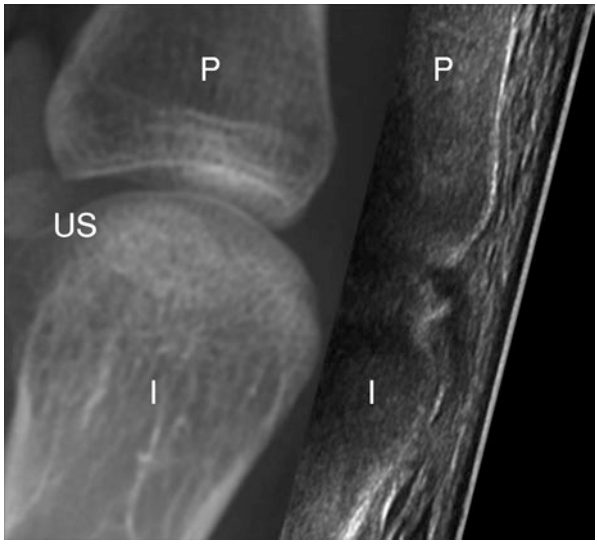

Fig. 3.24 First MCP joint. *I* First metacarpal bone, *US* ulnar sesamoid of the thumb, *P* proximal phalanx

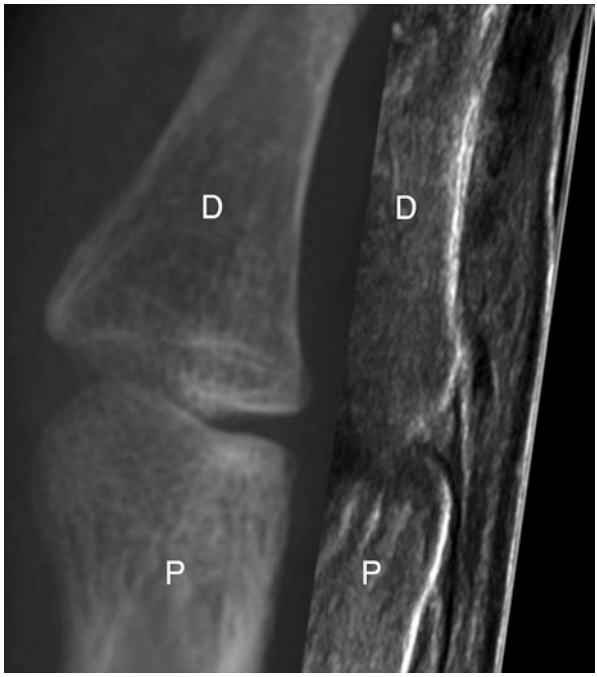

Fig. 3.25 First IP joint. *P* proximal phalanx, *D* distal phalanx

Fig. 3.26 Palmar side of the metacarpophalangeal, interphalangeal joints, and flexor tendons. *II* second metacarpal bone, *P* proximal phalanx, *M* middle phalanx, *D* distal phalanx, *FDP* flexor digitorum profundus tendon, *FDS* flexor digitorum superficialis tendon

Fig. 3.27 Palmar and dorsal panoramic ultrasound compared to X-ray of the index finger. *P* proximal phalanx, *M* middle phalanx, *D* distal phalanx

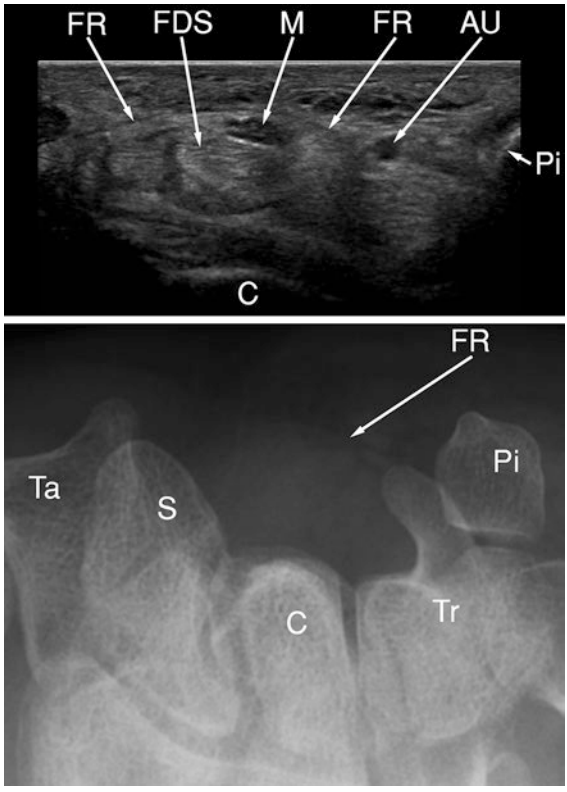

Fig. 3.28 Ultrasound and X-ray anatomy of the carpal tunnel. *C* capitate, *Pi* pisiform, *S* scaphoid, *Tr* triquetrum, *Ta* trapezium, *FR* flexor retinaculum, *FDS* flexor digitorum superficialis tendon, *M* median nerve, *AU* ulnar artery

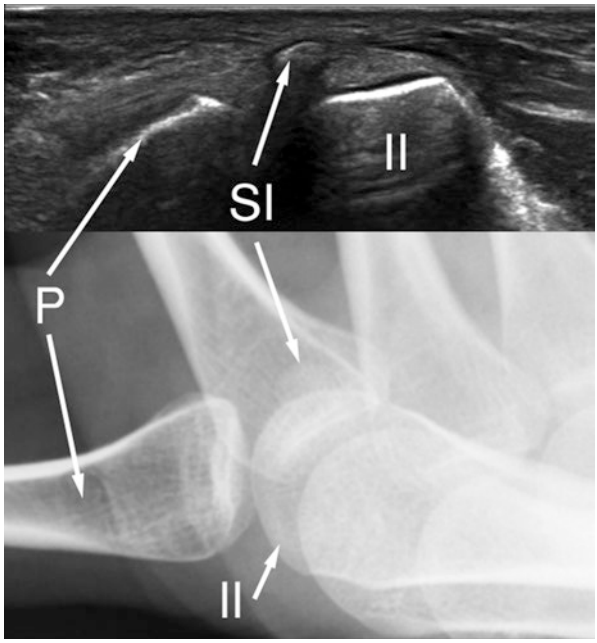

Fig. 3.29 Ultrasound and X-ray anatomy of the sesamoid bone of the index finger. *II* second metacarpal bone, *P* proximal phalanx, *SI* sesamoid bone of index finger

References

1. Isenberg DA, Renton P, editors. Imaging in rheumatology. 1st ed. Oxford: Oxford University Press; 2003.
2. McKinnis LN, editor. Fundamentals of musculoskeletal imaging. 3rd ed. Philadelphia: F. A. Davis Company; 2010.
3. Freyschmidt J, Brossmann J, Wiens J, Sternberg A. Koehler/Zimmer borderlands of normal and early pathological findings in skeletal radiography. 5th ed. Stuttgart: Thieme;2002.
4. Pope TL, Bloem HL, Beltran J, Morrison WB, Wilson DJ. Musculoskeletal imaging. 2nd ed. Philadelphia: Elsevier Health Sciences; 2014.
5. Whitley AS, Jefferson G, Holmes K, Sloane C, Anderson C, Hoadley G. Clark's positioning in radiography. 12th ed. London: Hodder Arnold Publication; 2005.
6. Martino F, Silvestri E, Grassi W, Garlaschi G, editors. Musculoskeletal sonography: technique, anatomy, semeiotics and pathological findings in rheumatic diseases. Mailand: Springer; 2007.
7. Uffmann M, Schaefer-Prokop C. Digital radiography: the balance between image quality and required radiation dose. Eur J Radiol. 2009;72:202–8.
8. Röntgen WC. Über eine neue Art von Strahlen. Sitzungsberichte der Physikalisch-medizinischen Gesellschaft zu Würzburg 1895;9:132–41.
9. O'Neill J, editor. Musculoskeletal ultrasound: anatomy and technique. New York: Springer; 2008.
10. Manaster BJ, editor. Diagnostic and surgical imaging anatomy: musculoskeletal. Philadelphia: Lippincott Williams & Wilkins; 2006.

4 Imaging Anatomy: Magnetic Resonance Imaging, Computed Tomography, Positron Emission Tomography and Other Novel Imaging Techniques

Franz Kainberger, Lena Hirtler, Hannes Platzgummer, Florian Huber, Janina Patsch, and Claudia Weidekamm

Imaging anatomy is strongly related to the workflow of reporting for planning the investigation and for the pattern analysis in image interpretation. In recent studies it was demonstrated that a clear, and in most cases, anatomically structured report yields more and better results than narrative reporting [1]. Recent trends are the indication-driven imaging workflow, the standardization of investigation techniques for the quantitative assessment of biomarkers and multimedia reports. For transmitting the often complex diagnostic information in arthritis, attempts have been made to display the anatomical distribution, the type and the severity of lesions graphically [2].

To what extent pathological lesions like synovial inflammation and erosions may be differentiated from normal anatomical structures or from changes seen in degenerative disease on magnetic resonance imaging (MRI) is still under discussion. By using the Rheumatoid Arthritis MRI Scoring System (RAMRIS), a high validity and clinical usefulness has been reported [3]. On the other hand, which anatomical structures or findings have to be assessed as normal or abnormal remains an open question. Indicators of synovial inflammation in the form of synovial thickening or enhancement after contrast media administration were reported in 21–69% [4–7]. For erosions or erosion-like anatomical variants, a rate between 2 and 47% has been reported in normal individuals [5, 8–11].

F. Kainberger, MD (✉) · H. Platzgummer, MD · F. Huber, MD · J. Patsch, MD, PhD.
C. Weidekamm, MD, MBA
Division of Neuro- and Musculoskeletal Radiology, Department of Biomedical Imaging and Image-Guided Therapy, Medical University of Vienna, Vienna, Austria
e-mail: franz.kainberger@meduniwien.ac.at

L. Hirtler, MA, MD, PhD
Division of Anatomy, Center for Anatomy and Cell Biology, Medical University of Vienna, Vienna, Austria

P. V. Balint, P. Mandl (eds.), *Ultrasonography of the Hand in Rheumatology*,
https://doi.org/10.1007/978-3-319-74207-6_4

Imaging Anatomy Embedded in the Diagnostic Workflow

The indication-driven workflow is a concept that aims to reduce the radiation exposure in patients by limiting the anatomical extent of the abnormalities to the minimal requirements [12]. Based on specified referrals, anatomical "regions of investigation" have been defined to smoothen the workflow and to yield optimal results. With MRI of the hand in arthritis, the documentation of both hands should be performed (Fig. 4.1) [13]. Regions of investigation are the hand as a whole, the wrist (sometimes with the metacarpus) and dedicated imaging of the thumb or groups of fingers. In case of suspected rheumatoid arthritis (RA), a field of view from the distal forearm to the proximal interphalangeal (PIP) joints has shown to be sufficient, as involvement of the distal interphalangeal (DIP) joints is only rarely observed. With regard to computed tomography (CT), depending on the indication, one or both whole hands are investigated.

With MRI, the slice orientation follows the three major anatomical planes. Anatomical landmarks for the assessment of the image quality of the wrist are the delineation of the hyaline cartilage and the triangular fibrocartilage complex (TFCC) to assess the quality of the spatial resolution [14]. In the metacarpophalangeal and interphalangeal joints, the delineation of the metacarpal heads and the phalangeal endings can be used to assess the spatial resolution with respect to the slice thickness. With CT, the trabecular structure of the bones is a useful anatomical landmark.

For the radiology report, there is a general consensus that the description should be structured anatomically. The order of listing the anatomical items generally varies between "inside out", i.e. starting with the bones and ending with the subcutaneous soft tissues, or "outside in". Variations on how to organize an anatomy-based checklist are based-in addition to anatomical origin and spread of disease-on the investigator's personal experience, the clinical relevance of findings and recently, on

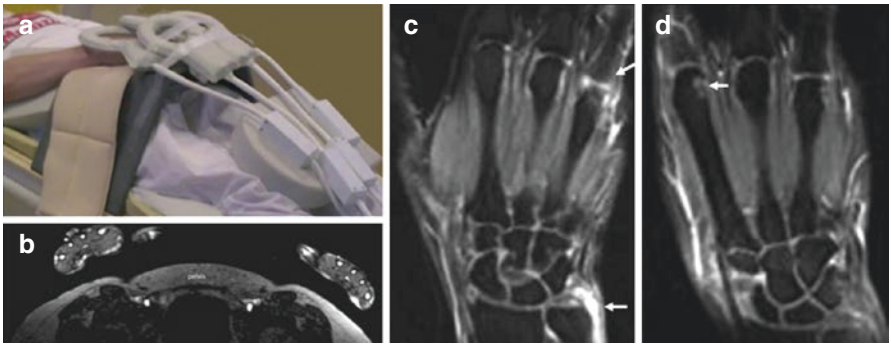

Fig. 4.1 Magnetic resonance imaging (**a**) of both hands of a patient with rheumatoid arthritis in a supine position. (**b**–**d**) Despite off-centre position of the hands and potential distortion of the magnetic field B0, the image quality, here with a 1.0 T, is sufficient for clinical purpose, (**c**) right-sided periulnar inflammation due to tenosynovitis of the extensor carpi ulnaris tendon and effusion in the second metacarpophalangeal joint (arrows), (**d**) erosion in the second metacarpophalangeal joint (arrow)

the rules of efficient diagnostic reasoning. Summarizing these aspects leads to an image analysis checklist which starts with alignment in order to get an overview of the arrangement of soft tissues, tendons, ligaments and bones. In case of arthritis, it makes sense to begin first with malalignment, since several studies have described a dependency of the distribution of erosions on anatomical and biomechanical factors with characteristic locations along the force-bearing axis of the wrist and in the metacarpophalangeal (MCP) joints adjacent to the radial collateral ligaments [10, 11]. This approach to analyzing radiographs is also known as the target area approach [15]. It may be applied in a similar way for the analysis of cross-sectional imaging with a focus on both macro- and microanatomical distribution of inflammation.

Investigation: Interactions of X-Rays, Gamma-Rays and Magnetic Fields with Anatomical Structures

High-resolution and dedicated post-processing techniques offer new insight into the patterns of arthritis and the potential to perform "virtual biopsies" [16]. In CT and projection radiography, X-rays are absorbed in human tissue in a process known as attenuation. Practically relevant parameters include radiodensity, expressed in Hounsfield units in CT as well as the thickness of the tissue. Cartilage, uric acid, fluids and fatty tissue have characteristic Hounsfield values. With dual-source CT and a dedicated post-processing software, the amount of monosodium urate (MSU) and of bone marrow oedema lesions (BMEL) can be estimated. A precise anatomical allocation of MSU deposits within or adjacent to collagen fibrils is possible. Certain anatomical structures, however, may show similar color encoding after post-processing, because the calculated values are not unique for a given tissue. In such a way, skin and nails with high keratin concentration, inadequate signal-to-noise ratio or metallic artefacts may appear with the same encoding. BMEL can be located and quantified with a "virtual noncalcium technique" by subtracting calcium from cancellous bone [17].

High-resolution peripheral quantitative computed tomography (HRpqCT) is a technique for the analysis of the bone architecture at the distal radius, the wrist and the distal tibia. With these systems, a 1 cm thick stack of parallel CT slices is obtained at the distal radius, the wrist or the tibia. With automated threshold segmentation, total, trabecular and cortical bone can be separated and quantified in vivo, enabling the non-invasive analysis of osseous anatomy. With a spatial resolution of 50–82 μm, bone erosions and other forms of osseous involvement of arthritis can be displayed. In contrast to two-dimensional methods like dual energy X-ray absorptiometry (DXA), it allows the assessment of cross-sectional bone geometry and of volumetric bone mineral density (vBMD). The vBMD can be differentiated into total and trabecular bone mineral density (expressed in mg hydroxyapatite (HA)/cm^3) and correlated with cortical thickness and other parameters of bone geometry [18, 19]. Typical microarchitecture parameters include cortical thickness (CTh, μm), trabecular number (TbN, mm^{-1}), thickness and

separation (TbTh, μm, TbSp, μm) and the distribution of trabecular separation (TbSpSD, μm). These parameters reflect the heterogeneity of the trabecular network [20]. For the detection of erosions, HRpqCT offers new insights in the subchondral, subenthesial and subtendinous lamellae, and normal anatomical representations of these structures have to be defined [21].

In MRI, the interaction of magnetic fields with human tissue mainly depends on the chemical binding of the water protons. The normal anatomy of the cortical bone is dark, because the water protons are strongly fixed in covalent bindings and only very low signal can be measured. If the binding is loose, like in fat, the signal will be bright on all sequences except on those generated with a fat-suppression technique. With 3 and 7 T, the spatial resolution can be significantly improved. For dynamic contrast-enhanced magnetic resonance imaging (DCE-MRI) and MR perfusion imaging, post-processing might be useful to quantify the flow rate of contrast media, thus calculating the severity of local inflammation in the synovium [22]. However, the precision of positioning of the regions of interest is low, and standardization remains difficult.

With hybrid and molecular imaging techniques in the form of positron emission tomography (PET)/CT, PET/MR and dedicated preclinical units, the normal and abnormal glucose metabolism and other forms of tracer accumulation may be exactly located [23]. PET depicts biological targets and can be used for the detection of inflammation at molecular and cellular levels. Multiple PET tracers have been investigated for their utility in imaging RA by using markers of cell proliferation; by targeting macrophages, B-cells or endothelial cells; and by using bone markers [24]. Macrophage-targeting PET tracers, such as 11C-(R)-PK11195 (1-(2-chlorophenyl)-*N*-methyl-*N*-(1-methylpropyl)-3-isoquinoline carboxamide), have been used for visualizing macrophage activity especially in clinically quiescent phases of RA [25]. Certain normal anatomical structures or benign lesions may be associated with an increased tracer uptake, thus simulating malignant diseases. With respect to the hand, such diagnostic pitfalls may occur in histiocytic, giant cell-containing or other benign bone lesions, especially in non-ossifying fibroma (or cortical desmoids), fibrous dysplasia or fibroxanthomas, granulomatous inflammation (including sarcoidosis) and many other forms of inflammation with increased macrophage and leukocyte activity [26].

Image Interpretation: Current Concepts in Imaging Anatomy

Over the years, anatomical concepts were developed to understand why synovitis and joint destruction develop in certain anatomical areas and progress by following predefined pathways. Traditional terms like bare areas, surface roughness, cysts, crypts or others have been used to describe these patterns. The dimensions of many of these definitions are often diffuse, so there is a need for a precise anatomical nomenclature with regard to CT and MRI as well as biomechanical and immunologic concepts. With a focus on inflammation, image interpretation should be performed by analysing general alignment, pattern of swelling, i.e. of synovitis

and enthesitis, cartilage loss (with joint space narrowing on projection radiographs), and changes in the subarticular bones. Especially for older patients with a higher prevalence of degenerative joint disease and clinically suspect arthralgia, anatomical terms and patterns should be used in a way that enables the differentiation of normal structures from true malalignment, synovitis, changes in joint space width and erosions.

Alignment: Kinetic Chains of Anatomical Compartments and Complexes

Malalignment due to subluxation in the wrist and the finger joints is a hallmark in the development of arthritis and may be observed not only in the advanced but also in the early stages of RA and other rheumatic diseases. The typical anatomical sites of any form of a destructive process may be regarded as the weak links in a "kinetic chain". This concept is used to understand joint compartments or anatomical complexes, especially tendons and ligaments, as links in a chain with the weaker parts being prone to destruction and impairment of the grip function [27]. Anatomical structures with a higher risk of being destroyed by inflammation, degeneration or trauma are called "critical zones" [28]. The "hot spots" of inflammation in RA are in the ulnocarpal compartment of the wrist, around the lunate bone and in the MCP joints, which all contribute to the development of ulnar drift with subsequent flattening of the transverse arch of the hand. In calcium pyrophosphate deposition disease (CPPD), the "hot spots" are the scapholunate space, the scapho-trapezio-trapezoid (triscaphe) compartment and the radial-sided MCP joints. Osteoarthritis (OA) primarily affects the first carpometacarpal joint (or compartment) with adjacent tendons as well as the interphalangeal joints.

The systematic approach to wrist malalignment has been newly defined by the Mayo classification system of carpal instability, a biomechanical approach which has now replaced earlier systems [29, 30]. The key anatomical concept of this classification is based on three principles: Firstly, there are two stable rows of carpal bones bound together by strong intercalated ligaments: proximally, the scaphoid, lunate and triquetral bones, stabilized by the intrinsic scapholunate ligament (SL) and the ulnotriquetral ligaments, and distally the distal carpal bones. A ligament rupture causes a dissociation of these two chain-like arrangements (carpal instability dissociative, CID). Scapholunate instability, as it occurs in CPPD, is a form of CID. Secondly, the radiocarpal and midcarpal compartments are the places where the normal motion of the wrist takes place with a different type of instability (carpal instability non-dissociative, CIND). Ulnar subluxation (ulnar drift) of the lunate, which occurs in RA, CPPD or other severe forms of synovitis, after trauma or with Madelung's deformity, may be regarded as a subform (CIND-trans). Thirdly, combinations in the form of a complex carpal instability or an adaptation of an underlying disease may occur as is the case in advanced forms of wrist arthritis (carpal instability complex and adaptive carpus).

The important kinetic chains causing instability in arthritis consist of synovial spaces and complexes, i.e. intimately interrelated ligaments, tendons and bones. Many anatomical variants have been described, and a different nomenclature is used for these structures that can be directly visualized with high-resolution MRI and US, especially if surrounded by effusion or inflammatory pannus [31]. For the diagnosis of arthritis, the following chains are of clinical relevance:

- In the ulnocarpal compartment (distal radioulnar joint), the ulnar recess of the radiocarpal compartment, the extensor carpi ulnaris tendon and the triangular fibrocartilage complex (TFCC)
- In the radiocarpal compartment, the dorsal radiocarpal "V"-ligament complex and the SL ligament complex
- In the midcarpal compartment, the distal components of the dorsal and palmar "V"-ligament complexes
- In the radial-sided part of the carpal tunnel, a new anatomical entity, the so-called scapho-trapezio-tunnel complex (STTC) can be delineated in close vicinity to the first carpometacarpal (CMC) joint and the scapho-trapezio-trapezoid (STT) or triscaphe joint
- In the metacarpophalangeal and interphalangeal joints, the capsular ligament complexes

The other carpal compartments which may be typically involved in inflammation due to overuse or degeneration and generally not in RA or related diseases: the first to the fifth extensor tendons, the central part of the carpal tunnel, Guyon's tunnel, the pisotriquetral compartment, the distal radioulnar joint and the second to fifth carpometacarpal joints with the amphiarthrotic intermetacarpal articulations.

The Ulnocarpal Wrist Compartment (Distal Radioulnar Joint)

The proximal borders of the ulnocarpal compartment are the ulnar styloid and the joint capsule. The proximal border is the TFCC. Its ulnar border is formed by the ulnar collateral ligament and the extensor carpi ulnaris tendon that runs in the sixth and most ulnarly located extensor tendon sheath through an osteofibrous channel that is formed by a shallow sulcus of the distal ulna. Inflammation in and around this tendon sheath causes the characteristic ulnar-sided swelling in arthritis.

The TFCC is fixed on its ulnar side to the extensor carpi ulnaris tendon and to the ulnar carpal collateral ligament (Fig. 4.2). Further, it is fixed to the ulna and to the adjacent bones by the ulnotriquetral, the volar distal radioulnar and other smaller ligaments [32]. These structures form the TFCC, also referred to as ulnocarpal complex and contain, in its centre loose connective tissue and a synovial fold, the meniscus homologue [33]. This is a small atavistic remnant of an ulnotriquetral joint that still exists in several other primates and is specifically prone to inflammation [34]. An inflammation of the meniscus homologue is typical in RA and may be related to erosions on the ulnar styloid. If an anatomical dissection of the TFCC is performed, it is difficult to separate the

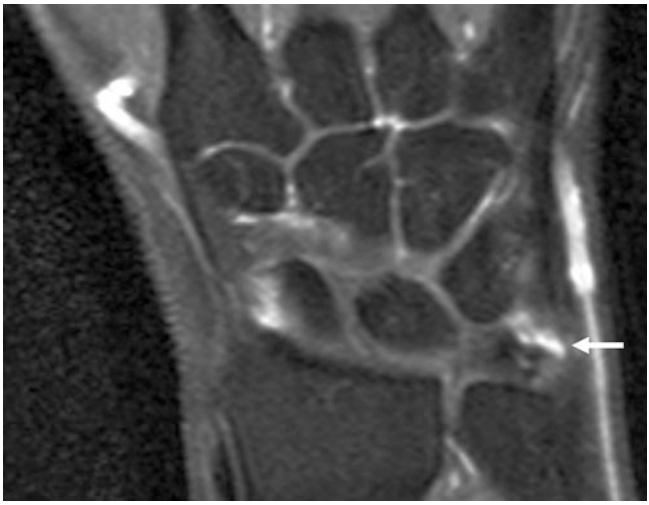

Fig. 4.2 Magnetic resonance imaging showing focal isolated effusion of the triangular fibrocartilage complex and ulnocarpal compartment (arrow) in a patient with rheumatoid arthritis

intimately connected structures of the TFCC, so it is not surprising that in arthritis the whole complex may be inflamed with subsequent destruction of the supporting ligaments and ulnar subluxation of the lunate. The TFCC plays an important role in stabilizing the wrist during pronation and supination.

The Radiocarpal and Midcarpal Compartments

Carpal stability is maintained by two complexes, the SL-ligament complex and the V-shaped palmar and carpal ligament complexes.

The scapholunate ligament complex consists of the SL-ligament, the volar-sided radioscaphocapitate ligament, the dorsal intercarpal ligament and other smaller supporting structures around it [35]. Therefore, SL instability is a function of both intrinsic SL-ligament and extrinsic SL-complex insufficiency [36, 37]. Insufficiency of the SL-ligament leads to an increase in the distance between the scaphoid and the lunate of more than 3–4 mm caused by an interruption of the biomechanically important dorsal component of this ligament. Scapholunar diastasis is, however, not always an indicator of instability. It may result from a stretched SL-ligament or may be observed in individuals with joint laxity, occurring bilaterally in this latter group (Fig. 4.3). In calcium pyrophosphate arthropathy, CPPD crystals are typically deposited in the TFCC, the dorsal and palmar part of which are true ligaments and its central part is fibrocartilage. CPPD may lead to non-traumatic rupture and in severe forms to scapholunate advanced collapse (SLAC).

The extrinsic ligaments of these compartments are summarized as two palmar and one dorsal "V"-ligament. Their proximal branches, especially the dorsal radio-luno-triquetral ligament, stabilize the lunate against drifting in the ulnar direction along the articular surface of the radius which has been compared to a slope for the lunate slipping in an ulnar direction (Fig. 4.4) [38]. (The proximal palmar and dorsal "V"-ligament branches, together with their neighboring structures, are also

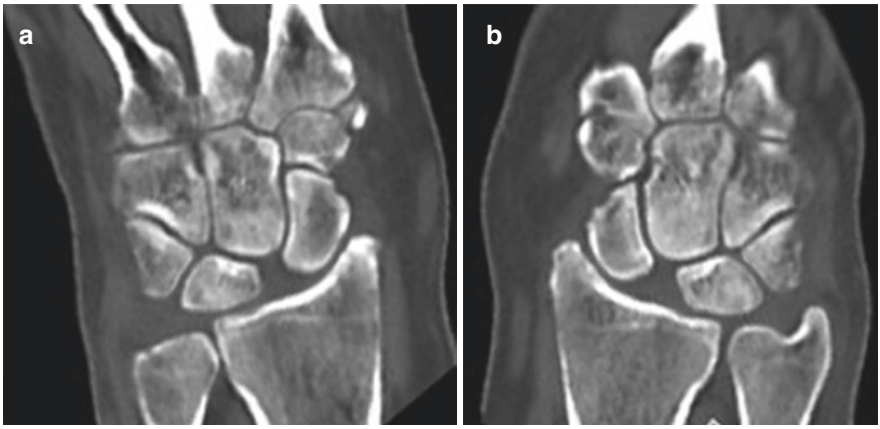

Fig. 4.3 Computed tomography of both hands in a patient with suspected gout. Bilaterally wide scapholunate spaces as a normal variant

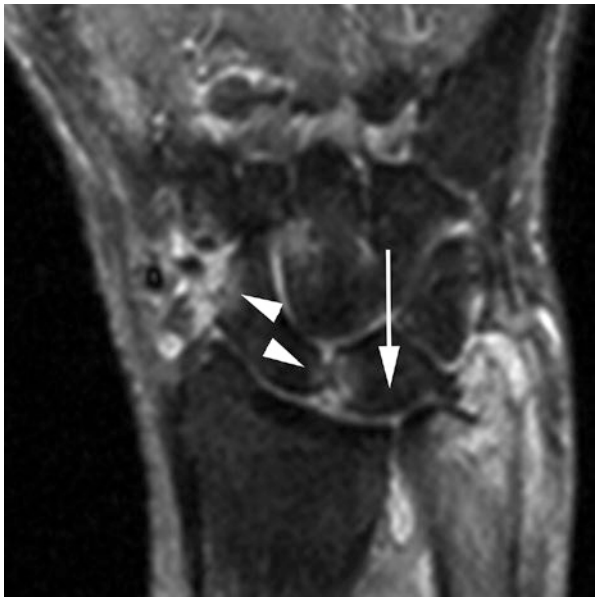

Fig. 4.4 Magnetic resonance imaging of a patient with rheumatoid arthritis and effusion which outlines the dorsal "V"-ligament: its proximal branch (arrow) is formed by the radiolunate and radio-luno-triquetral ligaments. The distal branch (arrowhead) indicates is the dorsal intercarpal ligament

known as "slingshot ligaments", a term which expresses their protective function in preventing the lunate and scaphoid from slipping.) The distal branch of the dorsal "V"-ligament is the strong dorsal intercarpal (DIC) ligament (also referred to as dorsal arcuate carpal ligament or Fick's arcuate ligament) that covers voluminous synovial tissue (Fig. 4.4). The pyramid-shaped triquetrum acts as a central anchor for the "V"-ligaments. Here, two components of the strong "V"-ligaments insert with formation of normal grooves (pseudoerosions): on its ulnar proximal side the ulnotriquetral ligament and on its dorsal aspect the DIC ligament. In CPPD with its high predilection for collagen, crystal deposits may be found in these ligaments.

A small palmar radio-scapholunate ligament (Testut's ligament) contains vessels and nerve endings. Its origin at the distal radius may be an inflammatory focus in RA with cystic destruction (Mannerfeldt's crypt) [39].

The Radial-Sided Carpal Tunnel, the Triscaphe and the First Carpometacarpal Joint

The carpal tunnel consists of two parts (also referred to as radial and ulnar "bursae"), which are divided incompletely by a fibrous septum. The radial bursa consists of the STTC and the central portion of the carpal tunnel part, containing the long flexor tendons and the median nerve. The STCC is a complex osseous and ligamentous hood for the synovial tendon sheaths of the flexor pollicis longus and the flexor carpi radialis tendons that cross the waist of the scaphoid on its palmar aspect [40]. It stabilizes the STT joint and the first CMC joint. Laterally, the hood is formed by the radial collateral carpal ligament and by the scaphoid tubercle (which may project at a palmar flexed scaphoid as "ring sign" on radiographs). The fibrous part of the hood consists of the radioscaphocapitate, the long radiolunate and other intercarpal ligaments. More distally, the tendons run over or insert at the trapezium where they are laterally bordered by the trapezial tuberosity. The radioscaphocapitate ligament is part of the distal palmar V-ligament and of the scapholunate ligament complex, thus acting as a rotatory stabilizer of the scaphoid [41].

The STT joint is additionally stabilized by the intrinsic scapho-trapezo-trapezoid ligament. The joint and the ligament are a predilection site for OA and CPPD.

The first carpometacarpal joint is stabilized by the STTC and many small capsular ligaments that provide a wide range of motion for the thumb and protect against subluxation in OA. Of importance among them are superficial and deep anterior oblique carpometacarpal ligaments and the dorsoradial carpometacarpal ligament [32]. With high-resolution MR, these structures may be directly visualized [42]. In females, the joint surfaces are flattened and less congruent which has been used as an explanation for the higher prevalence of OA in this population [43].

The Metacarpophalangeal and Interphalangeal Joints

The collateral ligament complexes are the main joint stabilizers of the MCP joints, in particular the stronger radial ligaments prevent from ulnar drift (Fig. 4.5) [11, 44]. The ligaments may appear inhomogeneous on MR images; this is probably related to a magic-angle phenomenon due to the different orientation of their three components (collateral ligament proprium, accessory collateral ligament and phalangoglenoid ligament) [45, 46]. The long extensor and flexor tendons share an intimate relationship with the joint capsule and are prone to subluxation and rupture in case of a severe ulnar drift. Their insertion as well as its thin and small capsular components can only be visualized in part with MRI and US, these include the ulnar and radial-sided sagittal ligaments which insert into the transverse profound

Fig. 4.5 Magnetic resonance imaging showing ulnar drift in a patient with rheumatoid arthritis and extensive bone marrow oedema with erosions of the distal ulna and subluxation of the lunate with more than 50% of its transverse diameter hanging over the ulnar edge of the radius (arrow). Insufficiency of the periscaphoid ligaments (arrowhead) with subenthesial oedema under the scapholunate ligament and radial-sided synovial folds

metacarpal ligament (parallel and directly proximal to the A1 ligament of the flexor tendon sheath), the fibrocartilaginous palmar plate with the checkrein ligaments and the volar-sided interconnections of all these ligaments (Zancolli complex) [46].

At the IP joints, the central slip of the extensor tendon hood plays a central role in the development of boutonnière deformity with flexion of the PIP and extension of the DIP. The central slip originates from the extensor hood and inserts on the middle phalanx. Capsular distension in arthritis leads to a rupture of this slip, so the extensor digitorum communis tendon loses its function. This results in the palmar migration of the collateral bands with subsequent loss of resistance against the pull of the lumbricals. The swan-neck deformity is a hyperextension of the PIP joint with flexion of the DIP due to both laxity of the joint capsule and rupture of the flexor tendon.

Synovial Recesses and Entheses

The macroscopic spread of inflammation and subsequent destruction (both typical and atypical) of joints and bone is commonly described in the context of anatomical compartment and complexes. The simple anatomical abstraction of a layered joint capsule composed of a superficial zone of macrophage-like A synoviocytes,

a deep zone of fibroblast-like B synoviocytes, a subsynovium (subintima) with loose connective tissue and blood vessels and a fibrous capsule with ligaments however, is too simplified a model to understand the pathways and distribution of inflammation. The synovial layers are not bordered by a basal lamina, and there are continuous overlaps and great regional differences in their thickness and composition. The superficial A synoviocytes may be totally absent, the fibroblasts are distributed in both the deep synovium and the subsynovium, the subsynovium contains strands of collagen fibres paralleling and intermingling the subjacent ligaments, and many ligaments are vascularized [47]. In RA and related diseases, the synovium with the subsynovial perivascular tissue are the anatomical site where the inflammatory reaction is triggered [48–50]. In psoriatic arthritis and other spondylarthropathies, the enthesis has been regarded as part of a synovio-entheseal complex which is characterised by a mixed pattern of inflammation due to stress dissipation and autoimmune processes [51]. From the entheses of the capsular ligaments of the joints and of tendons, the inflammation spreads into neighboring tissue by involving the subenthesial bone, the synovium and the periarticular soft tissue. In CPPD and other crystal deposition diseases, the crystal aggregates are primarily deposited in and around the collagen fibres of ligaments, tendon fibrocartilage or hyaline cartilage. In OA, the degenerative process starts in the structures which are under the heaviest biochemical load, such as cartilage and the fibres of the joint capsule or tendons. The resulting micro-instability leads to synovitis and degeneration of all joint components, which means that OA is regarded as a "whole-organ disease" [52].

For explaining the regional distribution of inflammation within the joints with erosions originating at the margins or at the entheses, two macroanatomical theories have been developed. The bare area concept emphasizes in areas covered by only thin hyaline cartilage or areas without such cover the synovium and synovial fluid are in direct contact with bone [48, 53]. In these transitional zones the synovium occupies the peripheral few millimetres of cartilage [47]. A second concept highlights the fact that in areas with big synovial volume, synovial duplications or folds, the inflammatory reaction is heavier. The dorsal prolongations of synovium in the midcarpal compartment or the thick synovial lining with prominent vessels around Testut's ligament are typical sites of inflammation in RA.

According to the classification of the above-mentioned kinetic chains within and around anatomical compartments, the following clinically relevant synovial spaces can be described [29]:

- In the ulnocarpal compartment, the tendon sheath of the extensor carpi ulnaris tendon and the small space around the meniscus homologue of the TFCC (Fig. 4.2)
- In the radiocarpal compartment, the ulnar (prestyloid, in wrist arthrography sometimes called "muddy pouch") recess around the neck of the ulnar styloid proximal to the TFCC (Fig. 4.6)
- In the midcarpal compartment, the dorsal space under the DIC ligament with a high volume of synovial tissue and the space between and around the lunate and

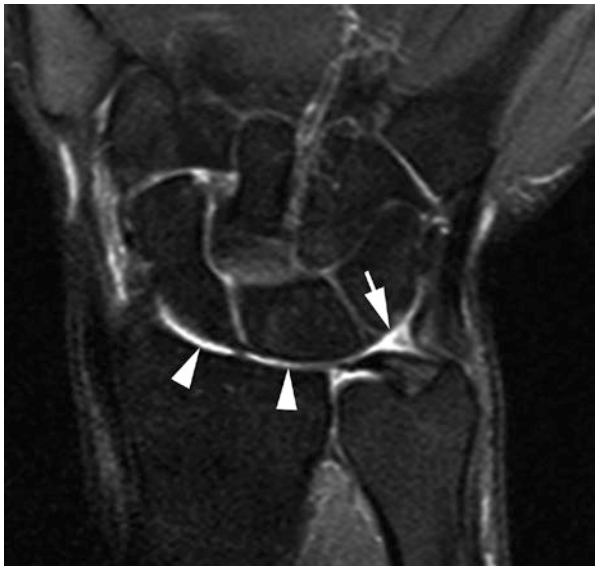

Fig. 4.6 Magnetic resonance imaging depicting a small effusion in the radiocarpal compartment between the articular surface of the radius and the proximal carpal row (arrowheads), extending to the ulnar side and ending with a sometimes pouch-like configuration (arrow) under the ulnar collateral ligament

the capitate bones (space of Poirier) with a gap between the branches of the supporting "V" -ligaments that predisposes to perilunate instability
- In the radial-sided part of the carpal tunnel, the tendon sheaths of the flexor carpi radialis and the flexor pollicis longus tendons (also referred to as "radial bursa")
- The CMC joint and the STT joint
- The MCP and IP joint space with a proximal recess along the metacarpal head and neck

The Osteocartilaginous Unit

The hyaline cartilage has a zonal architecture and consists, according to Beninghoff's arcade model, of four layers that can be readily identified with MRI [54–56]. Each zone is specifically prone to certain types of destruction. The superficial layer protects against shear, tensile and compressive forces as well. This layer is characterized by a high content of collagen fibres and it is here where we primarily find CPPD crystals, MSU aggregates and calcifications occurring in other crystal-induced or storage diseases. This layer, along with the middle and deep layers also features a high concentration of chondrocytes. In RA, these cells may produce matrix-degrading enzymes and induce chondrolysis with formation of empty lacunae [49, 57, 58]. At the border between uncalcified and calcified cartilage, numerous vascular channels exist, providing potential routes for molecular diffusion between the two compartments within the complex architecture of the chondro-osseous junction [59, 60]. This seems to be important in the progression of OA and

RA [48, 59]. The fourth layer, calcified cartilage, continues into the subchondral plate with its characteristic architecture around vascular sinusoids. Bone marrow oedema-like lesions with subsequent decalcification, resulting from synovial tissue-induced osteoclastogenesis and/or bony sclerosis may be observed in this layer [49, 60]. With high-resolution MRI and CT, an anatomical allocation of these processes within the ostocartilaginous unit is principally possible.

Subarticular and Subtendinous Bone

All anatomical sites with a predilection for arthritis share a common feature, in that they are not covered by periosteum. The subchondral bone with its peculiar trabecular structure and underlying vascular sinusoids and with its intimate relationship to the overlying calcified cartilage zone is a well-established anatomical unit [56]. For tendons and ligaments, a similar zonal structure has been described and termed the synovio-entheseal complex [62]. A third example of bone lacking periosteal coverage are osteofibrous channels or bone located adjacent to bursae, which are therefore in direct contact with fibrous and subsynovial tissue. The superficial aspect of the growth plate, during childhood and adolescence, may be regarded as a fourth example. These examples are also summarized under the term “calcified zones” or “laminae” [63, 64]. They may be of varying thickness and may be, apart from the periosteum, regarded as another type of bony border. With CT, the calcified zones can be displayed with spatial resolution in the submillimeter range.

If at such calcified zones a concavity or an interruption of the bony outline is observed, a differentiation of such a pseudoerosion from true inflammatory erosions in RA and related diseases may be difficult [63]. Pseudoerosions may be a normal concavity of the bone or may be artefact-related. They have to be differentiated from erosions or cysts in OA and from mucoid degeneration at ligament insertions, as well as from intraosseous ganglion cysts. Pseudoerosions are important pitfalls when scoring erosions occurring in arthritis [65]. They may appear more prominent in case of malalignment with a slight rotation of the bones due to ligament laxity or arthritic subluxation. In the elderly population characterized by a higher prevalence of degenerative changes, differentiation between pseudoerosions and true erosions may be difficult [66]. The scaphoid may be slightly deviated by postinflammatory scarring or after posttraumatic deformation, and its waist may be more prominently projected in the form of a pseudoerosion [65, 67, 68]. Anatomical pseudoerosions can be classified as grooves (notches or fossae) and jutties, sulci and roughnesses with or without a nutritional channel (Figs. 4.7 and 4.8).

A groove may be observed at a non-apophyseal direct tendon or ligament attachment, at an apophysis with overhanging edges of the bone or at the indirect attachments of a tendon or ligament with tangential transition into the periosteum. The latter are incompletely formed apophyseal structures and present rather as jutties than as real

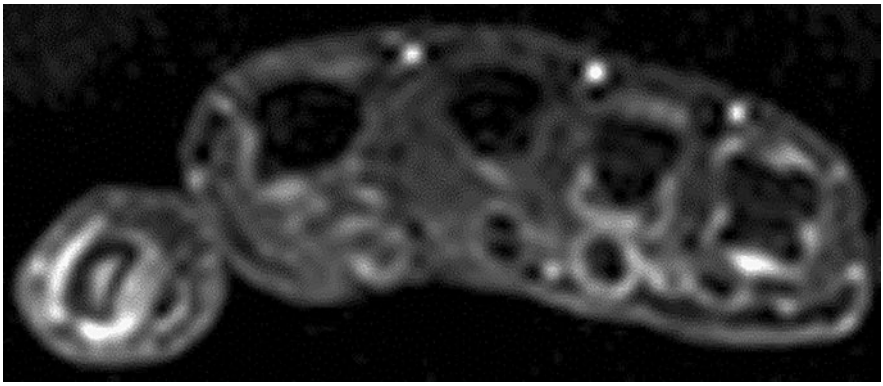

Fig. 4.7 Dynamic "film-like" perfusion imaging (which therefore appears blurry on the static image) showing the ulnar-sided collateral ligament complex of the third digit lying in a characteristic normal groove appearing as a pseudoerosion on cross-sectional images and the contrast media accumulating in the synovium of joints and tendon sheaths (bright signal). In the first metacarpophalangeal joint, a relevant synovitis is visible

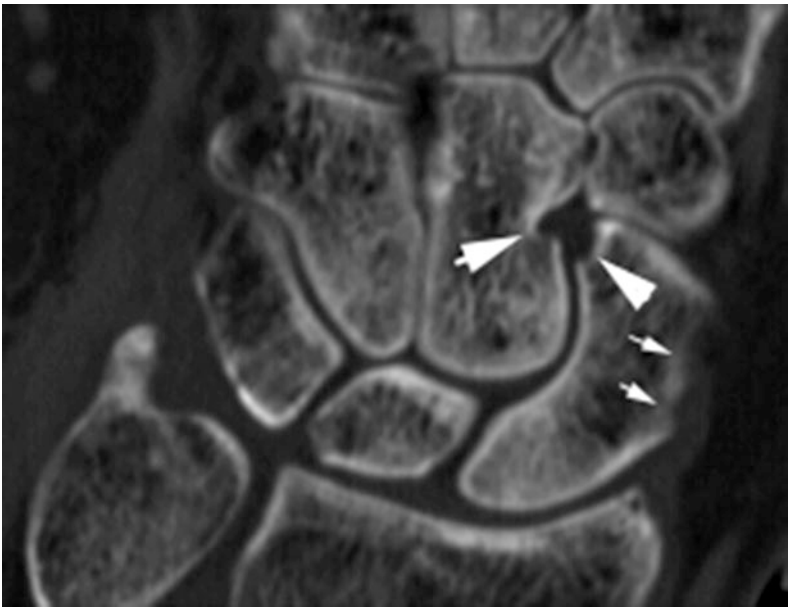

Fig. 4.8 Coronal CT image with grooves on the radial aspect of the capitate (arrow) and the ulnar aspect of the distal scaphoid (arrow head) representing characteristic pseudoerosions, the latter with slightly overhanging edges. Undulating shallow grooves on the radial aspect of the scaphoid (small arrows) represent insertions of innominate mucosal folds

grooves. Many such grooves exist in the hand, mainly at ligament insertions. A great variety of such grooves may be observed, particularly around the capitate and at its neighboring bones, not only at the strong "V"-ligament insertions but also at small intrinsic ligaments insertions [69]. On its radial surface, the capitate may have a prominent groove of varying size which forms an asymmetric capitate waist. At the carpometacarpal, the MCP and the finger joints, grooves occur at the bases of the metacarpal bones or at the phalangeal bases in the form of small round or oval subcapsular notches. The nonspherical form of metacarpal and metatarsal heads can be explained by the collateral ligament complexes with smoothly outlined shallow metacarpal grooves containing these structures [44]. At the metacarpals, these grooves are bordered by little tubercles for the proximal attachment of the collateral ligaments [44]. A focal decalcification on projection radiographs or CT images with hazy borders should not be assessed as a pseudoerosion but rather as a "pre-erosion" with increased focal osteoclast activity.

The roof of a bony sulcus is formed by a ligament, fascia or other fibrous tissue, thus forming an osteofibrous channel for a tendon within a synovial sheath. Pseudoerosions due to such a tangentially displayed channel may be typically observed at the waist of the scaphoid under the flexor pollicis longus and the flexor carpi radialis tendons.

A surface roughness is an area of bone, not covered by periosteum or cartilage. It is located adjacent to often innominate ligaments or synovial folds, to tendons or to nutritional vessels. A differentiation from shallow and in most cases chronic forms of erosions or from severe cartilage degeneration may be difficult. Some of them may be specified as crests or ridges that correspond to attachment sites for a redundant joint capsule. Nutritional channels of bone vessels may open to the surface of a bone with their orifice appearing hyperintense on T2-weighted MR images [65, 70].

Conclusion

Precise and detailed anatomical concepts and terms are necessary to meet today's requirement of diagnosing arthritis in its early, clinically suspected and preclinical stages. Especially with MRI, a continuous overlap is observed between normal osseous concavities and erosions as well as between synovitis due to overuse, degeneration or clinically suspected arthritis. A combined biomechanical and immunologic concept in understanding the origins and pathways of inflammation and degeneration might help improve the diagnostic accuracy and precision. This is a still ongoing process oriented to the increasing clinical demands of rheumatology.

References

1. Johnson AJ, Chen MY, Zapadka ME, Lyders EM, Littenberg B. Radiology report clarity: a cohort study of structured reporting compared with conventional dictation. J Am Coll Radiol. 2010;7:501–6.
2. Wick M, Peloschek P, Bogl K, Graninger W, Smolen JS, Kainberger F. The "X-ray Rheuma coach" software: a novel tool for enhancing the efficacy and accelerating radiological quantification in rheumatoid arthritis. Ann Rheum Dis. 2003;62:579–82.

3. Woodworth TG, Morgacheva O, Pimienta OL, Troum OM, Ranganath VK, Furst DE. Examining the validity of the rheumatoid arthritis magnetic resonance imaging score according to the OMERACT filter-a systematic literature review. Rheumatology (Oxford). 2017;56:1177–88.
4. Ejbjerg B, Narvestad E, Rostrup E, Szkudlarek M, Jacobsen S, Thomsen HS, Ostergaard M. Magnetic resonance imaging of wrist and finger joints in healthy subjects occasionally shows changes resembling erosions and synovitis as seen in rheumatoid arthritis. Arthritis Rheum. 2004;50:1097–106.
5. Palosaari K, Vuotila J, Soini I, Kaarela K, Kautiainen H, Hakala M. Small bone lesions resembling erosions can frequently be found in bilateral wrist MRI of healthy individuals. Scand J Rheumatol. 2009;38:450–4.
6. Partik B, Rand T, Pretterklieber ML, Voracek M, Hoermann M, Helbich TH. Patterns of gadopentetate-enhanced MR imaging of radiocarpal joints of healthy subjects. AJR Am J Roentgenol. 2002;179:193–7.
7. Robertson PL, Page PJ, McColl GJ. Inflammatory arthritis-like and other MR findings in wrists of asymptomatic subjects. Skelet Radiol. 2006;35:754–64.
8. Olech E, Crues JV 3rd, Yocum DE, Merrill JT. Bone marrow edema is the most specific finding for rheumatoid arthritis (RA) on noncontrast magnetic resonance imaging of the hands and wrists: a comparison of patients with RA and healthy controls. J Rheumatol. 2010;37:265–74.
9. Parodi M, Silvestri E, Garlaschi G, Cimmino MA. How normal are the hands of normal controls? A study with dedicated magnetic resonance imaging. Clin Exp Rheumatol. 2006;24:134–41.
10. Pierre-Jerome C, Bekkelund SI, Mellgren SI, Torbergsen T, Husby G, Nordstrom R. The rheumatoid wrist: bilateral MR analysis of the distribution of rheumatoid lesions in axial plan in a female population. Clin Rheumatol. 1997;16:80–6.
11. Tan AL, Tanner SF, Conaghan PG, Radjenovic A, O'Connor P, Brown AK, Emery P, McGonagle D. Role of metacarpophalangeal joint anatomic factors in the distribution of synovitis and bone erosion in early rheumatoid arthritis. Arthritis Rheum. 2003;48:1214–22.
12. Frija G. Quality and safety in radiology: a symbiotic relationship. Health Manage Forum. 2015;15.
13. Navalho M, Resende C, Rodrigues AM, Ramos F, Gaspar A, Pereira da Silva JA, Fonseca JE, Campos J, Canhão H. Bilateral MR imaging of the hand and wrist in early and very early inflammatory arthritis: tenosynovitis is associated with progression to rheumatoid arthritis. Radiology. 2012;264:823–33.
14. Friedrich KM, Chang G, Vieira RL, Wang L, Wiggins GC, Schweitzer ME, Regatte RR. In vivo 7.0-tesla magnetic resonance imaging of the wrist and hand: technical aspects and applications. Semin Musculoskelet Radiol. 2009;13:74–84.
15. Resnick D. Target area approach to articular disorders. A synopsis. In: Resnick D, Kransdorf M, editors. Bone and joint imaging, vol. 1. Philadelphia: Elsevier Sounders; 2005. p. 324–51.
16. Patsch JM, Burghardt AJ, Kazakia G, Majumdar S. Noninvasive imaging of bone microarchitecture Ann N Y Acad Sci. 2011;1240:77–87.
17. Pache G, Krauss B, Strohm P, Saueressig U, Blanke P, Bulla S, Schäfer O, Helwig P, Kotter E, Langer M, Baumann T. Dual-energy CT virtual noncalcium technique: detecting posttraumatic bone marrow lesions--feasibility study. Radiology. 2010;256:617–24.
18. Aeberli D, Eser P, Bonel H, Widmer J, Caliezi G, Varisco PA, Möller B, Villiger PM. Reduced trabecular bone mineral density and cortical thickness accompanied by increased outer bone circumference in metacarpal bone of rheumatoid arthritis patients: a cross-sectional study. Arthritis Res Ther. 2010;12:R119.
19. Fouque-Aubert A, Boutroy S, Marotte H, Vilayphiou N, Bacchetta J, Miossec P, Delmas PD, Chapurlat RD. Assessment of hand bone loss in rheumatoid arthritis by high-resolution peripheral quantitative CT. Ann Rheum Dis. 2010;69:1671–6.
20. Parfitt AM, Mathews CH, Villanueva AR, Kleerekoper M, Frame B, Rao DS. Relationships between surface, volume, and thickness of iliac trabecular bone in aging and in osteoporo-

sis. Implications for the microanatomic and cellular mechanisms of bone loss. J Clin Invest. 1983;72:1396–409.
21. Stok KS, Finzel S, Burghardt AJ, Conaghan PG, Barnabe C, SPECTRA Collaboration. The SPECTRA collaboration OMERACT special interest group: current research and future directions. J Rheumatol. 2017;44(12):1911–5.
22. Axelsen MB, Stoltenberg M, Poggenborg RP, Kubassova O, Boesen M, Bliddal H, Hørslev-Petersen K, Hanson LG, Østergaard M. Dynamic gadolinium-enhanced magnetic resonance imaging allows accurate assessment of the synovial inflammatory activity in rheumatoid arthritis knee joints: a comparison with synovial histology. Scand J Rheumatol. 2012;41:89–94.
23. Miese F, Scherer A, Ostendorf B, Heinzel A, Lanzman RS, Kröpil P, Blondin D, Hautzel H, Wittsack HJ, Schneider M, Antoch G, Herzog H, Shah NJ. Hybrid 18F-FDG PET-MRI of the hand in rheumatoid arthritis: initial results. Clin Rheumatol. 2011;30:1247–50.
24. Narayan N, Owen DR, Taylor PC. Advances in positron emission tomography for the imaging of rheumatoid arthritis. Rheumatology (Oxford). 2017;56(11):1837–46.
25. Gent YY, Ter Wee MM, Voskuyl AE, den Uyl D, Ahmadi N, Dowling C, van Kuijk C, Hoekstra OS, Boers M, Lems WF, van der Laken CJ. Subclinical synovitis detected by macrophage PET, but not MRI, is related to short-term flare of clinical disease activity in early RA patients: an exploratory study. Arthritis Res Ther. 2015;17:266.
26. Goodin GS, Shulkin BL, Kaufman RA, McCarville MB. PET/CT characterization of fibroosseous defects in children: 18F-FDG uptake can mimic metastatic disease. AJR Am J Roentgenol. 2006;187:1124–8.
27. Teixeira da Fonseca S, de Melo Ocarino J, Pereira da Silva P, Ferreira de Aquino C. Integration of stresses and their relationship to the kinetic chain. In: Magee D, Zachazewski J, William Q, editors. Scientific foundations and principles of practice in musculoskeletal rehabilitation. St. Louis: Saunders Elsevier; 2007. p. 476–86.
28. Kainberger F, Mittermaier F, Seidl G, Parth E, Weinstabl R. Imaging of tendons–adaptation, degeneration, rupture. Eur J Radiol. 1997;25:209–22.
29. Carlsen BT, Shin AY. Wrist instability. Scand J Surg. 2008;97:324–32.
30. Morco S, Bowden A. Ulnar drift in rheumatoid arthritis: a review of biomechanical etiology. J Biomech. 2015;48:725–8.
31. Taljanovic MS, Malan JJ, Sheppard JE. Normal anatomy of the extrinsic capsular wrist ligaments by 3-T MRI and high-resolution ultrasonography. Semin Musculoskelet Radiol. 2012;16:104–14.
32. Bateni CP, Bartolotta RJ, Richardson ML, Mulcahy H, Allan CH. Imaging key wrist ligaments: what the surgeon needs the radiologist to know. AJR Am J Roentgenol. 2013;200:1089–95.
33. Nobauer-Huhmann IM, Pretterklieber M, Erhart J, Bär P, Szomolanyi P, Kronnerwetter C, Lang S, Friedrich KM, Trattnig S. Anatomy and variants of the triangular fibrocartilage complex and its MR appearance at 3 and 7T. Semin Musculoskelet Radiol. 2012;16:93–103.
34. Lewis OJ, Hamshere RJ, Bucknill TM. The anatomy of the wrist joint. J Anat. 1970;106:539–52.
35. Shahabpour M, Staelens B, Van Overstraeten L, De Maeseneer M, Boulet C, De Mey J, Scheerlinck T. Advanced imaging of the scapholunate ligamentous complex. Skelet Radiol. 2015;44:1709–25.
36. Pappou IP, Basel J, Deal DN. Scapholunate ligament injuries: a review of current concepts. Hand (NY). 2013;8:146–56.
37. Theumann NH, Etechami G, Duvoisin B, Wintermark M, Schnyder P, Favarger N, Gilula LA. Association between extrinsic and intrinsic carpal ligament injuries at MR arthrography and carpal instability at radiography: initial observations. Radiology. 2006;238:950–7.
38. Schmitt R. Ulnokarpaler Komplex (TFCC). In: Schmitt R, Lanz W, editors. Bildgebende Diagnostik der Hand. 2nd ed. Stuttgart: Thieme; 2004. p. 96–102.
39. Dihlmann W, Stäbler A. Gelenke–Wirbelverbindungen. Stuttgart: Thieme; 2011.

40. Parellada AJ, Morrison WB, Reiter SB, Carrino JA, Kloss LA, Glickman PL, McLean M, Culp RW. Flexor carpi radialis tendinopathy: spectrum of imaging findings and association with triscaphe arthritis. Skelet Radiol. 2006;35:572–8.
41. Short WH, Werner FW, Green JK, Sutton LG, Brutus JP. Biomechanical evaluation of the ligamentous stabilizers of the scaphoid and lunate: part III. J Hand Surg Am. 2007;32:297–309.
42. Hirschmann A, Sutter R, Schweizer A, Pfirrmann CW. The carpometacarpal joint of the thumb: MR appearance in asymptomatic volunteers. Skelet Radiol. 2013;42:1105–12.
43. Ateshian GA, Rosenwasser MP, Mow VC. Curvature characteristics and congruence of the thumb carpometacarpal joint: differences between female and male joints. J Biomech. 1992;25:591–607.
44. Canella Moraes Carmo C, Cruz GP, Trudell D, Hughes T, Chung C, Resnick D. Anatomical features of metacarpal heads that simulate bone erosions: cadaveric study using computed tomography scanning and sectional radiography. J Comput Assist Tomogr. 2009;33:573–8.
45. Crim J, Grossman J. Hand MR atlas. In: Manster B, Crim J, editors. Imaging anatomy–musculoskeletal. Philadelphia: Elsevier; 2016. p. 456.
46. Streicher J, Pretterklieber M. Bewegungsapparat. In: Anderhuber F, Pera F, Streicher J, editors. Waldeyer–Anatomie des Menschen. Berlin: Walter de Gruyter; 2012. p. 218–23.
47. Adams M. Functional anatomy of the musculoskeletal system. In: Standring S, editor. Grey's anatomy. The anatomical basis of clinical practice. Philadelphia: Elsevier; 2016. p. 99.
48. Catrina AI, Svensson CI, Malmstrom V, Schett G, Klareskog L. Mechanisms leading from systemic autoimmunity to joint-specific disease in rheumatoid arthritis. Nat Rev Rheumatol. 2017;13:79–86.
49. Favalli EG, Becciolini A, Biggioggero M. Structural integrity versus radiographic progression in rheumatoid arthritis. RMD Open. 2015;1:e000064.
50. Harris ED Jr. Rheumatoid arthritis. Pathophysiology and implications for therapy. N Engl J Med. 1990;322:1277–89.
51. Sherlock JP, Joyce-Shaikh B, Turner SP, Chao CC, Sathe M, Grein J, Gorman DM, Bowman EP, McClanahan TK, Yearley JH, Eberl G, Buckley CD, Kastelein RA, Pierce RH, Laface DM, Cua DJ. IL-23 induces spondyloarthropathy by acting on ROR-gammat+ CD3+CD4-CD8-entheseal resident T cells. Nat Med. 2012;18:1069–76.
52. Benjamin M, McGonagle D. Basic concepts of enthesis biology and immunology. J Rheumatol Suppl. 2009;83:12–3.
53. Roemer FW, Crema MD, Trattnig S, Guermazi A. Advances in imaging of osteoarthritis and cartilage. Radiology. 2011;260:332–54.
54. Martel W, Stuck KJ, Dworin AM, Hylland RG. Erosive osteoarthritis and psoriatic arthritis: a radiologic comparison in the hand, wrist, and foot. AJR Am J Roentgenol. 1980;134:125–35.
55. Benninghoff A. Der funktionelle Aufbau des Hyalinknorpels. Ergeb Anat Entwickl Gesch. 1925;26:1–54.
56. Guermazi A, Roemer FW, Crema MD, Englund M, Hayashi D. Imaging of non-osteochondral tissues in osteoarthritis. Osteoarthr Cartil. 2014;22:1590–605.
57. Sophia Fox AJ, Bedi A, Rodeo SA. The basic science of articular cartilage: structure, composition, and function. Sports Health. 2009;1:461–8.
58. Blüml S, Redlich K, Smolen JS. Mechanisms of tissue damage in arthritis. Semin Immunopathol. 2014;36:531–40.
59. McInnes IB, Schett G. Cytokines in the pathogenesis of rheumatoid arthritis. Nat Rev Immunol. 2007;7:429–42.
60. Findlay DM, Kuliwaba JS. Bone-cartilage crosstalk: a conversation for understanding osteoarthritis. Bone Res. 2016;4:16028.
61. Imhof H, Sulzbacher I, Grampp S, Czerny C, Youssefzadeh S, Kainberger F. Subchondral bone and cartilage disease: a rediscovered functional unit. Investig Radiol. 2000;35:581–8.

62. Schett G, Gravallese E. Bone erosion in rheumatoid arthritis: mechanisms, diagnosis and treatment. Nat Rev Rheumatol. 2012;8:656–64.
63. Benjamin M, McGonagle D. The anatomical basis for disease localisation in seronegative spondyloarthropathy at entheses and related sites. J Anat. 2001;199:503–26.
64. Dihlmann W, Bandick J. Die Gelenksilhouette - das Informationspotential der Roentgenstrahlen. Berlin: Springer; 1995.
65. Hirtler L, Platzgummer H, Kainberger F. Pseudoerosions of the hands and feet in rheumatoid arthritis: anatomical concepts and redefinitions based on a systematic review. (in preparation) 2018.
66. McQueen F, Østergaard M, Peterfy C, Lassere M, Ejbjerg B, Bird P, O'Connor P, Genant H, Shnier R, Emery P, Edmonds J, Conaghan P. Pitfalls in scoring MR images of rheumatoid arthritis wrist and metacarpophalangeal joints. Ann Rheum Dis. 2005;64:i48–55.
67. Mangnus L, van Steenbergen HW, Lindqvist E, Brouwer E, Reijnierse M, Huizinga TW, Gregersen PK, Berglin E, Rantapää-Dahlqvist S, van der Heijde D, van der Helm-van Mil AH. Studies on ageing and the severity of radiographic joint damage in rheumatoid arthritis. Arthritis Res Ther. 2015;17:222.
68. Cimmino MA, Bountis C, Silvestri E, Garlaschi G, Accardo S. An appraisal of magnetic resonance imaging of the wrist in rheumatoid arthritis. Semin Arthritis Rheum. 2000;30:180–95.
69. Dohn UM, Ejbjerg BJ, Hasselquist M, Narvestad E, Moller J, Thomsen HS, Ostergaard M. Detection of bone erosions in rheumatoid arthritis wrist joints with magnetic resonance imaging, computed tomography and radiography. Arthritis Res Ther. 2008;10:R25.
70. Wawer R, Budzik JF, Demondion X, Forzy G, Cotten A. Carpal pseudoerosions: a plain X-ray interpretation pitfall. Skelet Radiol. 2014;43:1377–85.

Sonographic Terminology

5

Peter Vince Balint and Peter Mandl

Key to any sonographic technique is the position of the transducer in relation to the structure, organ or body part examined. This is achieved by providing first the anatomical, orthogonal plane utilized for the given scan (Table 5.1).

In addition to the anatomical plane describing the position of the transducer in relation to the axis of the examined structure, directional terms are commonly utilized to provide a more accurate location in relation to the structure itself (Table 5.2).

Furthermore, in particular for the purpose of joints, terms of motion may be provided when aiming to specify their position (Table 5.3). For the purpose of reporting the side examined (i.e. right-left, bilateral-unilateral) must also be specified.

When describing the scans performed, the two most commonly used transducer orientations are the long axis (or longitudinal) and short axis (or transverse) views (Table 5.4).

When reporting a sonographic finding, the echogenicity of a structure or lesion is a key property that needs to be addressed (Table 5.5).

Finally, when documenting images both for the purpose of keeping clinical records, as well as for scientific publication, the image must be oriented correctly. The orientation of images in this book follows the recommendations of the EULAR Standardized Procedures for Ultrasound Imaging in Rheumatology [2, 3] (Fig. 5.1). An exception to this are certain images in Chap. 7 Sonopathology (Articular and Periarticular) which are oriented inversely (proximal and radial on left). In order to make orientation clear, each ultrasound image is labelled accordingly.

P. V. Balint, MD, PhD, FRCP (✉)
3rd Rheumatology Department, National Institute of Rheumatology and Physiotherapy, Budapest, Hungary

P. Mandl, MD, PhD
Division of Rheumatology, Department of Internal Medicine III, Medical University of Vienna, Vienna, Austria

P. V. Balint, P. Mandl (eds.), *Ultrasonography of the Hand in Rheumatology*,
https://doi.org/10.1007/978-3-319-74207-6_5

Table 5.1 Anatomical planes[a]

1. Sagittal (or median) and parasagittal (or paramedian)
2. Coronal or frontal
3. Transverse or horizontal or axial

[a]The anatomical planes sagittal, coronal and transverse will be used in this book to describe the position of the transducer in relation to the evaluated structure(s) or region

Table 5.2 Directional terms[a]

1. Superior-inferior or cranial-caudal
2. Anterior-posterior or ventral-dorsal
3. Medial-lateral and intermediate
4. Proximal-distal
5. Superficial-profound/deep

[a]The directional terms superior-inferior, medial-lateral, ventral-dorsal, proximal-distal, superficial and deep will be used in this book to describe the position of the transducer in relation to the evaluated structure(s) or region. For the purpose of the hand, the term palmar is commonly utilized to describe the anterior direction. Similarly, the terms ulnar and radial are used at times to indicate the medial and lateral aspect, respectively. Anatomical terminology used in this book follows the guidelines set forth by the Federative Committee on Anatomical Terminology [1]

Table 5.3 Terms of motion

1. Flexion-extension
2. Abduction-adduction
3. Lateral (external) rotation-medial (internal) rotation
4. Supination and pronation

Table 5.4 Transducer orientation/view

1. Longitudinal or long axis view: Parallel to the long axis of the body, extremity or examined anatomical structure
2. Transverse or short axis view: Perpendicular to the long axis of the body, extremity or examined anatomical structure

Table 5.5 Terms of echogenicity

1. Anechoic: Area characterized by lack of echoes/interfaces (appearing as black)
2. Echoic: Area characterized by echoes/interfaces (appearing as white)
3. Hyperechoic: Area appearing more echoic as compared to its environment (appearing as various shades of light grey)
4. Hypoechoic: Area appearing less echoic as compared to its environment (appearing as various shades of dark grey)

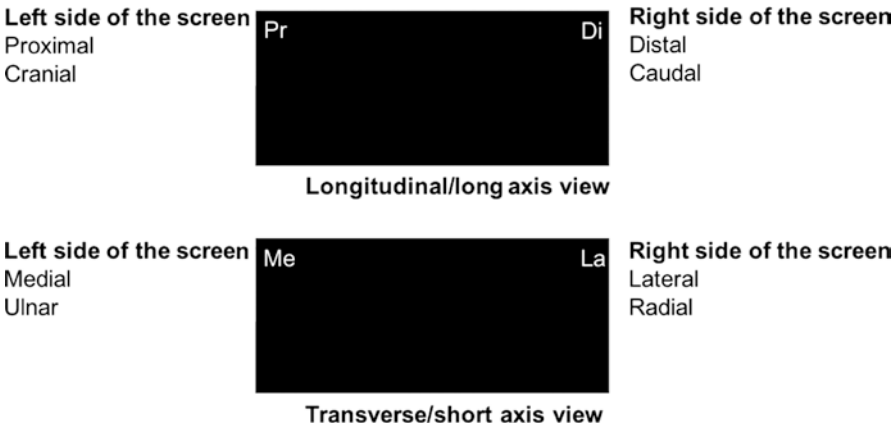

Fig. 5.1 Image orientation showing labels

References

1. Federative Committee on Anatomical Terminology (FCAT). Terminologia anatomica: international anatomical terminology. Stuttgart: Georg Thieme Verlag. p. 300. 1998. ISBN-10: 3-13-114361-4. ISBN-13: 978-3-13-114361-7.
2. Backhaus M, Burmester GR, Gerber T, Grassi W, Machold KP, Swen WA, Wakefield RJ, Manger B. Guidelines for musculoskeletal ultrasound in rheumatology. Ann Rheum Dis. 2001;60:641–9.
3. Möller I, Janta I, Backhaus M, Ohrndorf S, Bong DA, Martinoli C, Filippucci E, Sconfienza LM, Terslev L, Damjanov N, Hammer HB, Sudol-Szopinska I, Grassi W, Balint P, Bruyn GAW, D'Agostino MA, Hollander D, Siddle HJ, Supp G, Schmidt WA, Iagnocco A, Koski J, Kane D, Fodor D, Bruns A, Mandl P, Kaeley GS, Micu M, Ho C, Vlad V, Chávez-López M, Filippou G, Cerón CE, Nestorova R, Quintero M, Wakefield R, Carmona L, Naredo E. The 2017 EULAR standardised procedures for ultrasound imaging in rheumatology. Ann Rheum Dis. 2017;76:1974–9.

Sonoanatomy: Physiological Structures (Articular and Periarticular)

6

Peter Mandl, Emilio Filippucci, Irina Gessl, Walter Grassi, and Peter Vince Balint

Examination Technique

As with any small, superficial joint, the wrist and the hand joints are best examined with high-frequency linear array transducers. Frequencies of 10–22 MHz are preferable [1]. Most commercially available high-resolution ultrasound systems have built-in presets for small joints and allow the user to manually save the settings selected for each type of joint as a preset. The wrist and the small joints of the hand are usually examined with the patient seated at the examination table and the palms facing up or down depending on the examined region. In certain cases, however, it may become necessary or easier to examine the hands and wrists with patient is lying either prone or supine. Care should be taken when handling the transducer to avoid putting too much pressure on the examined region as this can easily lead to erroneous findings or to the non-detection of actual pathological phenomena, in particular small fluid collections. Transducer pressure also has a significant impact on Doppler signals, either quelling the signal or generating artefacts. The transducer should be held similarly as one holds a wallet, between the thumb and the four remaining digits, with the little finger preferably resting on the examined region or on the examination table, which allows the performer to control the amount of

P. Mandl, MD, PhD (✉) · I. Gessl, MD
Division of Rheumatology, Department of Internal Medicine III, Medical University of Vienna, Vienna, Austria
e-mail: peter.mandl@meduniwien.ac.at; irina.gessl@meduniwien.ac.at

E. Filippucci, MD, PhD · W. Grassi, MD
Clinica Reumatologica, Università Politecnica delle Marche, Ospedale "C. Urbani", Ancona, Italy
e-mail: walter.grassi@univpm.it

P. V. Balint, MD, PhD, FRCP
3rd Rheumatology Department, National Institute of Rheumatology and Physiotherapy, Budapest, Hungary
e-mail: pvbalint@gmail.com

P. V. Balint, P. Mandl (eds.), *Ultrasonography of the Hand in Rheumatology*,
https://doi.org/10.1007/978-3-319-74207-6_6

pressure introduced to the region (Fig. 6.1a). An appropriate amount of ultrasound gel should be applied to the scanned joint or area (Fig. 6.1b). This technique also enables the sonographer to perform very subtle movements with the transducer and may help eliminate slight unintentional hand motion (either that of the examiner or of the patient) as seen in systole or in various forms of tremor. The transducer can be manipulated in a number of ways such as sliding, tilting, rocking, rotating and compressing to allow more adequate assessment of structures [2].

Depending on the position of the transducer in relation to the axis of the examined structure, sonographers commonly use the terms long axis (generally, but not always corresponding to the longitudinal plane) or short axis view (generally, but not always corresponding to the transverse plane). Scanning in both the longitudinal and transverse planes is also mandatory to adequately identify certain phenomena, e.g. osteophytes, tenosynovitis, etc. [3]. Most sonographers begin the examination of the small joints of the hand in the sagittal plane which allows the assessment of most small joints (e.g. metacarpophalangeal (MCP), proximal and distal interphalangeal (PIP and DIP), radiocarpal, etc.) in the long axis, which in certain cases may be sufficient for the detection and assessment of pathology (Fig. 6.2a). It is important to note that unlike many other joints of the body, almost all of the joints of the hand are accessible to ultrasound (acoustic window); however, because bone is a strong reflector, we cannot acquire an image showing any given joint in its entirety.

Tendon and nerve pathology, particularly in the wrist as well as several other important structures such as the scapholunate ligament, may be more readily detected in the transverse plane (short axis) (Fig. 6.2b), while the coronal plane is indispensable for the examination of, e.g. the radius and the ulna as well as the collateral ligaments of the second and fifth MCP joints, etc. (Fig. 6.2c). Most sonographers begin their examination at the dorsal aspect before moving to the radial and ulnar aspects and finish by examining the palmar (also known as volar) aspect.

Finally, the authors advise the reader to adhere to the EULAR standardized procedures for ultrasound imaging in rheumatology [4]. Beyond these guidelines, we advise sonographers to perform real-time scans of each region in all necessary planes before

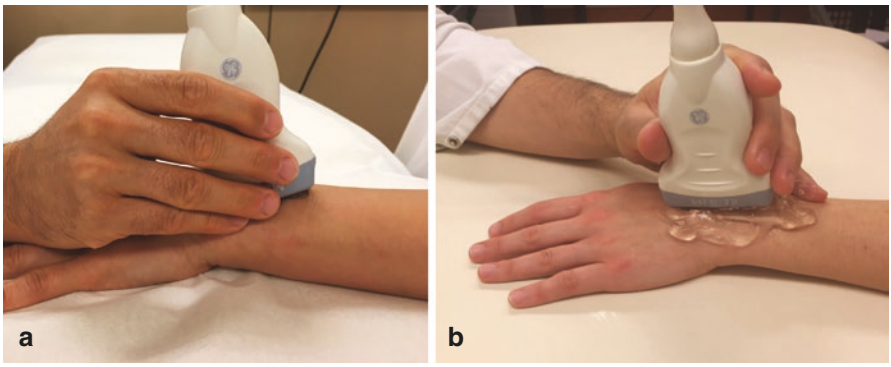

Fig. 6.1 (**a**) Appropriate handling of the ultrasound transducer; (**b**) Appropriate amount of gel during the examination

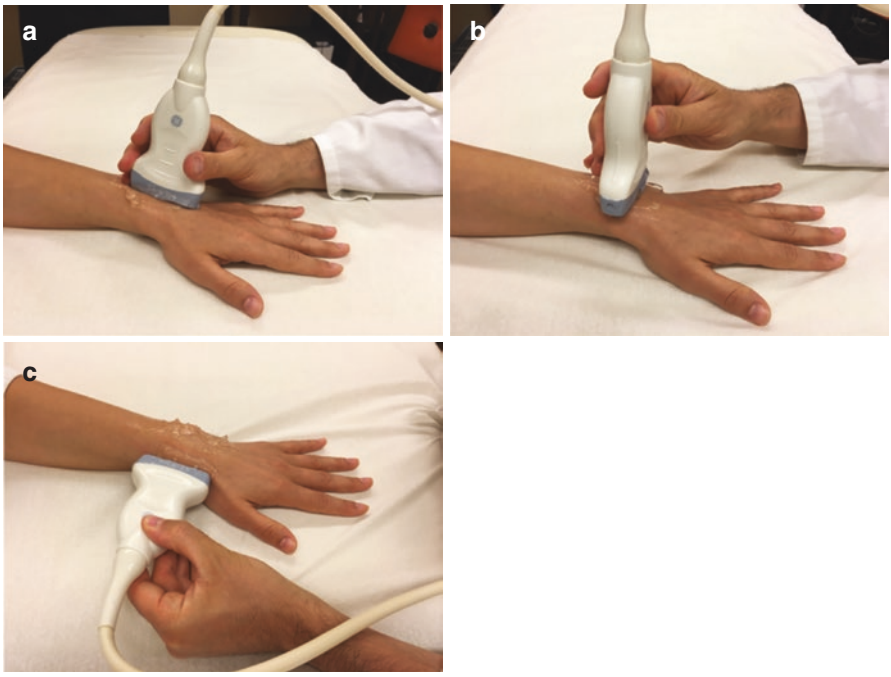

Fig. 6.2 Scanning of the wrist in various planes. (**a**) sagittal; (**b**) transverse; (**c**) coronal plane

attempting to detect and diagnose pathology using ultrasound. Dynamic imaging, i.e. moving the joints, tendons or muscles and acquiring video clips help obtain vital information about the function of the examined structure and may also improve the identification of different interfaces, especially that of nerves and tendons within the image. It is also important to try to assess, as far as possible, the entire anatomical structure or pathological lesion of interest and in case of pathology to correctly identify cases where the extent or type of lesion requires the performance of additional imaging methods, such as computer tomography or magnetic resonance tomography.

Sonoanatomy of the Wrist and Hand

Based on the specific clinical presentation and pathology, different scanning planes and patient positions may be utilized to obtain the best possible images required for the appropriate evaluation of the ultrasound findings. Appropriate positioning of the joint may aid the evaluation of certain structures. Hyperextension of the MCP joints may facilitate the visualization of small amounts of fluid in the dorsal aspect. Forming a fist is useful when attempting to assess the cartilage coating of the metacarpal head or that of the phalanges in the PIP joints. These positions may also aid in detecting small irregularities of the bony cortex in these areas. Care should be taken, however, as the same position may quell or eliminate Doppler signal [2, 5] and may also displace small fluid collections. The authors have observed a similar

phenomenon during abduction or extension of the thumb. A simple dynamic examination may also aid in delineating adjacent anatomical structures and consequently pathological lesions, e.g. flexing the distal phalanx helps in distinguishing the superficial and profound flexor tendons.

Dorsal Aspect of the Wrist

The ultrasound examination of the dorsal wrist commonly begins with a longitudinal scan in the midline of the hand (third ray). In this view, the bony landmarks from proximal to distal include the distal radial epiphysis, the lunate and the capitate as well as the base of the third metacarpal bone. The extensor tendons of the fourth compartment, the extensor retinaculum and the intercarpal joint recesses can also be visualized clearly (Fig. 6.3). This image is particularly helpful when evaluating joint fluid and synovial thickening and is particularly useful for distinguishing intercarpal synovitis from extensor tendon tenosynovitis which may have very similar clinical

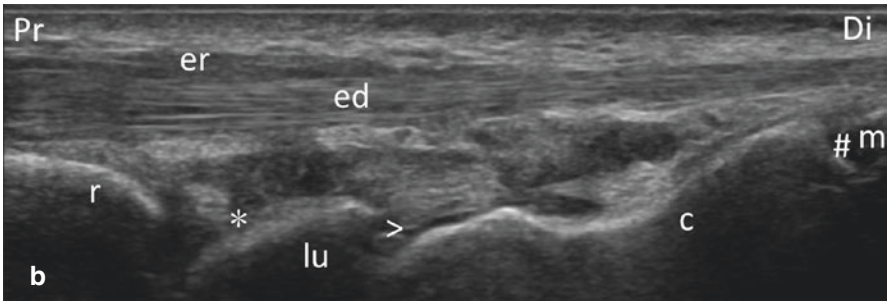

Fig. 6.3 Dorsal midline scan of the wrist. (**a**) Transducer position for the longitudinal scan; (**b**) ultrasound image of the longitudinal scan. ***c*** capitate, *ed* extensor digitorum, *er* extensor retinaculum, *lu* lunate, *m* metacarpal bone, *r* radius, *arrowhead* intercarpal recess, *asterisk* radiocarpal recess, *hashtag* carpometacarpal joint, *Pr* proximal, *Di* distal

presentation. Shifting the transducer in a sweeping motion from midline in the radial or ulnar direction allows the assessment of each group of extensor tendons in the long axis (see compartments below) as well as a view of the carpal bones and metacarpals. Moving the transducer proximally and to the radial or ulnar side provides an extensive view of the bony contour of the radius or ulna and of the triangular fibrocartilage complex on the ulnar side (Figs. 6.4 and 6.5).

The gap between the styloid process of the ulna and the triquetrum contains the triangular fibrocartilage complex (TFCC), a structure which can be evaluated only partially by ultrasound by means of coronal images. The TFCC is optimally visualized with the forearm pronated, and the humerus internally rotated at the shoulder before the body with the hand resting on its edge on the table, i.e. halfway between pronation and supination. With the transducer positioned in line with the ulna, just distal to the ulnar styloid, the TFCC appears as a homogeneous, echogenic triangular structure deep to the extensor carpi ulnaris tendon (Fig. 6.5) [6]. Care should be taken when judging findings with regard to the TFCC as we can evaluate this structure only partly by ultrasound.

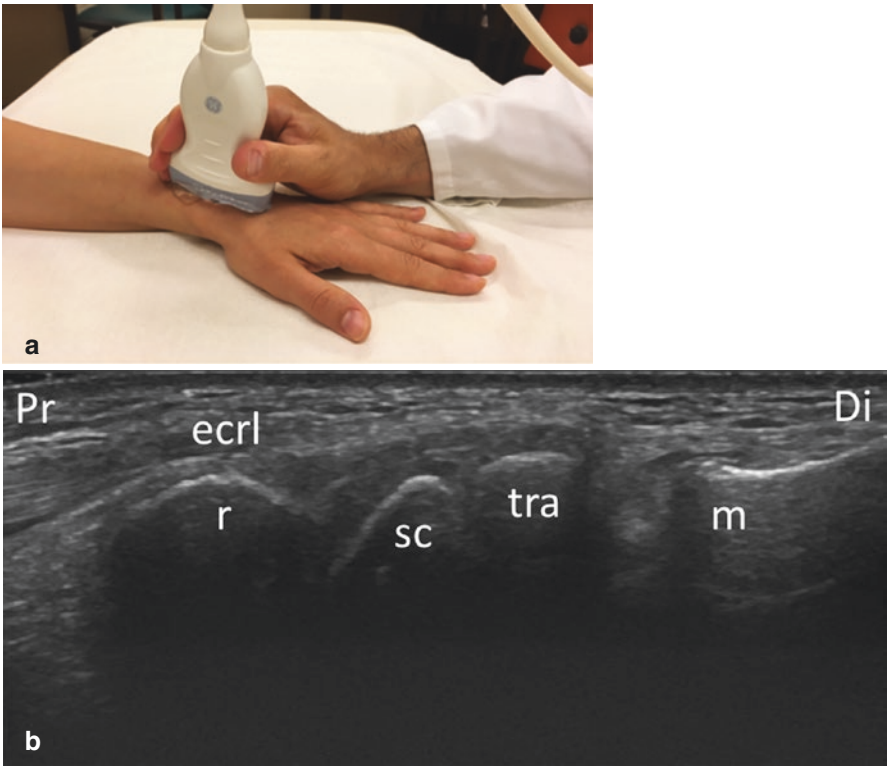

Fig. 6.4 Dorsal scan of the radiocarpal joint over the scaphoid. (**a**) Transducer position for the longitudinal scan; (**b**) ultrasound image of the longitudinal scan. *ecrl* extensor carpi radialis longus, *m* metacarpal bone, *r* radius, *sc* scaphoid, *tra* trapezium, *Pr* proximal, *Di* distal

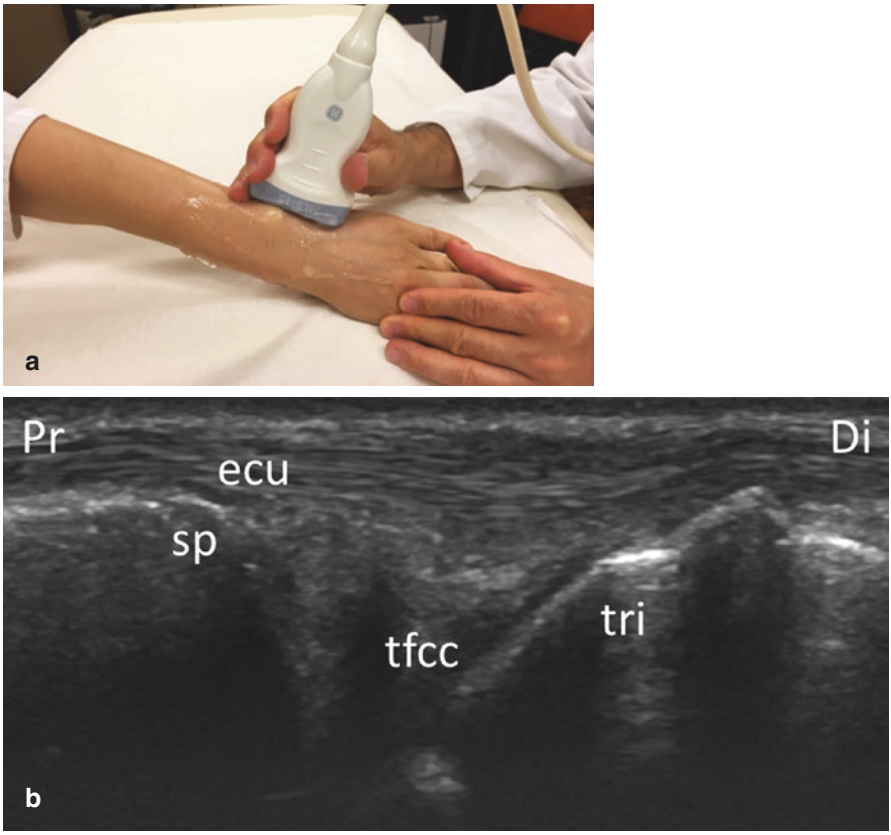

Fig. 6.5 Coronal scan of the ulnar styloid and the triangular fibrocartilage complex. (**a**) Transducer position for the coronal scan; (**b**) ultrasound image of the coronal scan. *ecu* extensor carpi ulnaris tendon, *sp* ulnar styloid process, *tfcc* triangular fibrocartilage complex; *tri* triquetrum, *Pr* proximal, *Di* distal

We continue the ultrasound examination of the dorsal wrist with the transverse scan. While individual extensor tendons may also be recognized and evaluated for changes in tendon integrity and tendon function on the longitudinal scan, it is the dorsal transverse scan which enables their proper identification in their respective compartments. Longitudinal scans of the extensor tendons may help in evaluating the integrity of tendons and assess their dynamic motion in detail. Dynamic scanning of the tendons may be facilitated by moving the appropriate fingers. Respective tendons may be identified according to their position and appearance in relation to the prominent bony landmark on the dorsal radius known as Lister's tubercle, which separates the second and third compartments (Fig. 6.6).

Particular care must be taken, when scanning tendons, as they commonly exhibit artefacts [7]. Anisotropy, an angle-generated artefact which is characteristic of tissues containing multiple parallel linear sound interfaces (e.g. tendons, ligaments), leads to the preferential reflection of the ultrasound beam in one direction.

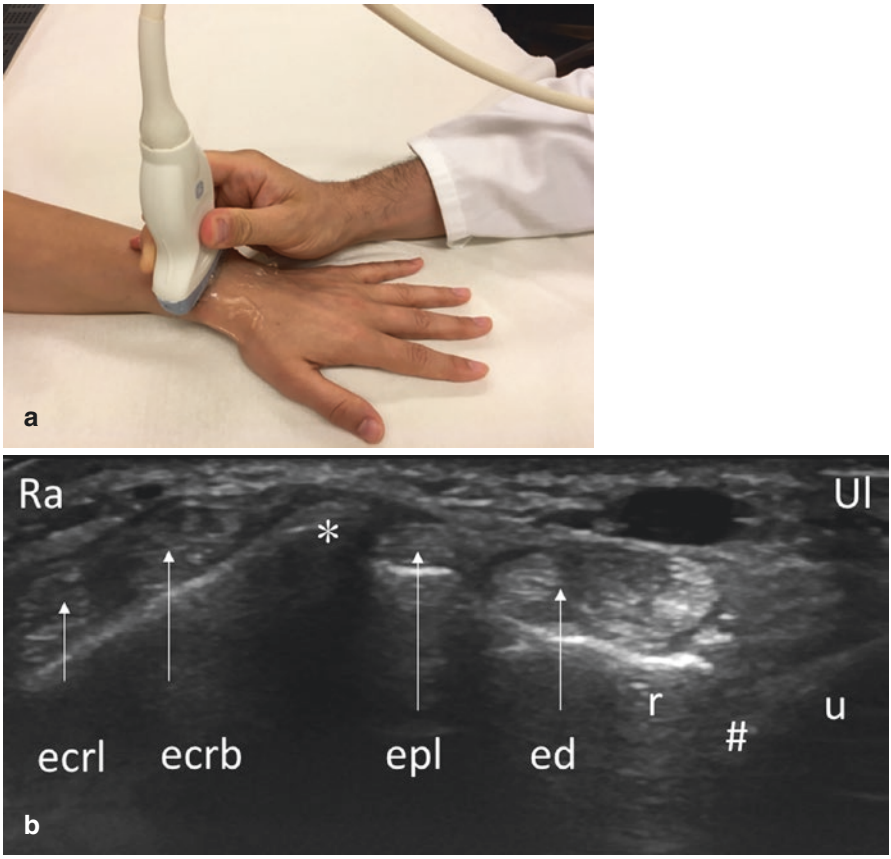

Fig. 6.6 Transverse scan of the wrist depicting Lister's tubercle. (**a**) Transducer position; (**b**) ultrasound image. *ecrb* extensor carpi radialis brevis tendon, *ed* extensor digitorum tendon, *ecrl* extensor carpi radialis longus tendon, *epl* extensor pollicis longus tendon, *r* radius, *u* ulna, *asterisk* Lister's tubercle, *hashtag* distal radioulnar joint, *Ra* radial, *Ul* ulnar

Anisotropy may also be useful when identifying tendons and can be corrected by modifying the insonation angle of the ultrasound beam (i.e. by tilting the transducer). Slice thickness or edge artefacts consist of loss of signal and distal acoustic shadowing at the edge of the tendons that can mimic or obscure fluid or inflammation in the paratenon. Slice thickness artefacts can be reduced by the use of multiple focal zones. If a single focal zone is used, it must be set to the depth of the main interest [7].

Extensor Compartments

The first extensor compartment contains the abductor pollicis longus (APL) and extensor pollicis brevis (EPB) tendons. It is situated lateral to the radial styloid process (Fig. 6.7); therefore it is best examined with the ulnar edge of the hand resting on

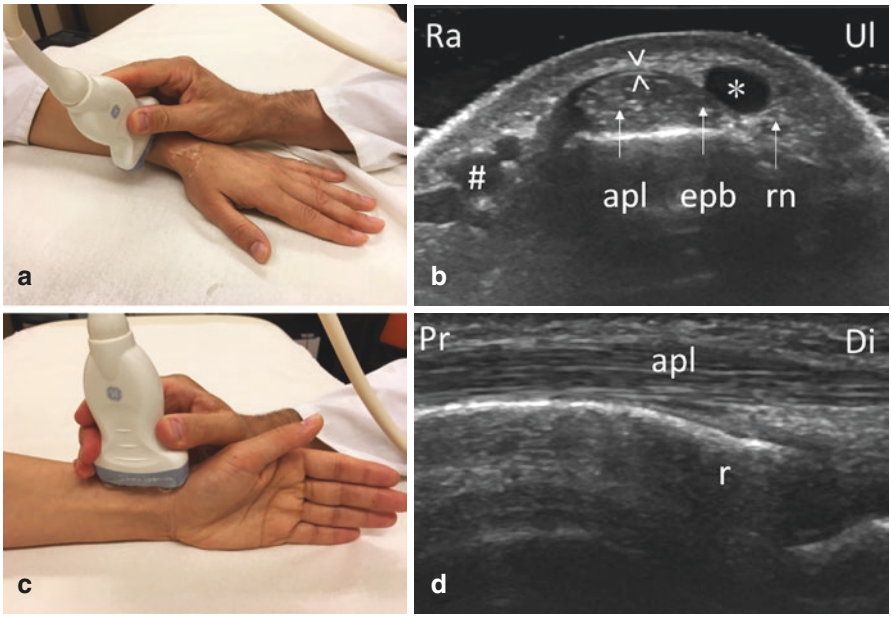

Fig. 6.7 Transverse and longitudinal scans of the first extensor compartment. (**a**) Transducer position for the transverse scan; (**b**) ultrasound image of the transverse scan; (**c**) transducer position for the longitudinal scan; (**d**) ultrasound image of the longitudinal scan. *apl* abductor pollicis longus, *epb* extensor pollicis brevis, *r* radius, *rn* radial nerve, *asterisk* cephalic vein, *hashtag* radial artery, *arrowheads* extensor retinaculum, *Di* distal, *Pr* proximal, *Ra* radial, *Ul* ulnar

the table, i.e. the hand held halfway between pronation and supination. With the transducer positioned over the lateral aspect of the radial styloid, the APL is the slightly thicker-appearing tendon in the palmar position, and EPB is the relatively thinner tendon in the dorsal position. The first compartment travels through and constitutes the lateral or radial border of a region known as the anatomic snuffbox, whose floor is formed by the radial styloid, the scaphoid, the trapezium and the metacarpal base of the thumb [6]. In addition to the second extensor compartment, it also contains the superficial branch of the radial nerve, running superficial to the compartment, and the radial artery and accompanying veins running deep to the compartment. The cephalic vein positioned dorsal to the EPB tendon as well as individual branches of the radial nerve running ventral to dorsal to the tendons may also be observed in this scanning position. In general, extensor tendons are known to exhibit different variations with respect to their attachment and anatomic variation [8]. The APL tendon should be followed distally over the scaphoid to assess for possible accessory tendons and slips [9] as these were shown to be associated with the development of de Quervain's tenosynovitis, a thickening of the tendon sheath of the APL and EPB tendons [10].

With the hand positioned palm down on the examination table, shifting the transducer medially in the transverse plane allows the visualization of the second

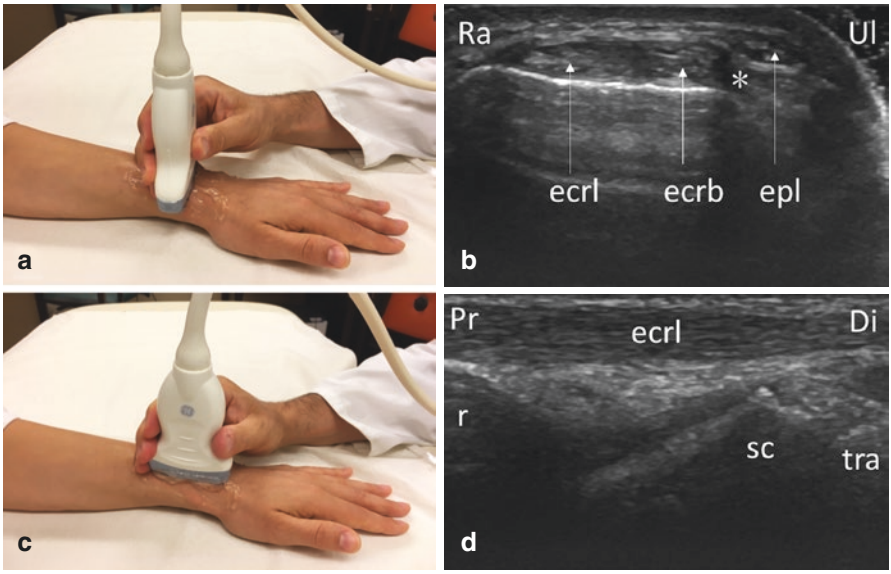

Fig. 6.8 Transverse and longitudinal scans of the second extensor compartment. (**a**) Transducer position for the transverse scan; (**b**) ultrasound image of the transverse scan; (**c**) transducer position for the longitudinal scan; (**d**) ultrasound image of the longitudinal scan. *ecrb* extensor carpi radialis brevis tendon, *ecrl* extensor carpi radialis longus tendon, *epl* extensor pollicis longus tendon, *rad* radius, *sc* scaphoid, *tra* trapezium, *asterisk* Lister's tubercle, *Di* distal, *Pr* proximal, *Ra* radial, *Ul* ulnar

compartment, which contains the twin tendons of extensor carpi radialis longus (ECRL) on the radial side of the compartment and extensor carpi radialis brevis (ECRB) on the ulnar side of the compartment (Fig. 6.8). Located on the radial side of Lister's tubercle, the two tendons, which are of almost identical size, run side by side over the radial styloid process and are among the most easily recognizable of the compartments. Sweeping the transducer proximally over the tendons demonstrates the APL and EPB muscles appearing superficial to them at the level of the distal forearm to reach the first compartment (Fig. 6.9). The ECRL and ECRB tendons insert onto the base of the second and third metacarpal bone, respectively. Moving the transducer over and slightly distal to Lister's tubercle allows us to visualize the scapholunate ligament, which appears as an echogenic fibrillar structure between the lunate and scaphoid bones (Fig. 6.10). The ligament is depicted under ultrasound in approximately 80% of individuals with normal anatomy [11]; however, the absence thereof under ultrasound does not necessarily indicate injury [12]. Moving the transducer slightly to the ulnar side allows the visualization of the dorsal lunotriquetral ligament which appears similar (Fig. 6.10). Ulnar deviation of the wrist may be useful to assess the integrity of this ligament. Shifting the transducer in the proximal direction allows the assessment of the dorsal radiotriquetral

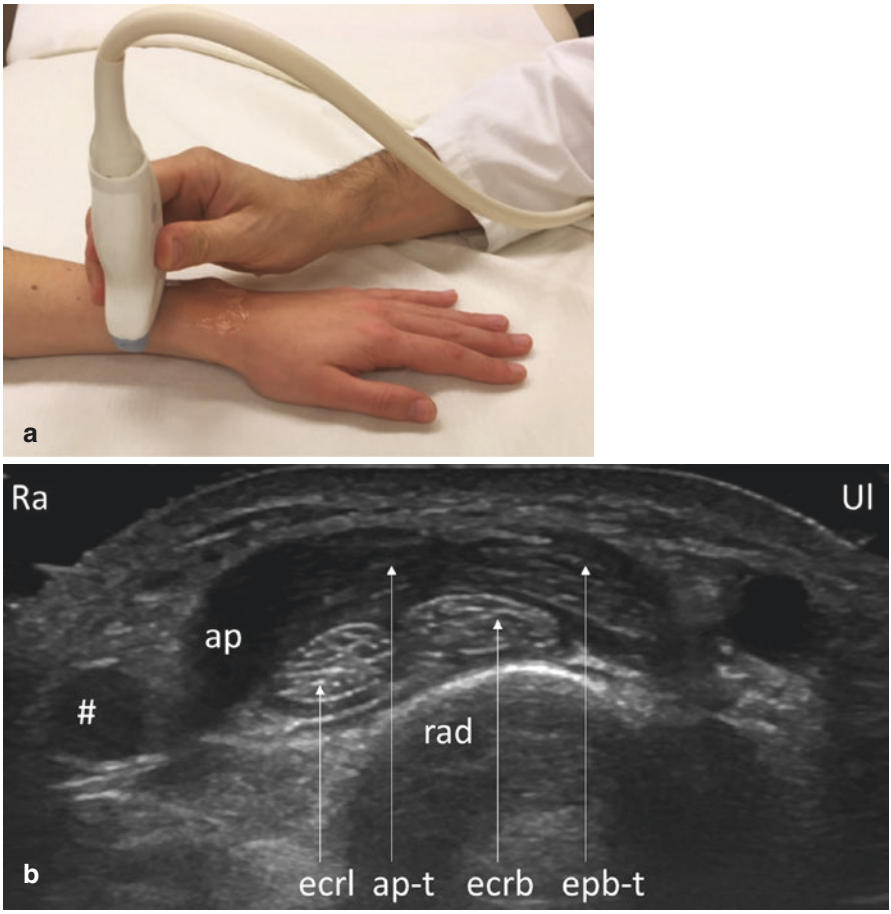

Fig. 6.9 Transverse scan of extensor pollicis brevis and abductor pollicis longus tendons crossing over the second compartment (extensor carpi radialis brevis and longus tendons). (**a**) Transducer position for the transverse scan; (**b**) ultrasound image of the transverse scan. *ap* abductor pollicis muscle, *ap-t* abductor pollicis tendon, *ecrb* extensor carpi radialis brevis tendon, *ecrl* extensor carpi radialis longus tendon, *epb* extensor pollicis brevis tendon, *hashtag* radial artery, *Ra* radial, *Ul* ulnar

ligament which originates from the dorsal side of the distal radius, passes over the lunate and inserts on the dorsal side of the triquetrum (Fig. 6.11).

Lister's tubercle separates the second from the third compartment, with the latter compartment located on the ulnar side of the tubercle and containing the extensor pollicis longus (EPL) tendon. The EPL tendon curves around the tubercle (Fig. 6.12). A variation of Lister's tubercle features a groove; in such cases the EPL tendon may run in this groove instead of curving around the tubercle [13]. The EPL tendon forms the ulnar border of the region known as the anatomical

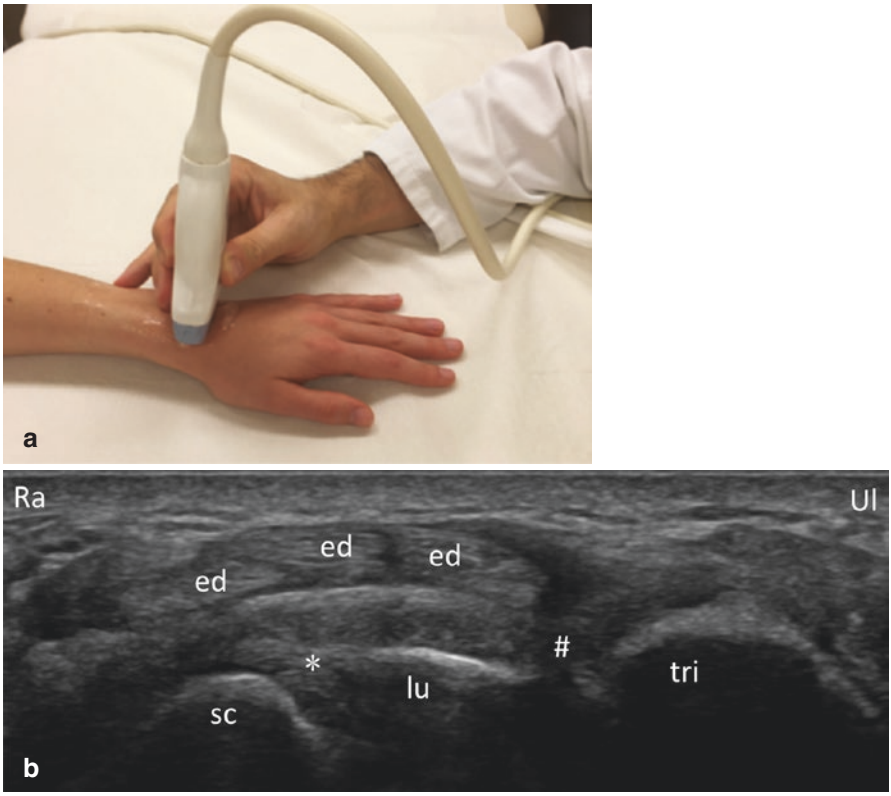

Fig. 6.10 Transverse scan of the wrist depicting the scapholunate and lunotriquetral ligaments. (**a**) Transducer position for the transverse scan; (**b**) ultrasound image of the transverse scan. *ed* extensor digitorum tendons. *lu* lunate, *sc* scaphoid, *tri* triquetrum, *asterisk* scapholunate ligament, *hashtag* lunotriquetral ligament, *Ra* radial, *Ul* ulnar

snuffbox and crosses the ECRL and ECRB tendons of the second compartment before passing up the thumb to the site of its insertion at the base of the distal phalanx (Fig. 6.13).

The fourth compartment is located over the distal radius, ulnar to the third compartment, and contains the extensor digitorum (ED) and extensor indicis (EI) tendons (Fig. 6.14). Shifting the probe in the short axis proximally and distally over the compartment facilitates the differentiation of the EI tendon, similarly to the flexion/extension of the index finger. Finger flexion/extension may also aid the differentiation of the individual tendons of the fourth compartment. The extensor retinaculum is thickest over the fourth compartment [6]. High-resolution sonography can reliably identify the distal posterior interosseous nerve; a small (1–3 mm) hypoechoic structure which can be located on the floor of this compartment as confirmed also by dissection in a recent study on cadavers [14].

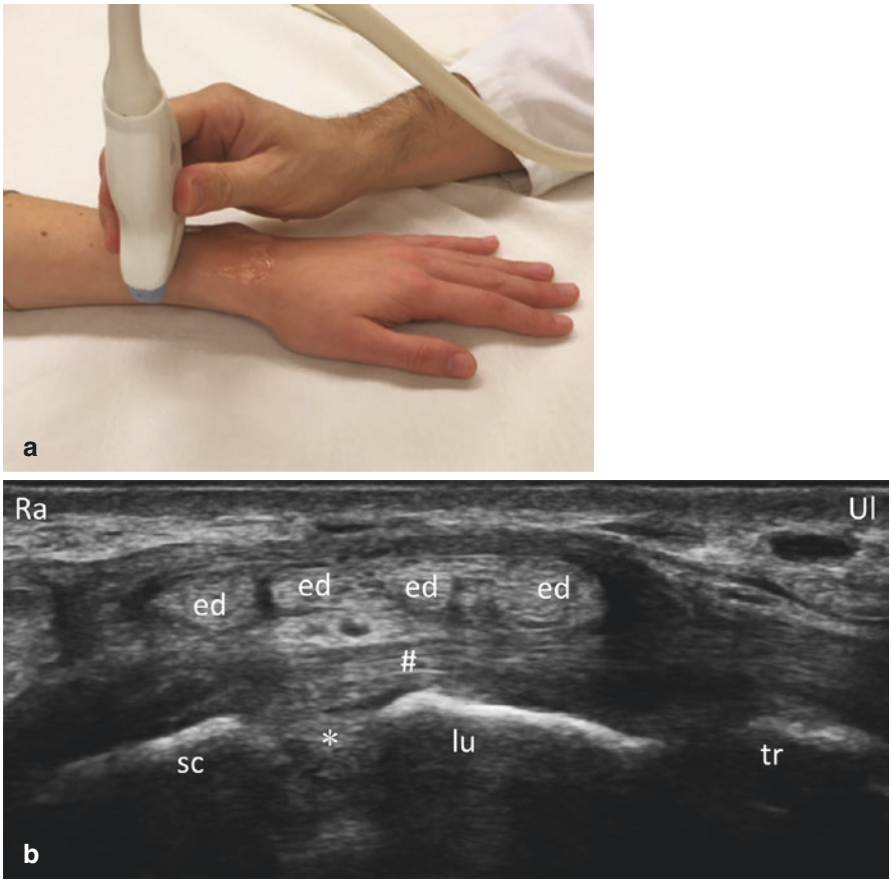

Fig. 6.11 Transverse scan of the wrist depicting the dorsal radiotriquetral ligament. (**a**) Transducer position for the transverse scan; (**b**) ultrasound image of the transverse scan. *ed* extensor digitorum tendons, *lu* lunate, *sc* scaphoid, *tr* triquetrum, *asterisk* scapholunate ligament, *hashtag* dorsal radiotriquetral ligament, *Ra* radial, *Ul* ulnar

The fifth compartment is dorsal to the distal radioulnar joint and contains the extensor digiti minimi (EDM) tendon (Fig. 6.15). Dynamic scanning in the short axis is also useful to identify this small tendon which attaches to the base of the proximal phalanx of the fifth digit.

The sixth and final compartment is located between the ulnar head and the styloid process of the ulna and contains the thick extensor carpi ulnaris (ECU) tendon (Fig. 6.16). The ECU tendon travels within a groove formed by the ulna and the styloid process of the ulna and is displaced during normal wrist or forearm movement; awareness of its movements is crucial to diagnose its dislocation or instability [15]. Tenosynovitis of the ECU tendon and erosions on the ulnar styloid are frequent findings in rheumatoid arthritis and often constitute a very early sign of disease [16].

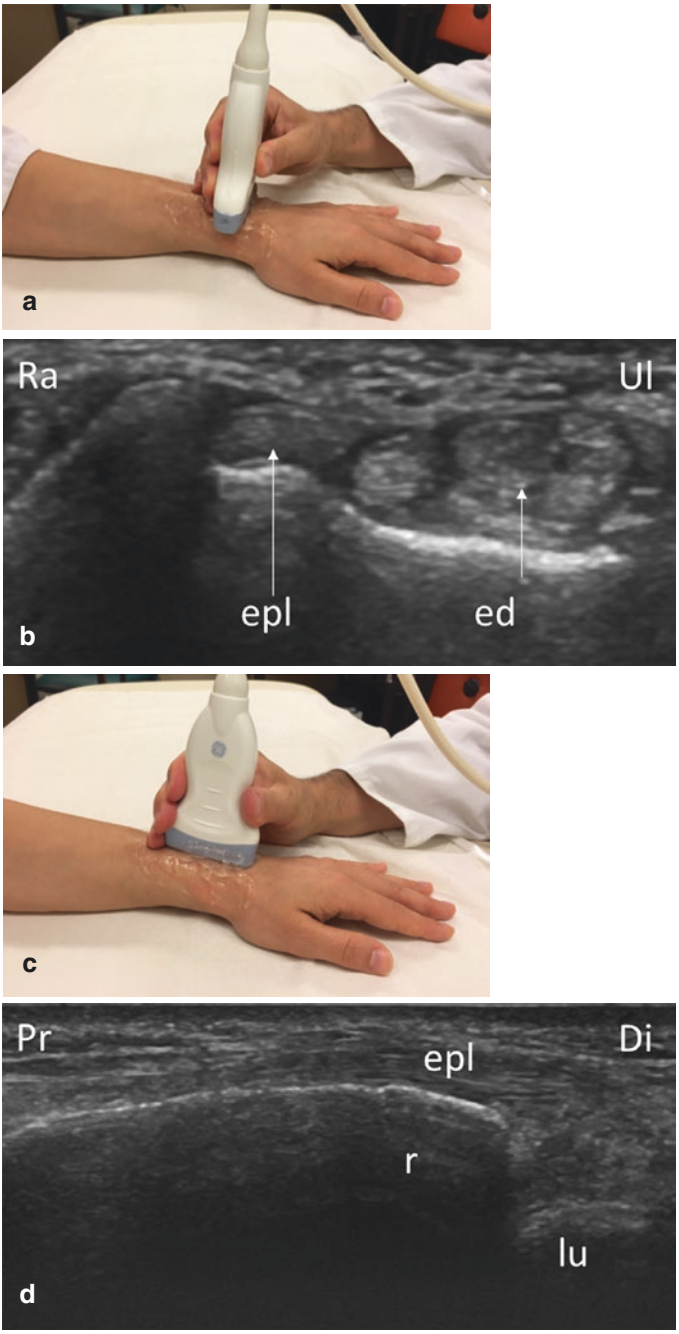

Fig. 6.12 Transverse and longitudinal scans of the third extensor compartment. (**a**) Transducer position for the transverse scan; (**b**) ultrasound image of the transverse scan; (**c**) transducer position for the longitudinal scan; (**d**) ultrasound image of the longitudinal scan. *ed* extensor digitorum tendons, epl extensor pollicis longus tendon, *lu* lunate, *r* radius, *Di* distal, *Pr* proximal, *Ra* radial, *Ul* ulnar

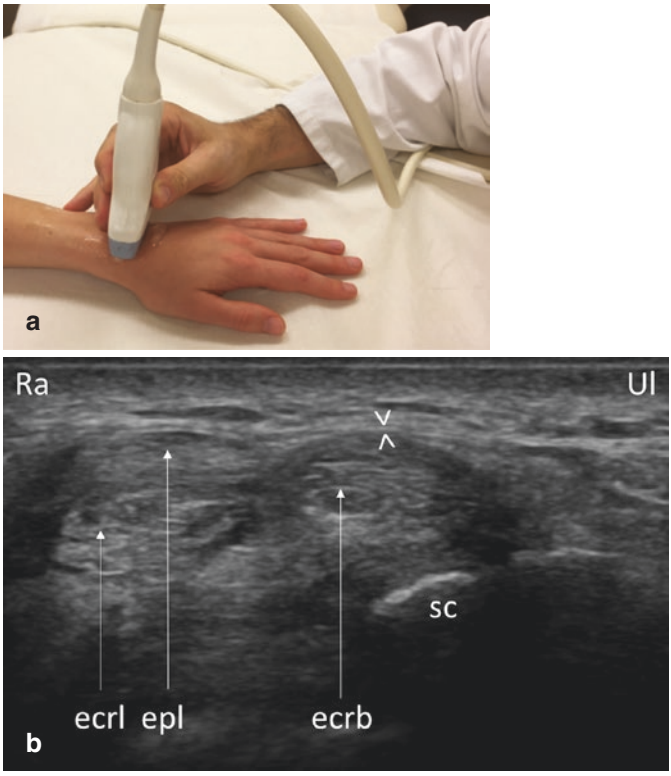

Fig. 6.13 Transverse scans of extensor pollicis longus tendon crossing over the second compartment (extensor carpi radialis brevis and longus tendons). *ecrb* extensor carpi radialis brevis tendon, *ecrl* extensor carpi radialis longus tendon, *epl* extensor pollicis longus tendon, *sc* scaphoid, *arrowheads* extensor retinaculum, *Ra* radial, *Ul* ulnar

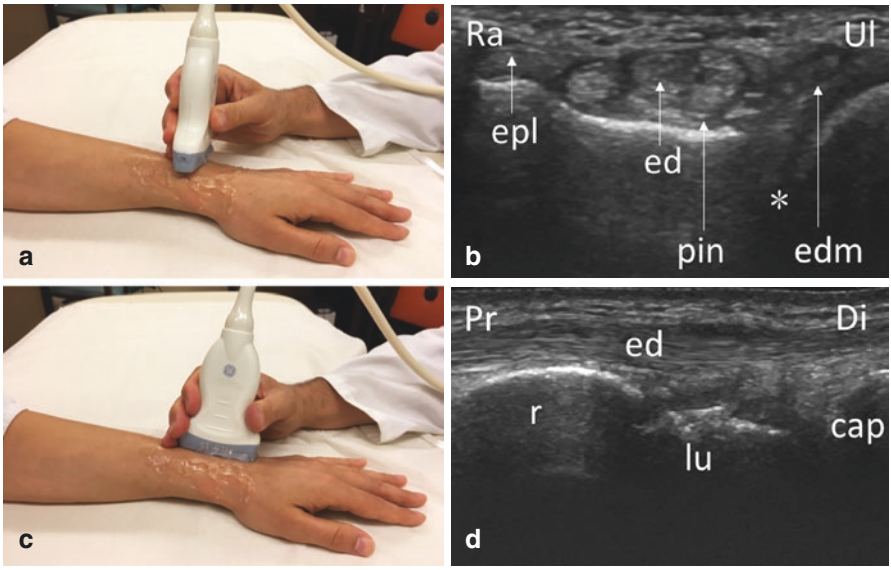

Fig. 6.14 Transverse and longitudinal scans of the fourth extensor compartment. (**a**) Transducer position for the transverse scan; (**b**) ultrasound image of the transverse scan; (**c**) transducer position for the longitudinal scan; (**d**) ultrasound image of the longitudinal scan. *cap* capitate, *ed* extensor digitorum tendons, *edm* extensor digiti minimi, epl extensor pollicis longus tendon, *lu* lunate, *pin* posterior interosseous nerve, *r* radius, *Di* distal, *Pr* proximal, *Ra* radial, *Ul* ulnar

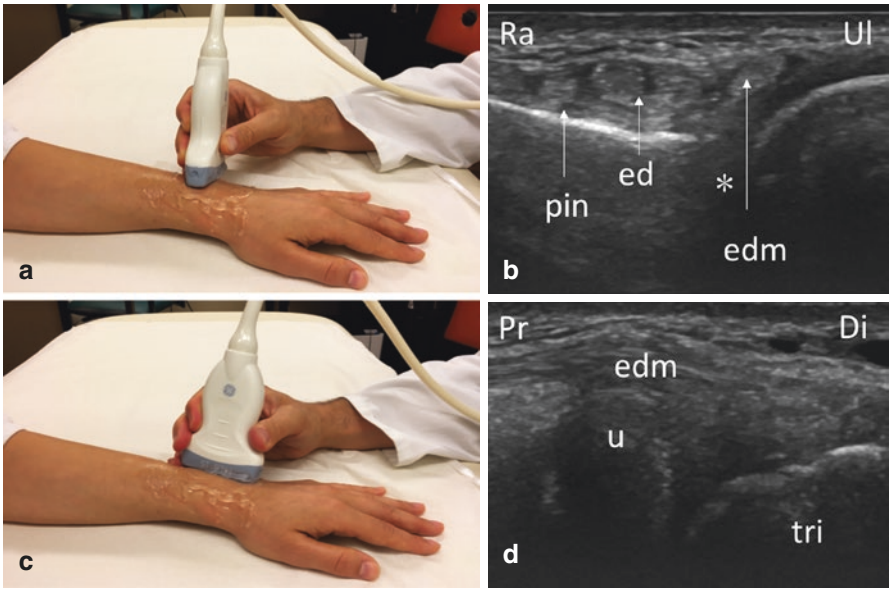

Fig. 6.15 Transverse and longitudinal scans of the fifth extensor compartment. (**a**) Transducer position for the transverse scan; (**b**) ultrasound image of the transverse scan; (**c**) transducer position for the longitudinal scan; (**d**) ultrasound image of the longitudinal scan. *ed* extensor digitorum tendons, *edm* extensor digiti minimi, *pin* posterior interosseous nerve, *tri* triquetrum, *u* ulna, *Di* distal, *Pr* proximal, *Ra* radial, *Ul* ulnar

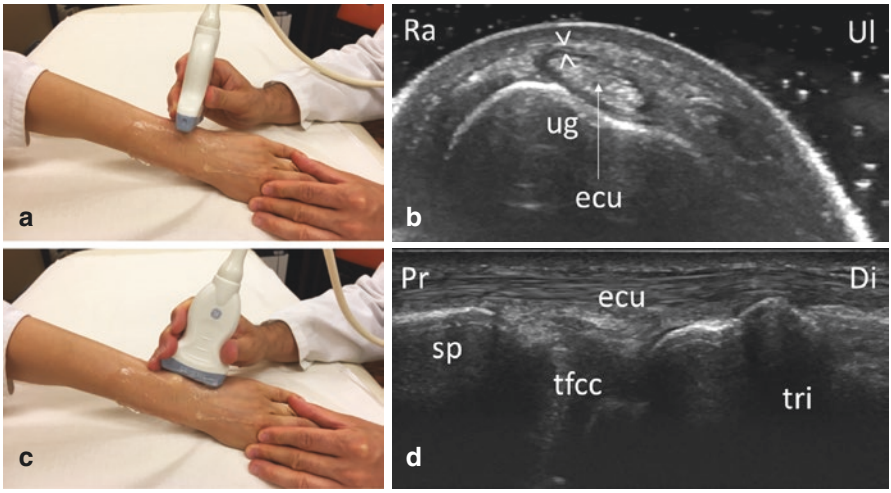

Fig. 6.16 Transverse and longitudinal scans of the sixth extensor compartment. (**a**) Transducer position for the transverse scan; (**b**) ultrasound image of the transverse scan; (**c**) transducer position for the longitudinal scan; (**d**) ultrasound image of the longitudinal scan. *ecu* extensor carpi ulnaris, *sp* ulnar styloid process, *tfcc* triangular fibrocartilage complex, *tri* triquetrum, *ug* ulnar groove, *arrowheads* extensor retinaculum, *Pr* proximal, *Di* distal, *Ra* radial, *Ul* ulnar

Palmar Aspect of the Wrist

The wrist is placed with the palm facing upward on the examination table. Pertaining to synovitis of the wrist, the longitudinal scan of the palmar wrist is somewhat less informative than the corresponding scan acquired from the dorsal aspect. It is however very helpful when evaluating flexor tendons or median nerve pathology. The bony landmarks from proximal to distal include the radius, proximal and distal carpal row and the metacarpal bones. The transverse scan of the palmar wrist provides an overview of the important structures of the flexor aspect of the wrist. The flexor retinaculum, also known as the transverse carpal ligament of the wrist, is a strong fibrous band, analogous with its extensor counterpart in function, which houses the structures of the carpal tunnel: the flexor tendons and the median nerve (Fig. 6.17).

The Carpal Tunnel

The flexor retinaculum is one of the key structures defining the carpal tunnel, which attaches medially to the pisiform bone and the hook of the hamate, splitting laterally into a superficial and a deep lamina. The thick tendon of flexor carpi radialis (FCR), housed in its synovial sheath, travels between the two laminae, separated from the tendons within the carpal tunnel. At the proximal inlet of the carpal tunnel, the FCR tendon lies ulnar to the radial artery, which is usually accompanied by one or more

veins (Fig. 6.17). Within the carpal tunnel, the flexor pollicis longus (FPL) tendon is located on the radial side followed by the four flexor digitorum superficialis (FDS) tendons, of which the third and fourth tendon lies superficial to the second and fifth tendon. Under these two tendons, we find the four flexor digitorum profundus (FDP) tendons running side by side to each other. The median nerve travels through the carpal tunnel and is commonly observed immediately under the retinaculum, deep to the tendon of the palmaris longus, when present, and superficial and ulnar to the FPL tendon (Fig. 6.18). On transverse scan, the nerve may appear elliptic, round or triangular in shape and appears to flatten progressively as it runs through the tunnel. As all peripheral nerves, the median nerve is characterized by

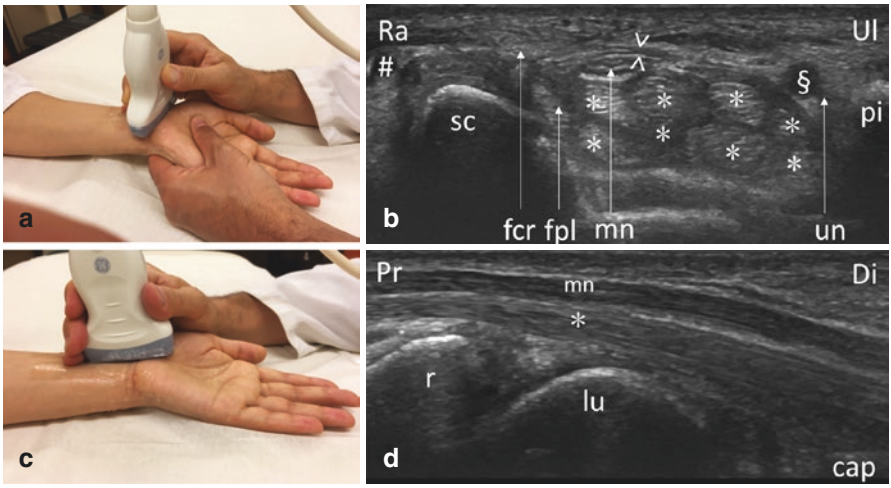

Fig. 6.17 Palmar midline scans of the wrist. (**a**) Transducer position for the transverse scan; (**b**) ultrasound image of the transverse scan; (**c**) transducer position for the longitudinal scan; (**d**) ultrasound image of the longitudinal scan. *cap* capitate, *fcr* flexor carpi radialis, *fpl* flexor pollicis longus, *lu* lunate, *mn* median nerve, *pi* pisiform, *r* radius, sc scaphoid, *u* ulnar artery, *un* ulnar nerve, *arrowheads* flexor retinaculum, *asterisk* flexor digitorum tendons, *hashtag* radial artery, *paragraph* ulnar artery, *Pr* proximal, *Di* distal, *Ra* radial, *Ul* ulnar

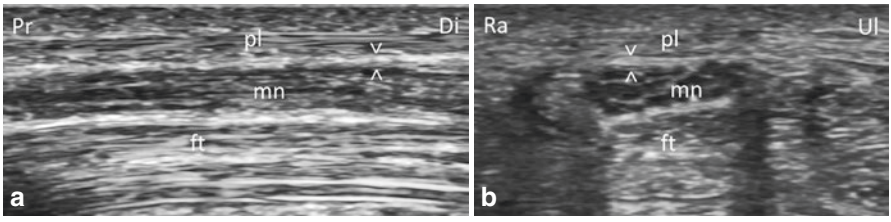

Fig. 6.18 Longitudinal and transverse image showing the different echostructure of the tendons and nerves. (**a**) Longitudinal scan; (**b**) transverse scan. *ft* flexor tendon, *mn* median nerve, *pl* palmaris longus tendon, *arrowheads* flexor retinaculum, *Pr* proximal, *Di* distal, *Ra* radial, *Ul* ulnar

discrete hyperechoic bundles on a hypoechoic background delimited by a hyperechoic margin, the epineurium, granting its characteristic honeycombed structure. It can be distinguished from tendons on longitudinal scan by performing a dynamic examination, during which tendons demonstrate motion (the nerve may also move passively during motion of the fingers) and more pronounced anisotropy (change in echogenicity according to the angle of insonation) as compared to the nerve [17]. A persistent median artery may accompany the median nerve in the forearm and wrist; this is considered a normal anatomical variant. Patients who have a persistent median artery often have a bifid proximal median nerve [18], which can be readily detected by sonography [19] (see also Fig. 7.38 in Chap. 7).

Guyon's Canal

In relation to the carpal tunnel, Guyon's canal is a much narrower, fibrosseous, oblique tunnel formed by the flexor retinaculum and the pisohamate ligament, between the pisiform bone and the hook of the hamate tunnel. The ulnar nerve bifurcates within the canal into superficial (more ulnar) and deep (more radial) branches. On transverse scan, the ulnar nerve appears as a rounded, honeycomb structure that lies medial to the ulnar artery (Fig. 6.19) and can be followed into the forearm.

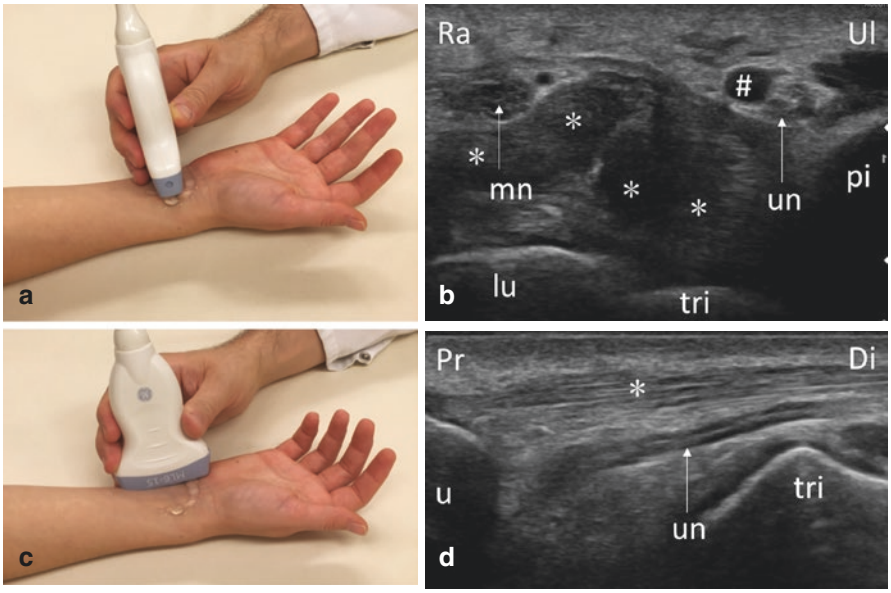

Fig. 6.19 Transverse and longitudinal scans of the ulnar nerve. (**a**) Transducer position for the transverse scan; (**b**) ultrasound image of the transverse scan; (**c**) transducer position for the longitudinal scan; (**d**) ultrasound image of the longitudinal scan. *lu* lunate, *mn* median nerve, *pi* pisiform, *tr* triquetrum, *u* ulna, *un* ulnar nerve, *asterisk* flexor digitorum tendons, *hashtag* ulnar artery, *Pr* proximal, *Di* distal, *Ra* radial, *Ul* ulnar

The Thenar Eminence

Shifting the transducer distally and turning it in an oblique fashion until it lies perpendicular to the thumb resting on the thenar, allows the visualization of the thenar eminence. This scan provides a very clear transverse image of the FPL tendon, travelling between the abductor pollicis brevis and opponens pollicis muscles. By turning the transducer 90°, the tendon can be followed, and its integrity may be assessed (Fig. 6.20). This tendon is surrounded by a synovial tendon sheath which extends from the carpal tunnel to the volar aspect of the thumb until the insertion of the FPL tendon into the base of the distal phalanx.

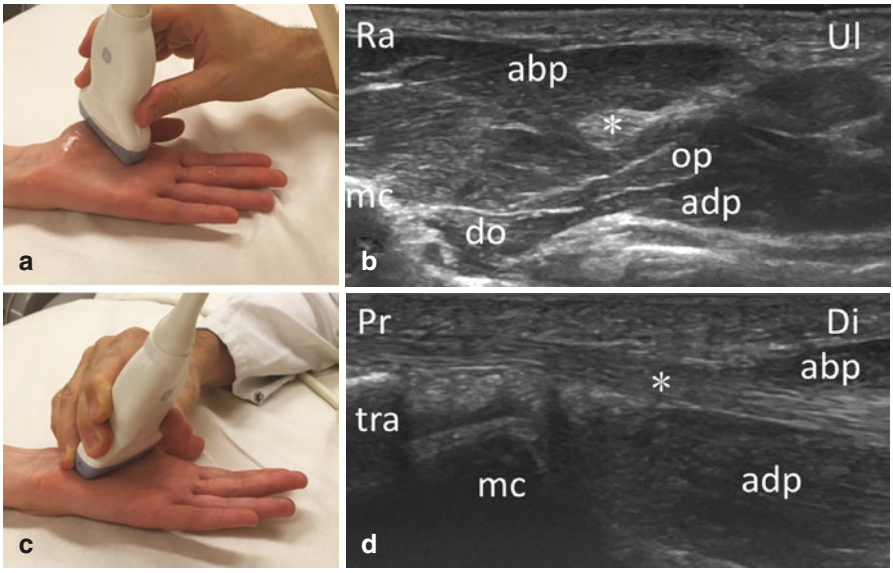

Fig. 6.20 Transverse and longitudinal scans of the flexor pollicis longus tendon. (**a**) Transducer position for the transverse scan; (**b**) ultrasound image of the transverse scan; (**c**) transducer position for the longitudinal scan; (**d**) ultrasound image of the longitudinal scan. *abp* abductor pollicis brevis muscle, *adp* adductor pollicis muscle, *do* dorsal interosseous muscle, *mc* metacarpal bone, *op* opponens pollicis muscle, *tra* trapezium, *asterisk* flexor pollicis tendon, *Pr* proximal, *Di* distal, *Ra* radial, *Ul* ulnar

Carpometacarpal Joint

The carpometacarpal (CMC) joints of the wrist link the distal row of carpal bones and the proximal bases of the metacarpal bones. Of these joints, the CMC joint of the thumb, known also as first CMC joint or trapeziometacarpal (TMC) joint, differs significantly from the other four CMC joints and is the joint, which is routinely scanned by rheumatologist experts in ultrasound, mainly due to its common involvement in trapeziometacarpal osteoarthritis (Fig. 6.21). This joint can be scanned on the dorsal, lateral and volar sides, while the ulnar aspect is impossible to be visualized by ultrasound.

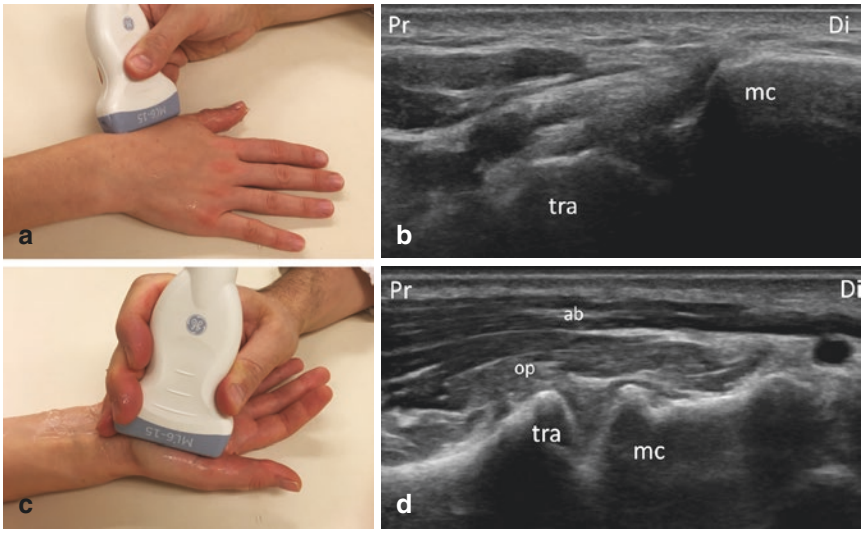

Fig. 6.21 Longitudinal scans of the first carpometacarpal (trapeziometacarpal) joint. (**a**) Transducer position for the coronal aspect; (**b**) ultrasound image of the coronal aspect; (**c**) transducer position for the volar aspect; (**d**) ultrasound image of the volar aspect. *ab* abductor pollicis, *mc* metacarpal bone, *op* opponens muscle, *tr* trapezium, *Di* distal, *Pr* proximal

Metacarpophalangeal Joint

The metacarpophalangeal (MCP) joint is a frequently involved joint in patients with different rheumatic diseases. While the anatomical features of the metacarpal bones and of the MCP joints differ slightly depending on the digit, they all share the same basic structure and function [20] (Fig. 6.22). The head of the metacarpal bone is oblong and slightly elongated in the dorso-palmar axis; although it may be irregular, the head has a smooth convex intraarticular part, while the extra-articular areas of the head are rough and contain a medial and lateral tubercle for the attachment of the collateral ligaments, as well as an elevated ridge surrounding the intraarticular smooth area. At the margin of the articular surface, multiple small vascular foramina house vessels known as nutritional or feeding vessels (see also Fig. 7.8 in Chap. 7). The dorsal aspect of the MCP joint also contains a triangular soft-tissue structure known as the triangular or dorsal fat pad which is continuous with the joint capsule. On longitudinal images the dorsal fat pad appears as a slightly echoic homogeneous triangular structure located between the metacarpal head and the base of the proximal phalanx under the extensor tendon. Above the dorsal fat pad, the respective extensor tendon may be visualized based on its characteristic fibrillar pattern; finger movement often facilitates detection. This structure has a rich vascular network and may act among many things, as a spacer, similar in function to the fat pad in the dorsal aspect of the joint (Fig. 6.23). On the palmar aspect, the MCP joint contains the volar plate. One difference between the two structures, however, is that unlike the dorsal fat pad, the volar plate is attached also to the base of the phalanx. This,

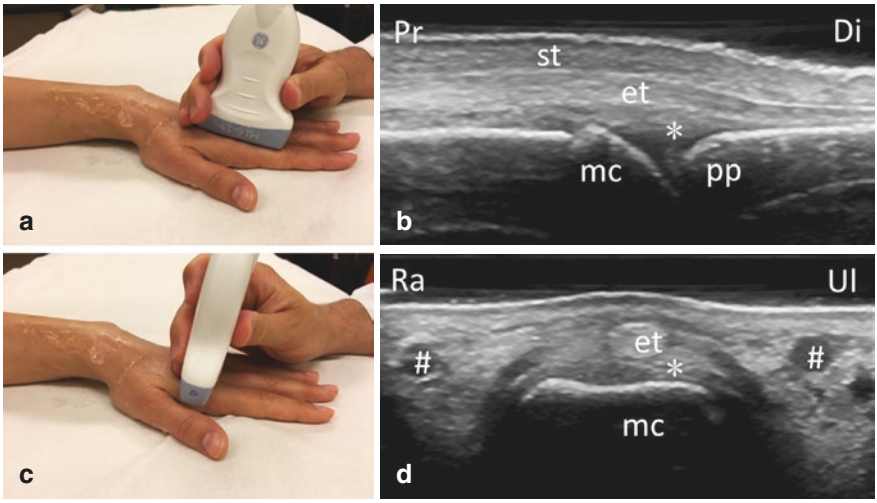

Fig. 6.22 Longitudinal and transverse dorsal scans of the metacarpophalangeal joint. (**a**) Transducer position for the transverse scan; (**b**) ultrasound image of the longitudinal scan; (**c**) transducer position for the longitudinal scan; (**d**) ultrasound image of the transverse scan. *et* extensor tendon, *mc* metacarpal bone, *pp* proximal phalanx, *st* subcutaneous tissue, *asterisk* dorsal fat pad, *hashtag* digital veins, *Pr* proximal, *Di* distal, *Ra* radial, *Ul* ulnar

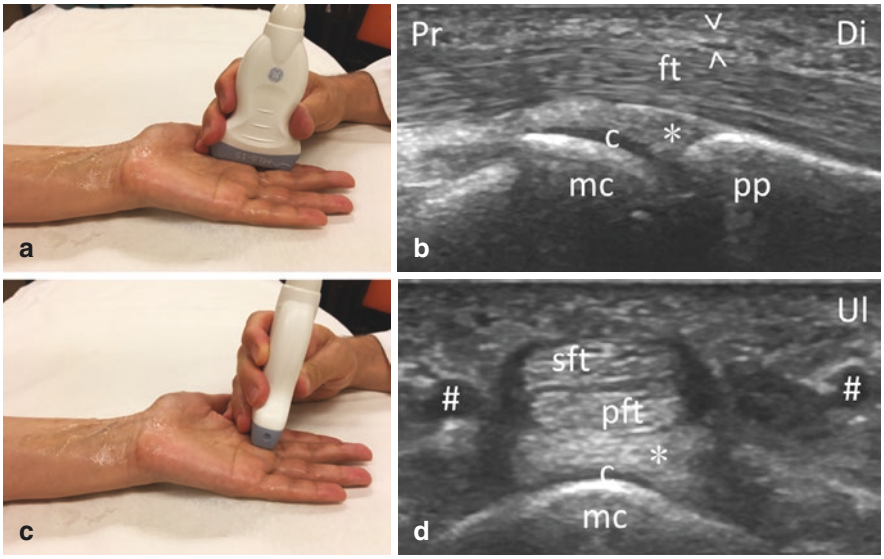

Fig. 6.23 Longitudinal and transverse volar scans of the metacarpophalangeal joint. (**a**) Transducer position for the longitudinal scan; (**b**) ultrasound image of the longitudinal scan; (**c**) transducer position for the transverse scan; (**d**) ultrasound image of the transverse scan. *c* cartilage, *ft* flexor tendons, *mc* metacarpal bone, *pp* proximal phalanx, *hashtags* digital artery, *asterisk* volar plate, *arrowheads* A1 pulley, *Pr* proximal, *Di* distal, *Ra* radial, *Ul* ulnar

coupled with the fact that it contains fibrocartilage which renders it more rigid than the fat pad, also limits the expansion of the palmar recess of the MCP joint. Small amounts of fluid have been observed in normal subjects with varying frequency within MCP recesses [21, 22]. When these recesses contain no fluid or only small amounts of fluid, they may not be properly visualized by ultrasound.

Each MCP joint also possesses both radial and ulnar collateral ligaments, which can be visualized by ultrasound (Figs. 6.24, and 6.25). On the radial aspect of the second MCP joint, the lateral collateral ligament, lying just on top of (and originating and inserting on to) the bones, must be distinguished from the tendon of the first dorsal interosseous inserting into the proximal phalanx. By following these structures proximally, the tendons and the ligaments can be therefore distinguished from one another (i.e. tendons become muscles, while the ligaments are attached to bones).

The cartilage covering the metacarpal head is one of the few areas of the human body where hyaline cartilage can be appropriately assessed and evaluated by ultrasound (Fig. 6.26). Anechoic articular cartilage follows the cortical contours of both the metacarpal head and the phalangeal base; however, the cartilage covering the phalangeal head cannot be appropriately assessed, due to the lack of an acoustic window. The fully flexed position of the MCP joint, the so-called "flick" view,

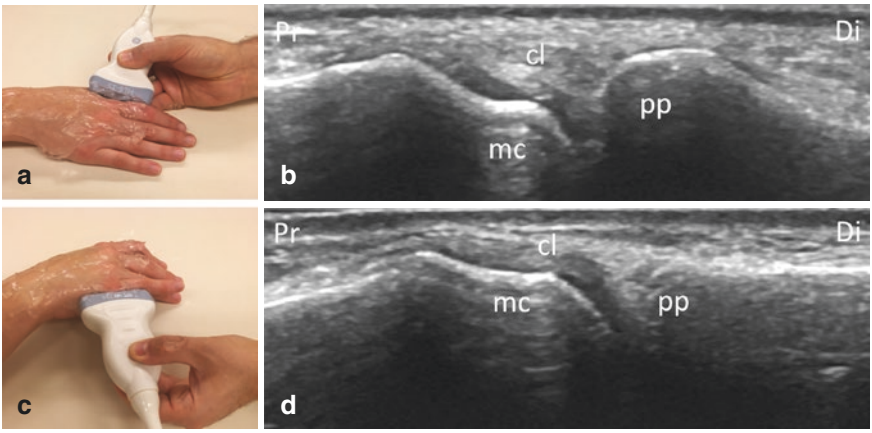

Fig. 6.24 Coronal scans of metacarpophalangeal joints. (**a**) Transducer position for the coronal scan of the second metacarpophalangeal joint (radial aspect); (**b**) ultrasound image of the coronal scan of the second metacarpophalangeal joint (radial aspect); (**c**) transducer position for the coronal scan of the fifth metacarpophalangeal joint (ulnar aspect); (**d**) ultrasound image of the fifth metacarpophalangeal joint (ulnar aspect). *cl* collateral ligament, *mc* metacarpal bone, *pp* phalanx, *Pr* proximal, *Di* distal

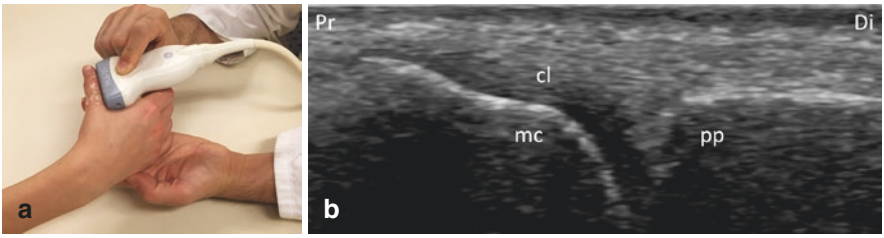

Fig. 6.25 Ulnar collateral ligament of the thumb. (**a**) Transducer position for the longitudinal scan; (**b**) ultrasound image of the longitudinal scan. *cl* collateral ligament, *mc* metacarpal bone, *pp* proximal phalanx, *Pr* proximal, *Di* distal

facilitates the assessment of the cartilage of the metacarpal head [23]. Care should be taken when evaluating the cartilage interface sign, a hyperechoic line seen on the outer margin of the cartilage, which should be clearly distinguished from the double contour sign seen in gout (see also Chap. 7).

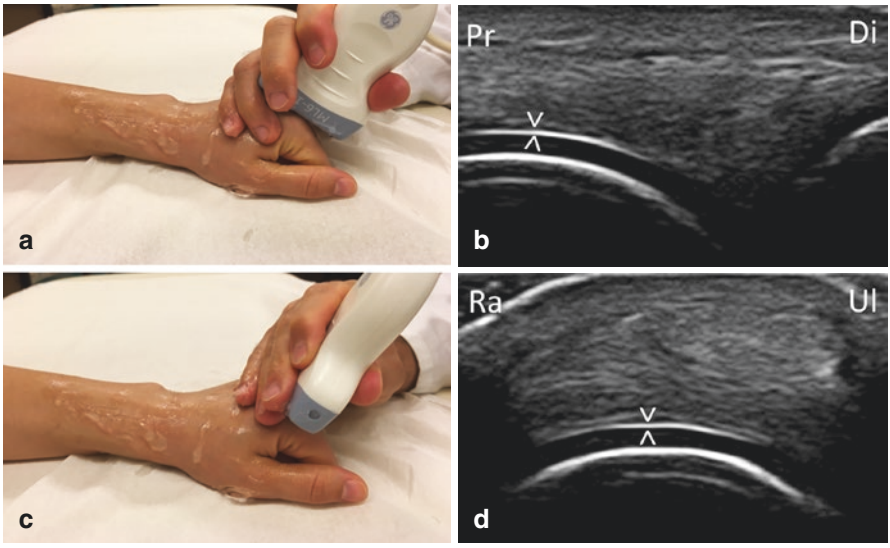

Fig. 6.26 Longitudinal and transverse scans of the cartilage covering of the metacarpal head. (**a**) Transducer position for the longitudinal scan; (**b**) ultrasound image of the longitudinal scan; (**c**) transducer position for the transverse scan; (**d**) ultrasound image of the transverse scan. *arrowhead* chondro-synovial interface, *Di* distal, *Pr* proximal, *Ul* ulnar, *Ra* radial

Palmar Aspect of the Finger

The FDS and FDP tendons should be identified independently as they pass over the MCP joints into the flexor tendon sheath of the fingers. The FDS tendons split at the level of the proximal third of the proximal phalanx (Fig. 6.27). The two halves of the FDS tendon then encircle and reunite under the FDP tendon, attaching to the proximal half of the middle phalanx. The FDP tendon passes through the divided FPS tendon, inserting at the base of the distal phalanx. Annular pulleys are a series of retinacular thickenings along five distinct regions of the flexor synovial sheath (pulleys A1–A5). The A1 annular pulley can be visualized by ultrasound as a very thin, hyperechoic band of connective tissue surrounded by a hypo-/anechoic rim overlying the flexor tendons and the volar plate at the level of the joint (Fig. 6.28). In transverse view finger movement allows the separation of the two flexor tendons. The tendons pass in close proximity to the proximal phalanges where they are held in position by the A2 pulley during finger flexion. The A2 pulley appears similar to the A1 and is situated above the superficial flexor tendon at the level of the proximal third of the proximal phalanx [24]. Cruciate pulleys (pulleys C1–C3), a series of additional fibres which interlink the annular pulleys, generally can not be visualized by ultrasound [25].

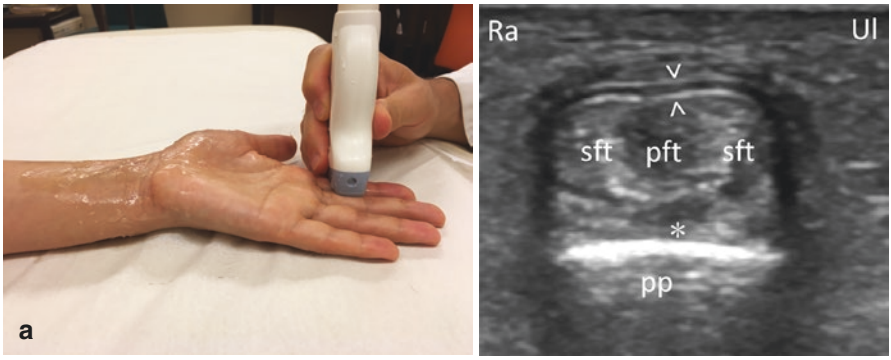

Fig. 6.27 Transverse scan of the flexor superficialis tendon at the level of the proximal third of the proximal phalanx. (**a**) Transducer position for the transverse scan; (**b**) ultrasound image of the transverse scan. *pft* profound flexor tendon, *pp* proximal phalanx, *sft* superficial flexor tendon, *asterisk* volar plate, *arrowheads* tendon sheath, *Ra* radial, *Ul* ulnar

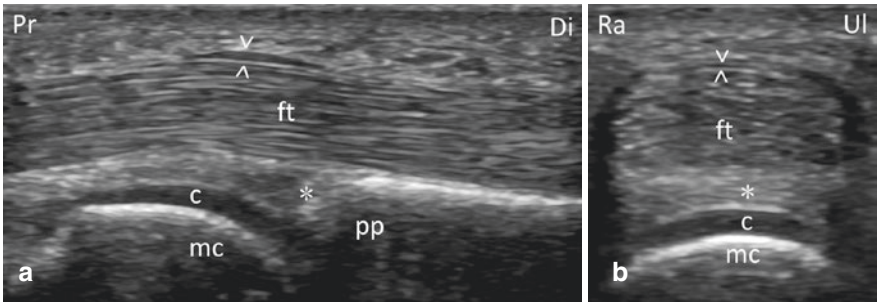

Fig. 6.28 Longitudinal and transverse image of the A1 annular pulley. (**a**) Ultrasound image of the longitudinal scan; (**b**) ultrasound image for the transverse scan. *c* hyaline cartilage, *ft* flexor tendons, *mc* metacarpal bone, *pp* proximal phalanx, *arrowheads* A1 pulley, asterisk volar plate, *Pr* proximal, *Di* distal, *Ra* radial, *Ul* ulnar

Interphalangeal Joints

Generally speaking, the anatomy of both proximal interphalangeal (PIP) and distal interphalangeal (DIP) joints mimics closely that of the MCP joints (Figs. 6.29, 6.30, 6.31, 6.32, and 6.33). The capsule, volar plate and dorsal fat pad may all be identified; they will however appear as much smaller and thinner structures as compared to the corresponding structures in MCP joints. The extensor tendons in particular are hard to visualize, when scanning PIP and DIP joints. The A4 pulley at the level of the midpoint of the middle phalanx in the sagittal plane, as well as the A3 and A5 pulleys (in the region of the PIP and DIP joints, respectively), may also be occasionally identified by sonography [6]. Sonography can also depict the extensor hood, a triangular, fibrous expansion, which surrounds the ED (or EPL to the thumb) tendon

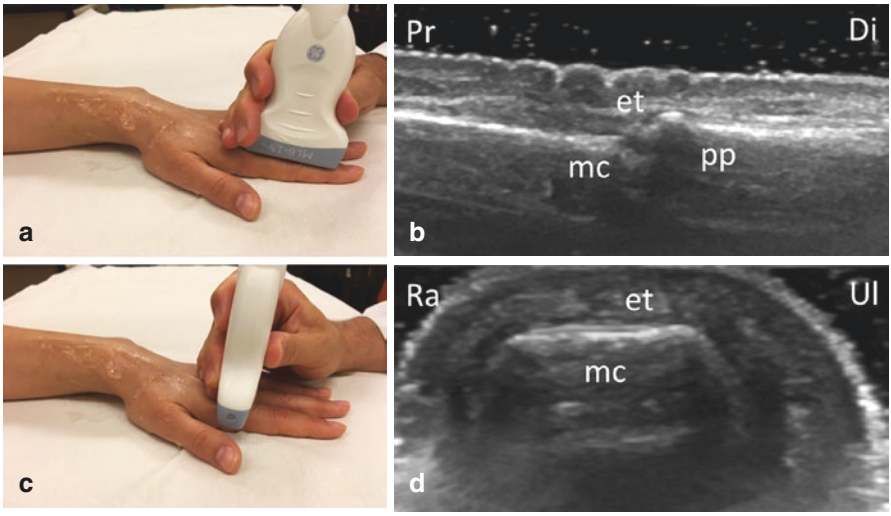

Fig. 6.29 Longitudinal and transverse dorsal scans of the proximal interphalangeal joint. (**a**) Transducer position for the longitudinal scan; (**b**) ultrasound image of the longitudinal scan; (**c**) transducer position for the transverse scan; (**d**) ultrasound image of the transverse scan. *et* extensor tendon, *mc* metacarpal bone, *pp* proximal phalanx, *Pr* proximal, *Di* distal, *Ra* radial, *Ul* ulnar

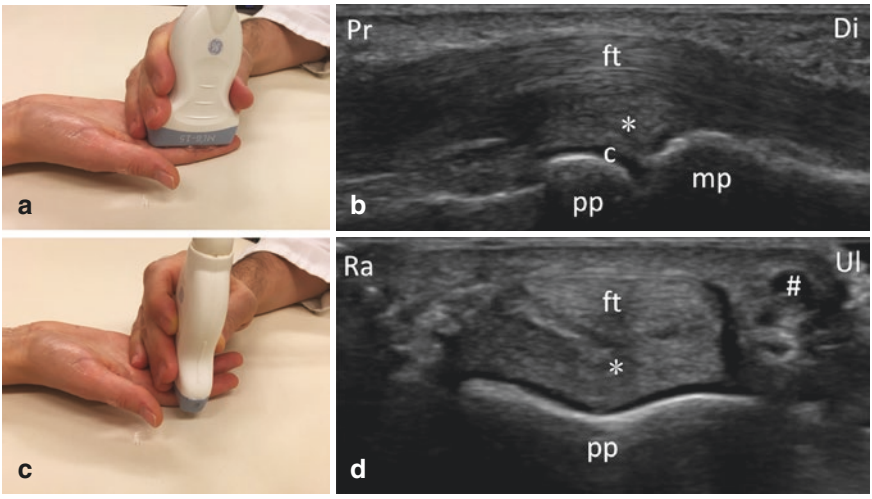

Fig. 6.30 Longitudinal and transverse palmar scan of the proximal interphalangeal joint. (**a**) Transducer position for the longitudinal scan; (**b**) ultrasound image of the longitudinal scan; (**c**) transducer position for the transverse scan. *c* hyaline cartilage, *ft* flexor tendon, *mp* middle phalanx, *pp* proximal phalanx, *asterisk* volar plate, *hashtag* digital artery, *Di* distal, *Pr* proximal, *Ra* radial, *Ul* ulnar

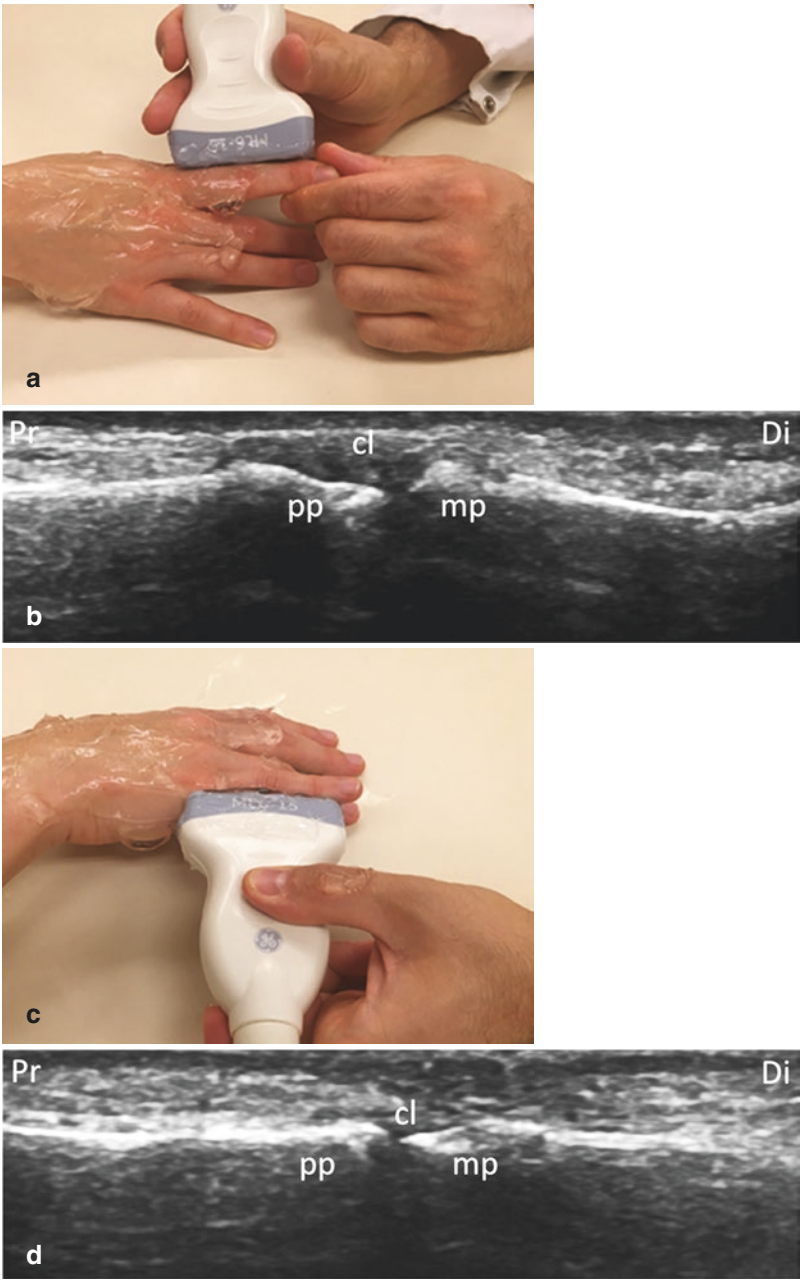

Fig. 6.31 Coronal scans of the proximal interphalangeal joints. (**a**) Transducer position for the coronal scan of the second proximal interphalangeal joint (radial aspect); (**b**) ultrasound image of the coronal scan of the second proximal interphalangeal joint (radial aspect); (**c**) transducer position for the coronal scan of the fifth proximal interphalangeal joint (ulnar aspect); (**d**) ultrasound image of the fifth proximal interphalangeal joint (ulnar aspect). *cl* collateral ligament, *mp* middle phalanx, *pp* phalanx, *Pr* proximal, *Di* distal

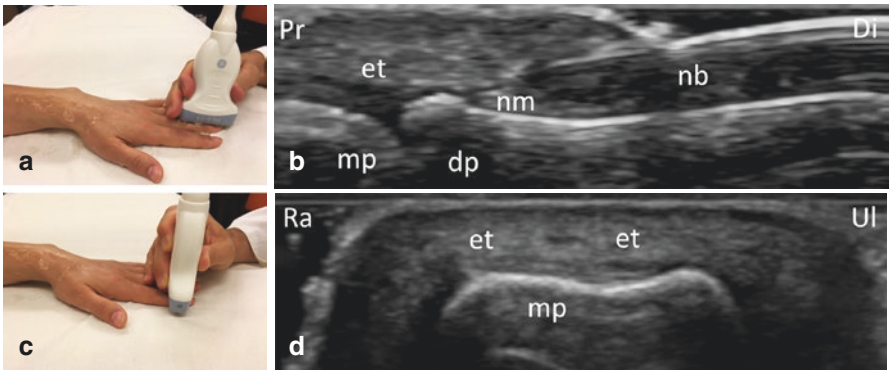

Fig. 6.32 Longitudinal and transverse dorsal scan of the distal interphalangeal joint showing the two lateral slips of the extensor tendon. (**a**) Transducer position for the longitudinal scan; (**b**) ultrasound image of the longitudinal scan; (**c**) transducer position for the transverse scan; (**d**) ultrasound image of the transverse scan. *dp* distal phalanx, *et* extensor tendon, *mp* middle phalanx, *nb* nail bed, *nm* nail matrix, *Pr* proximal, *Di* distal, *Ra* radial, *Ul* ulnar

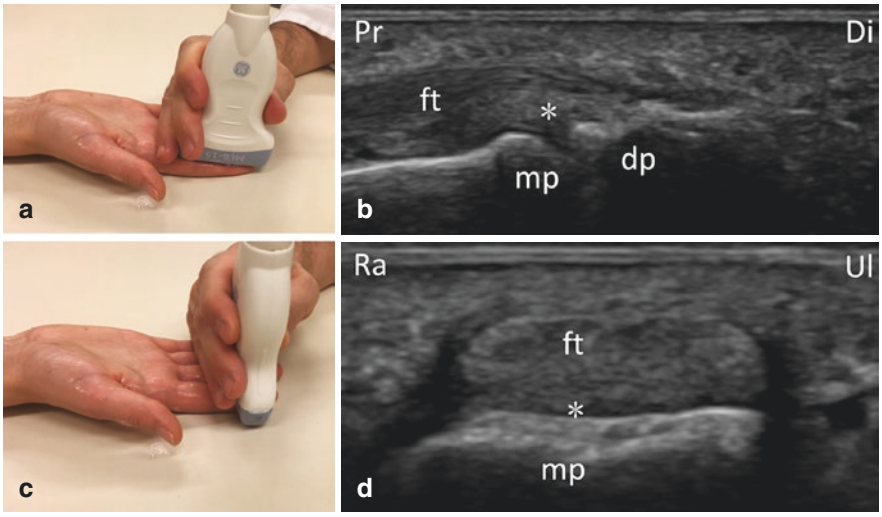

Fig. 6.33 Longitudinal and transverse palmar scan of the distal interphalangeal joint. (**a**) Transducer position for the longitudinal scan; (**b**) ultrasound image of the longitudinal scan; (**c**) transducer position for the transverse scan. *dp* distal phalanx, *ft* flexor tendon, *mp* middle phalanx, *asterisk* volar plate, *Di* distal, *Pr* proximal, *Ra* radial, *Ul* ulnar

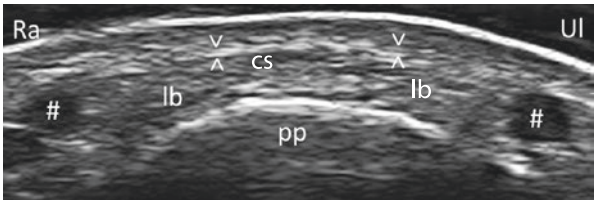

Fig. 6.34 Transverse image of the extensor apparatus over the proximal phalanx. *cs* central slip of the extensor tendon, *lb* lateral band of the extensor tendon, *pp* proximal phalanx, *arrowheads* transverse retinacular ligament, *hashtags* digital veins, *Ra* radial, *Ul* ulnar

on the dorsal aspect of the proximal phalanx of each digit, and connects to the dorsal and collateral aspects of the respective MCP joint (Fig. 6.34) [26].

Muscles, Vasculature and Innervation

The muscles, vasculature and innervation of the hand and digits are rarely the specific focus of rheumatological examinations but may be evaluated in certain cases. The dorsal and palmar interossei of the hand originate from the metacarpal bones and insert on the proximal phalanges and abduct/adduct the digits. They receive innervation from the deep branch of the ulnar nerve. The four lumbrical, of the hand are unique in that they originate from tendons (FDP tendons) rather than bones and insert onto the extensor hood of their respective digits (first lumbrical, first digit; second and third lumbrical, third digit; fourth lumbrical, fourth digit). These muscles flex MCP joints and extend the interphalangeal joints. They receive innervation from the deep branch of the ulnar nerve (3. and 4. lumbrical) and the median nerve (1. and 2. lumbrical). The vasculature of the fingers is provided chiefly by two digital arteries for each digit and features a complex microvasculature of capillaries and small veins (Figs. 6.30 and 6.34). The fingers are innervated by the median, ulnar and radial nerve and their respective branches; a detailed description of the neural architecture of the digits is beyond the scope of this chapter. Finally, the skin and nail (plate, matrix and bed) may also be assessed by ultrasound, which may be

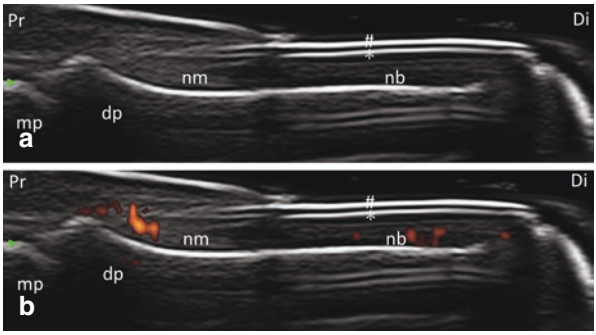

Fig. 6.35 Longitudinal image of the distal interphalangeal joint and the nail plate. (**a**) grayscale image; (**b**) power Doppler image. *dp* distal phalanx, *et* extensor tendon, *mp* middle phalanx, *nb* nail bed, *nm* nail matrix, *asterisk* ventral plate, *hashtag* dorsal plate, *Pr* proximal, *Di* distal

particularly relevant in patients with psoriatic arthritis (Fig. 6.35). The nail bed is a region where we can expect to see Doppler signals in normal individuals; therefore particular attention must be devoted to the assessment of Doppler in this area.

References

1. Filippucci E, Iagnocco A, Meenagh G, Riente L, Delle Sedie A, Bombardiei S, et al. Ultrasound imaging for the rheumatologist II. Ultrasonography of the hand and wrist. Clin Exp Rheumatol. 2006;24:118–22.
2. Mandl P, Benis S, Patonay L, Balint PV. The normal joint. In: D'Agostino MA, Wakefield RJ, editors. Essential applications of ultrasound in rheumatology. Philadelphia: Elsevier; 2010. p. 51–67.
3. Wakefield RJ, Balint PV, Szkudlarek M, Filippucci E, Backhaus M, D'Agostino MA, et al. Musculoskeletal ultrasound including definitions for ultrasonographic pathology. J Rheumatol. 2005;32:2485–7.
4. Möller I, Janta I, Backhaus M, Ohrndorf S, Bong DA, Martinoli C, et al. The 2017 EULAR standardised procedures for ultrasound imaging in rheumatology. Ann Rheum Dis. 2017;76:1974–9.
5. Husic R, Lackner A, Stradner MH, Hermann J, Dejaco C. Joint positions matter for ultrasound examination of RA patients-increased power Doppler signal in neutral versus flat position of hands. Rheumatology. 2017;56:1312–9.
6. Lee JC, Healy JC. Normal sonographic anatomy of the wrist and hand. Radiographics. 2005;25:1577–90.
7. Irsay L, Mandl P, Balint PV. Pitfalls of gray-scale artifacts. In: D'Agostino MA, Wakefield RJ, editors. Essential applications of ultrasound in rheumatology. Philadelphia: Elsevier; 2010. p. 29–43.
8. Von Schroeder HP, Botte MJ. Anatomy of the extensor tendons of the fingers: variations and multiplicity. J Hand Surg [Am]. 1995;20:27–34.
9. Gonzalez MH, Sohlberg R, Brown A, Weinzweig N. The first dorsal extensor compartment: an anatomic study. J Hand Surg [Am]. 1995;20:657–60.
10. Yuasa K, Kiyoshige Y. Limited surgical treatment of de Quervain's disease: decompression of only the extensor pollicis brevis subcompartment. J Hand Surg [Am]. 1998;23:840–3.
11. Griffith JF, Chan DP, Ho PC, Zhao L, Hung LK, Metreweli C. Sonography of the normal scapholunate ligament and scapholunate joint space. J Clin Ultrasound. 2001;29:223–9.
12. Jacobson JA, Oh E, Propeck T, Jebson PJL, Jamadar DA, Hayes CW. Sonography of the scapholunate ligament in four cadaveric wrists: correlation with MR arthrography and anatomy. Am J Roentgenol. 2002;179:523–7.

13. De Maeseneer M, Marcelis S, Osteaux M, Jager T, Machiels F, Van Roy P. Sonography of a rupture of the tendon of extensor pollicis longus muscle: initial clinical experience and correlation with findings at cadaveric dissection. Am J Roentgenol. 2005;184:175–9.
14. Smith J, Rizzo M, Finnoff JT, Sayeed YA, Michaud J, Martinoli C. Sonographic appearance of the posterior interosseous nerve at the wrist. J Ultrasound Med. 2011;30:1233.
15. Lee KS, Ablove RH, Singh S, De Smet AA, Haaland B, Fine JP. Ultrasound imaging of normal displacement of the extensor carpi ulnaris tendon within the ulnar groove in 12 forearm-wrist positions. Am J Roentgenol. 2009;193:651–5.
16. Filippucci E, Gabba A, Di Geso L, Girolimetti R, Salaffi F, Grassi W. Hand tendon involvement in rheumatoid arthritis: an ultrasound study. Semin Arthritis Rheum. 2012;41:752–60.
17. Silvestri E, Martinoli C, Derchi LE, Bertolotto M, Chiaramondia M, Rosenberg I. Echotexture of peripheral nerves: correlation between US and histologic findings and criteria to differentiate tendons. Radiology. 1995;197:291–6.
18. Gassner EM, Schocke M, Peer S, Schwabegger A, Jaschke W, Bodner G. Persistent median artery in the carpal tunnel: color Doppler ultrasonographic findings. J Ultrasound Med. 2002;21:455–61.
19. Propeck T, Quinn TJ, Jacobson JA, Paulino AF, Habra G, Darian VB. Sonography and MR imaging of bifid median nerve with anatomic and histologic correlation. Am J Roentgenol. 2000;175:1721–5.
20. Singh I. Variations in the metacarpal bones. J Anat. 1959;93:262–7.
21. Schmidt WA, Schmidt H, Schicke B, Gromnica-Ihle E. Standard reference values for musculoskeletal ultrasonography. Ann Rheum Dis. 2004;63:988–94.
22. Padovano I, Costantino F, Breban M, D'Agostino MA. Prevalence of ultrasound synovial inflammatory findings in healthy subjects. Ann Rheum Dis. 2016;75:1819–23.
23. Mandl P, Supp G, Baksa G, Radner H, Studenic P, Gyebnar J, et al. Relationship between radiographic joint space narrowing, sonographic cartilage thickness and anatomy in rheumatoid arthritis and control joints. Ann Rheum Dis. 2015;74:2022–7.
24. Martinoli C, Bianchi S, Nebiolo M, Derchi LE, Garcia JF. Sonographic evaluation of digital annular pulley tears. Skelet Radiol. 2000;29:387–91.
25. Hauger O, Chung CB, Lektrakul N, Botte MJ, Trudell D, Boutin RD, Resnick D. Pulley system in the fingers: normal anatomy and simulated lesions in cadavers at MR imaging, CT, and US with and without contrast material distention of the tendon sheath. Radiology. 2000;217:201–12.
26. Kichouh M, Vanhoenacker F, Jager T, Van Roy P, Pouders C, Marcelis S, Van Hedent E, De Mey J. Functional anatomy of the dorsal hood or the hand: correlation of ultrasound and MR findings with cadaveric dissection. Eur Radiol. 2009;19:1849–56.

Sonopathology: Pathological Findings (Articular and Periarticular)

7

Emilio Filippucci, Peter Mandl, Peter Vince Balint, and Walter Grassi

Synovial Hyperplasia and Fluid

Synovitis represents the most readily identifiable and detectable pathology in the wrist and the small joints of the hand. Intra-articular fluid appears as an anechoic or hypoechoic area within the joint capsule and in its early stages may facilitate the detection of the capsule, which is otherwise not clearly detectable by ultrasound (US) in the small joints (Fig. 7.1a, b). Intra-articular synovial fluid is not compressible but displaceable except in case of high intra-articular pressure. Synovial hyperplasia is poorly compressible and nondisplaceable. Rheumatoid synovial hyperplasia may appear either hypoechoic or hyperechoic on US. Hypoechogenic and more exudative forms of synovitis predominantly featuring synovial fluid probably indicate more active grayscale synovitis compared with the more hyperechoic synovial hyperplasia; however, biopsy studies are needed to confirm this observation. Synovial hyperplasia may be difficult to distinguish from normal connective tissue as they both appear quite similar with regard to echogenicity; increased amount of synovial fluid however may facilitate differentation (Fig. 7.2). Synovial hyperplasia generally appears somewhat more heterogeneous as compared to normal connective tissue especially in cases of synovitis due to the deposition of crystals (Figs. 7.3 and

E. Filippucci, M.D., PhD. (✉) · W. Grassi, M.D.
Clinica Reumatologica, Università Politecnica delle Marche, Ospedale "C. Urbani", Ancona, Italy
e-mail: emilio_filippucci@yahoo.it; walter.grassi@univpm.it

P. Mandl, M.D., PhD.
Division of Rheumatology, Department of Internal Medicine III, Medical University of Vienna, Vienna, Austria
e-mail: peter.mandl@meduniwien.ac.at

P. V. Balint, M.D., PhD., FRCP.
3rd Rheumatology Department, National Institute of Rheumatology and Physiotherapy, Budapest, Hungary
e-mail: pvbalint@gmail.com

P. V. Balint, P. Mandl (eds.), *Ultrasonography of the Hand in Rheumatology*,
https://doi.org/10.1007/978-3-319-74207-6_7

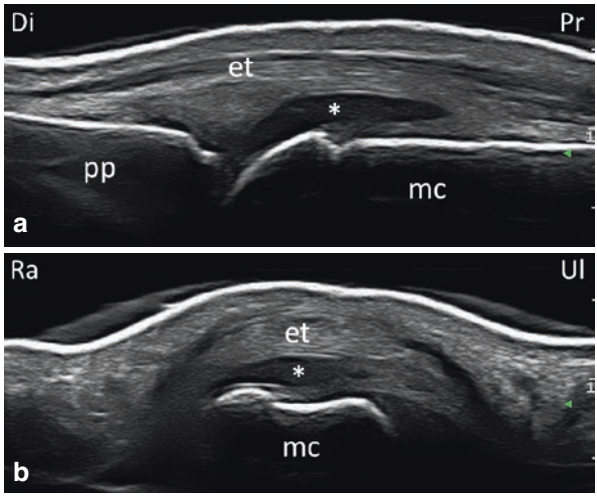

Fig. 7.1 Dorsal longitudinal (**a**) and transverse (**b**) scans of a metacarpophalangeal joint. Exudative synovitis in early rheumatoid arthritis. Joint cavity enlargement due to an abnormal amount of synovial fluid (asterisk). *et* finger extensor tendon, *mc* metacarpal head, *pp* proximal phalanx, *Di* distal, *Pr* proximal, *Ra* radial, *Ul* ulnar

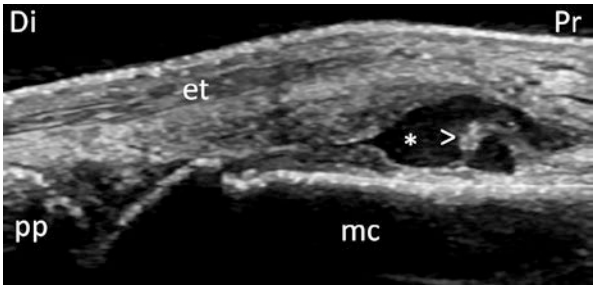

Fig. 7.2 Dorsal longitudinal scan of a metacarpophalangeal joint. Synovitis. Joint cavity enlargement due to both synovial fluid (asterisk) and synovial hyperplasia (arrowhead). *et* finger extensor tendon, *mc* metacarpal head, *pp* proximal phalanx, *Di* distal, *Pr* proximal

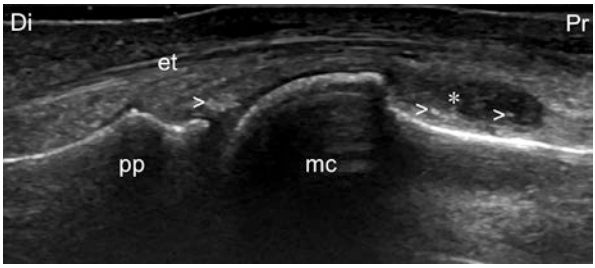

Fig. 7.3 Dorsal longitudinal scan of a metacarpophalangeal joint. Synovitis in gout. Joint enlargement due to synovial fluid and synovial hyperplasia (asterisk) with hyperechoic structures (arrowhead) corresponding to urate deposits. *et* finger extensor tendon, *mc* metacarpal head, *pp* proximal phalanx, *Di* distal, *Pr* proximal

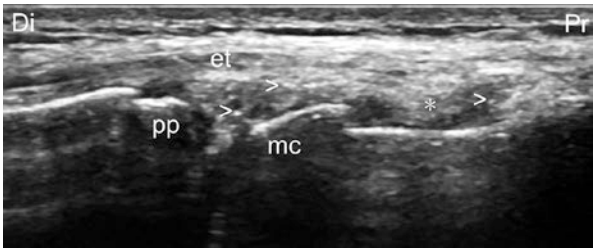

Fig. 7.4 Dorsal longitudinal scan of a metacarpophalangeal joint. Synovitis in calcium pyrophosphate deposition disease (CPPD). Joint enlargement due to synovial fluid and synovial hyperplasia (asterisk) with hyperechoic structures (arrowhead) corresponding to calcium pyrophosphate deposits. *et* finger extensor tendon, *mc* metacarpal head, *pp* proximal phalanx, *Di* distal, *Pr* proximal

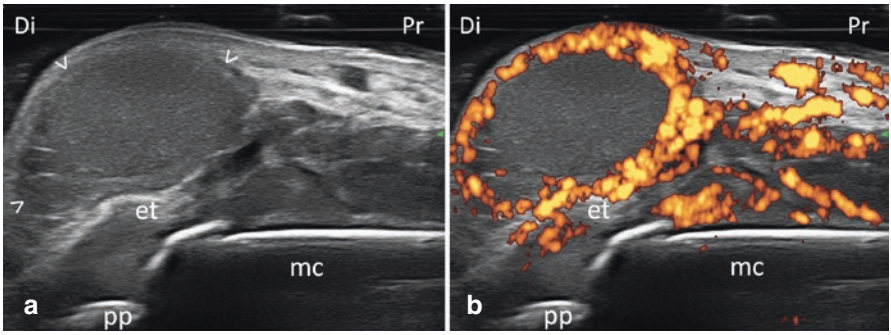

Fig. 7.5 Dorsal longitudinal scan of a metacarpophalangeal joint. Septic arthritis. Grayscale (**a**) and power Doppler (**b**) images. The arrowheads indicate a purulent collection, surrounded by power Doppler signal. *et* finger extensor tendon, *mc* metacarpal head, *pp* proximal phalanx, *Di* distal, *Pr* proximal

7.4) or in case of septic arthritis (Fig. 7.5). Differentiating synovial hyperplasia from normal anatomical structures is particularly challenging in small joints; however, a clear understanding of anatomy facilitates assessment (Fig. 7.6a, b). Tendons and ligaments in particular exhibit a high degree of anisotropy, the artifact of directional dependence which can be helpful when attempting to differentiate these structures from their surroundings. Several semi-quantitative scoring systems have been developed, which rate the individual components as well as the combination thereof [1]. Scores based on a reduced number of joints have generally demonstrated similar or even better metric properties than corresponding joint evaluations featuring a large number of joints [2]. The quantitative measurement of synovitis in grayscale based on the volume or thickness of synovial tissue is not widely practiced due to low feasibility. Several studies have advocated scanning only certain aspects of the small joints of the hand. This has led to proposals limiting the examination to only certain aspects of such joints (e.g., only the dorsal or the palmar aspect joints) by claiming that these are either superior for detecting synovitis in both grayscale and Doppler signal or are more frequently involved [3–6]. Few

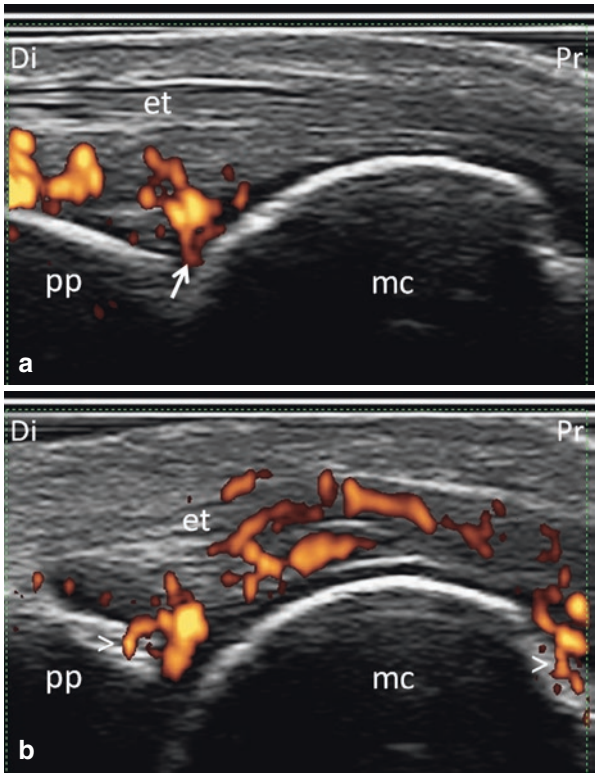

Fig. 7.6 Dorsal longitudinal scan of second (**a**) and third (**b**) metacarpophalangeal joint of the dominant hand in a patient with established rheumatoid arthritis. Different patterns of joint damage. (**a**) Complete reabsorption of the hyaline cartilage and active pannus attached to the subchondral bone (arrow). (**b**) Active pannus is damaging the base of the proximal phalanx and the bare area of the metacarpal head (arrowheads). Hyaline cartilage of the metacarpal head is still detectable. *et* finger extensor tendon, *mc* metacarpal head, *pp* proximal phalanx, *Di* distal, *Pr* proximal

studies examined the lateral distribution of synovitis within a single joint and have shown a predilection for radial-sided synovitis in certain metacarpophalangeal (MCP) and proximal interphalangeal (PIP) joints [4, 5]. Whenever feasible, all aspects should be evaluated in order to avoid underestimating synovial fluid and/or hyperplasia.

Intra-articular color or power Doppler (CD/PD) signal is considered to indicate either the vasodilation of normally existing vessels, angiogenesis, hyperemia, anastomosis, shunt, and increased density of intra-articular vascular network without angiogenesis or a combination thereof [7, 8]. Doppler signal, either CD or PD, is commonly utilized to differentiate "active" inflamed synovium from inactive pannus, fibrous tissue, and joint debris (Fig. 7.7); however, one study demonstrated vessels in 7% of MCP joints of healthy subjects [9]. Questionable objectivity, due to varied machine settings, artifacts, and the absence of information related to the topographic distribution of the CD/PD signal, continues to pose important limitations to the evaluation of Doppler signal in the small joints of the hand. The increased sensitivity of the latest-generation high-resolution US equipment allows the visualization of intra-articular Doppler signal corresponding to the presence of physiological vessels, a finding not obtainable, with older, less sensitive equipment (Fig. 7.8). Such developments question the earlier paradigm of intra-articular Doppler signal being by

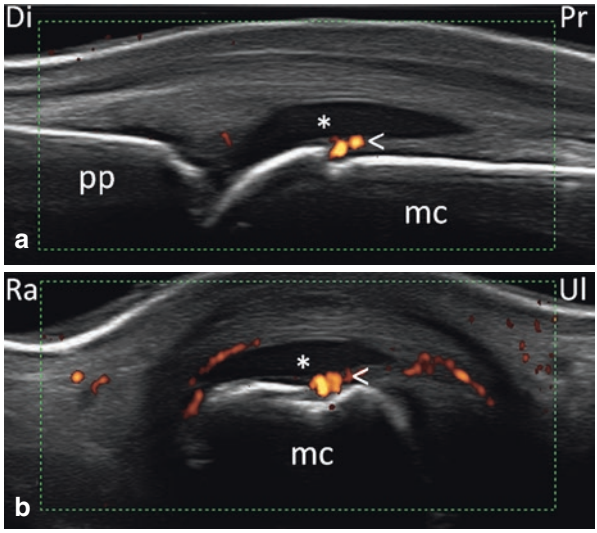

Fig. 7.7 Dorsal longitudinal (**a**) and transverse (**b**) scans of a metacarpophalangeal joint. Exudative synovitis in early rheumatoid arthritis. Joint cavity enlargement due to an abnormal amount of synovial fluid (asterisk) with surrounding power Doppler signal. The arrowheads indicate a hyperemic feeding vessel. *et* finger extensor tendon, *mc* metacarpal head, *pp* proximal phalanx, *Di* distal, *Pr* proximal, *Ra* radial, *Ul* ulnar

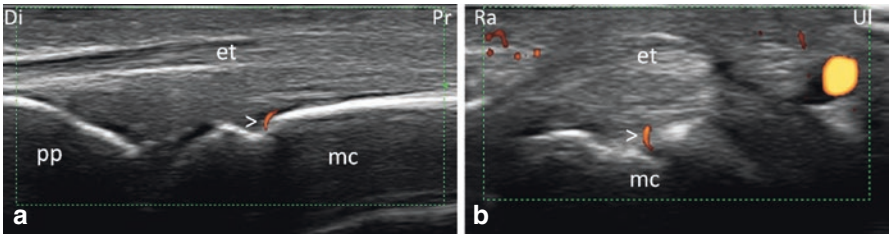

Fig. 7.8 Dorsal longitudinal (**a**) and transverse (**b**) scans of a metacarpophalangeal joint. Healthy subject. The arrowheads indicate the power Doppler signal generated by a feeding vessel. *et* finger extensor tendon, *pp* proximal phalanx, *mc* metacarpal head, *Di* distal, *Pr* proximal, *Ra* radial, *Ul* ulnar

definition pathological. Binary grading and semi-quantitative scoring were also adapted for evaluating Doppler signal in small joints. Various quantitative approaches have also been introduced, including pixel counting, calculation of pulsatility and resistance indices, and microbubble contrast material [10, 11]. While semi-quantitative and quantitative scoring correlate well, the former is naturally limited especially in cases when the Doppler pixel count is close to the cutoffs between the semi-quantitative grades [12]. Synovial fluid does not commonly exhibit Doppler signal, although such signals may indeed be detected occasionally. Erroneous Doppler signal may be due to the movement of fluid caused by transducer pressure or movement of the joint, correctly classified as artifactual signals. It can also be due to the fact that a structure (most often synovial hyperplasia), which exhibits Doppler signal and which is not visualized in grayscale US in that particular plane shows through, due to slice thickness or incorrect positioning of the focal zone or gain setting.

Tenosynovitis and Tendon Damage

Ultrasound is an ideal tool for evaluating or detecting tendon involvement in various rheumatic conditions, particularly since it allows dynamic examination, which is key to the accurate diagnosis. The US image of tenosynovitis generally corresponds to the OMERACT definition, i.e., hypoechoic or anechoic thickened tissue with or without fluid within the tendon sheath, which is seen in two perpendicular planes and which may exhibit Doppler signal [13, 14] (Fig. 7.9). Having a clear understanding of the anatomical structure of tendons is crucial for the evaluation of tenosynovitis and for interpreting Doppler signal within the tendon sheath as well as for the evaluation of tendon involvement. Collagen fibrils are arranged into collagen fibers, which subsequently form bundles. A fascicle is a larger group of fibers separated by loose connective tissue, the endotenon. Fascicles grouped together form the tendon, surrounded by the epitenon. Tendons lacking a tendon sheath may possess a paratenon or false tendon sheath, which can be affected by a similar pathological entity known as paratenonitis [15] (Figs. 7.10 and 7.11).

Due to the neurovascular supply of tendons, Doppler signal accompanying tenosynovitis will appear in the tendon sheath rather than the actual tendon itself, which normally has only a very limited blood supply via the mesotendon, the musculotendinous junction, and the osteotendinous junction and vessels from various surrounding connective tissue such as the paratenon and vincula. In case of tendinitis or mechanical intratendon damage, the tendon is characterized by loss of fibrillar pattern, with or without enlargement, loss of continuity involving part of the tendon or the entire tendon with intervening hypoechoic or anechoic region, as well as Doppler signals within the tendon, due to neovascularization (Fig. 7.12). In severe cases of tendon rupture, retraction of ruptured tendon ends may require dynamic maneuver for demonstrating the lesion. Partial or full tearing of the extensor tendons commonly occurs in chronic tendon damage and may be evaluated also by US.

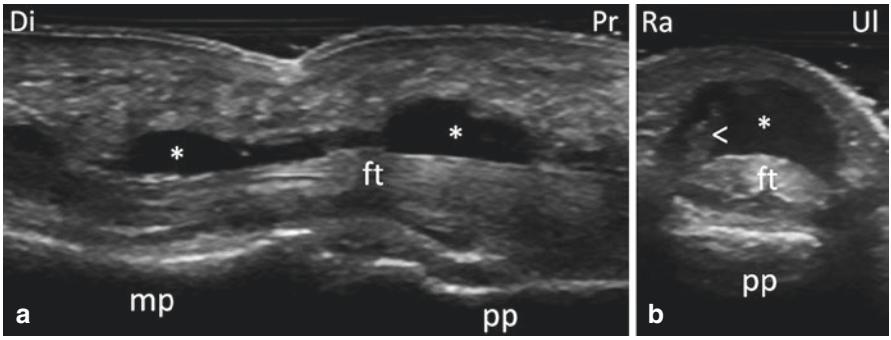

Fig. 7.9 Volar longitudinal (**a**) and transverse (**b**) scans of the finger flexor tendons at the proximal interphalangeal joint. Exudative tenosynovitis of the finger flexor tendon in psoriatic arthritis. The images show a mainly anechoic tendon sheath widening. The arrowhead indicates a small area of synovial proliferation. *ft* finger flexor tendons, *mp* middle phalanx, *pp* proximal phalanx, *Di* distal, *Pr* proximal, *Ra* radial, *Ul* ulnar

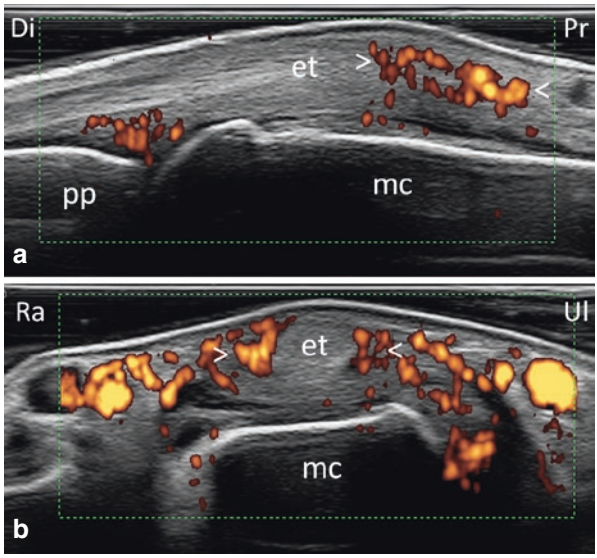

Fig. 7.10 Dorsal longitudinal (**a**) and transverse (**b**) scans of a metacarpophalangeal joint. Psoriatic arthritis. The arrowheads indicate power Doppler signal surrounding the finger extensor tendon. *mc* metacarpal head, *pp* proximal phalanx, *Di* distal, *Pr* proximal, *Ul* ulnar, *Ra* radial

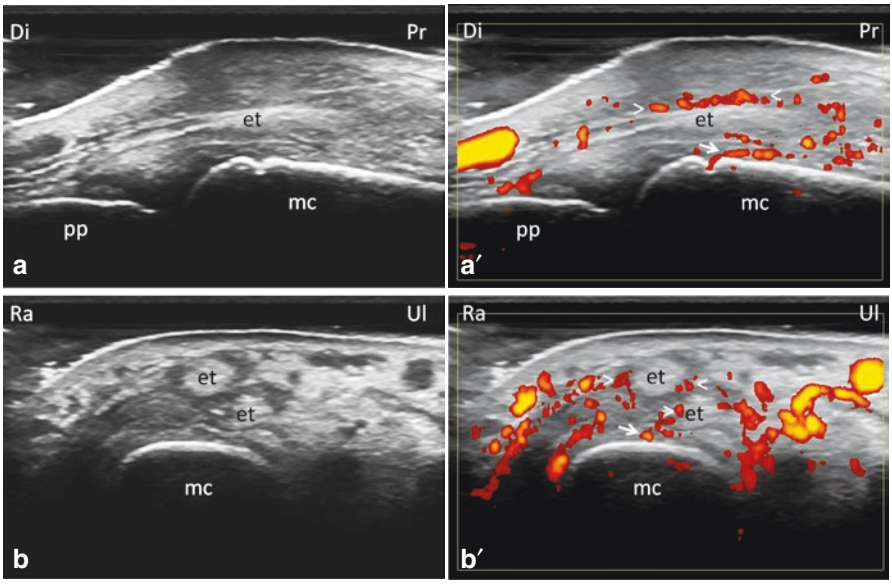

Fig. 7.11 Dorsal longitudinal (**a**, **a′**) and transverse (**b**, **b′**) scans of a metacarpophalangeal joint. Peritenon inflammation of the extensor tendon (arrowheads) in psoriatic arthritis. The arrows indicate a feeding vessel. *et* finger extensor tendon, *mc* metacarpal head, *pp* proximal phalanx, *Di* distal, *Pr* proximal, *Ra* radial, *Ul* ulnar

Global or nodular thickening and hypervascularization of the A1 pulley are the key ultrasonographic findings in the condition known as trigger finger (Fig. 7.13). Notch formation on the surface of the pulley, tendinosis, or tenosynovitis of the

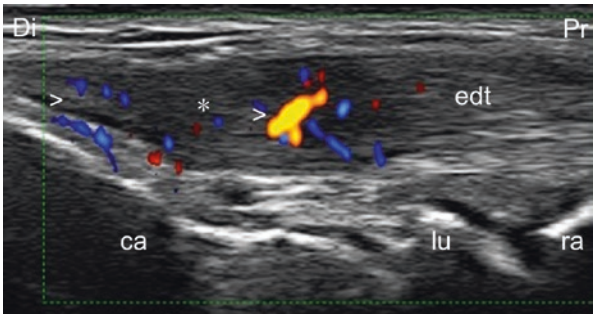

Fig. 7.12 Dorsal longitudinal midline scan of the wrist. Tendinitis of the extensor digitorum tendon as indicated by decreased echogenicity of the tendon (asterisk) accompanied by intratendinous power Doppler signal (arrowheads). *edt* extensor digitorum tendon, *ca* capitate, *lu* lunate, *ra* radius, *Di* distal, *Pr* proximal

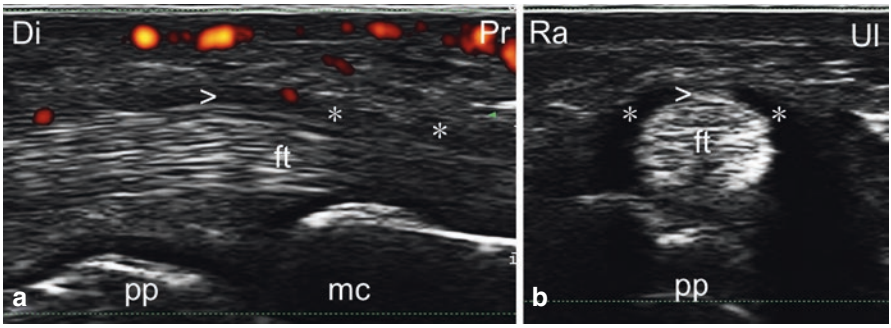

Fig. 7.13 Volar longitudinal (**a**) and transverse (**b**) scans of a metacarpophalangeal joint. Tenosynovitis of the flexor tendons (asterisk) accompanied by nodular thickening and hypervascularization of the A1 pulley in trigger finger (arrowhead). *ft* finger flexor tendons, *mc* metacarpal head, *pp* proximal phalanx, *Di* distal, *Pr* proximal, *Ra* radial, *Ul* ulnar

finger flexor tendons, diverticular cystic appearance of the synovial sheath in the absence of tenosynovitis, as well as MCP joint involvement are additional phenomena accompanying this condition [16, 17].

Dactylitis

Dactylitis, referring to "sausage-like" digits, is a peculiar characteristic of seronegative spondyloarthritides and in particular psoriatic arthritis. The definition of dactylitis as well as its corresponding US findings remains controversial. In the past, it was thought that the sausage-like appearance was due to concomitant flexor tenosynovitis and arthritis of the MCP, metatarsophalangeal or interphalangeal joints. Recent US and MRI studies have confirmed however that dactylitis is due to flexor tenosynovitis and marked adjacent soft tissue swelling (subcutaneous edema) with

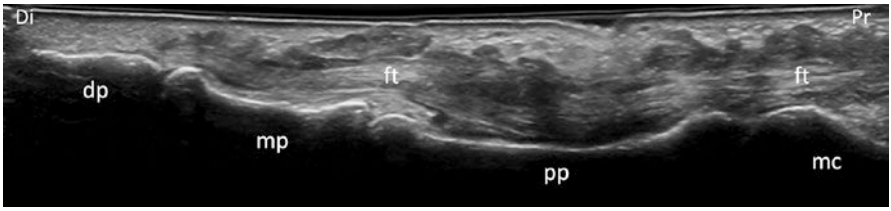

Fig. 7.14 Volar longitudinal scan of the finger acquired using the extended view showing tenosynovitis of the finger flexor tendons in dactylitis in psoriatic arthritis. *dp* distal phalanx, *ft* finger flexor tendons, *mc* metacarpal head, *mp* middle phalanx, *pp* proximal phalanx, *Di* distal, *Pr* proximal

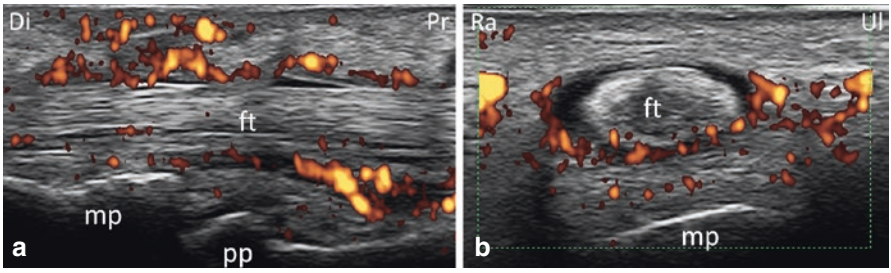

Fig. 7.15 Volar longitudinal (**a**) and transverse (**b**) scans of the finger show evident power Doppler signal in the synovial tissue surrounding the finger flexor tendons in dactylitis in psoriatic arthritis. *ft* finger flexor tendons, *mp* middle phalanx, *pp* proximal phalanx, *Di* distal, *Pr* proximal, *Ra* radial, *Ul* ulnar

a variable degree of small joint synovitis, although several studies have indicated the involvement of extensor tendons as well (Figs. 7.14 and 7.15) [18].

Enthesitis

Ultrasound is used extensively for the evaluation of enthesitis primarily in the context of spondyloarthropathies. Although the hand includes a number of entheseal regions, these are not generally assessed by US in routine practice. It has been suggested that enthesitis might be the primary lesion in spondyloarthropathies and that the synovitis evident in various adjacent structures (joint, tendon, or bursa) is only a secondary phenomenon to the inflamed entheses [18–23]. In dactylitis, enthesitis could occur at the numerous "functional entheses" that the flexor digitorum tendon forms with retinacula or pulleys [19]. These "functional entheses" are frequently associated with the presence of fibrocartilage that reduces compression and shear strain. The distal interphalangeal (DIP) joint capsule and the distal insertion of the finger extensor tendon were found to be intimately linked with the nail complex, with the dorsal, volar, and lateral aspects of the nail bed being ensheathed in fibers extending from the entheses, suggesting that the nail is an integral part of the

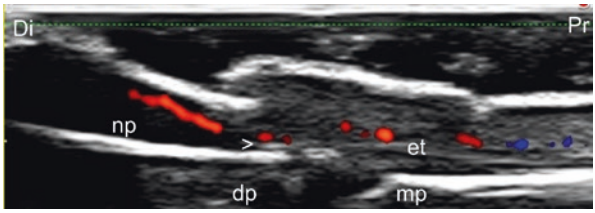

Fig. 7.16 Dorsal longitudinal scan of a distal interphalangeal joint. Power Doppler signal along the extensor tendon and at its insertion on the distal phalanx (arrowhead) as a sign of enthesitis in psoriatic arthritis with nail involvement. *mp* middle phalanx, *dp* distal phalanx, *et* finger extensor tendon, *Di* distal, *Pr* proximal

enthesis organ [22] (Fig. 7.16). Anchorage mechanisms including fibers tether the nail plate to the underlying periosteum, which itself was found to be closely anchored to the extensor tendon [23]. Psoriatic nail involvement appears as a minimal loss of the hyperechoic definition of the ventral plate in the early stages, thickening and fusion of both nail plates, loss of the intermediate anechoic layer, increased flow along the extensor tendon, and other involved tissues except nail plate and nail bed thickening in the later stages. Ultrasound may also be used to assess not only enthesitis and nail involvement in psoriatic arthritis; the skin, including psoriatic plaques, can also be evaluated.

Cartilage Destruction, Bone Erosion, and Osteophytes

Inflammation generally leads to structural damage, although the frequency and rate of progression differ among the various inflammatory arthritides. Joint damage typically follows a pattern beginning with cartilage loss, development of subchondral irregularities which deepen to become erosions, and finally malalignment and subluxation occurs (Fig. 7.17). Cartilage loss begins with the destruction of the cartilage matrix, which facilitates the attachment of the inflamed synovial tissue to the cartilage. This leads to subsequent breaks in the chondro-synovial margin (Fig. 7.18) followed by the inflamed active pannus invading the hyaline cartilage (Fig. 7.19) [24, 25].

Grayscale signs of synovitis are commonly accompanied by early bone erosions (Fig. 7.20), and in many cases, the intimate relationship between the invading pannus and the resulting erosion (Figs. 7.21 and 7.22) can be appropriately demonstrated on US [26]. Bone erosion appears as an interruption of the bony cortex detectable on at least two perpendicular planes. In patients with rheumatoid arthritis (RA), at the level of the hand and wrists, bone erosions are usually located on the lateral and dorsal aspects of the second and fifth metacarpal heads together with the ulnar styloid process [27]. It is suggested that bone erosions occur mainly on the radial side of the second, third, and fourth metacarpal heads, but not the fifth metacarpal head, due to the involvement of the radial collateral ligament, highlighting the need for lateral scans to avoid missing erosions on the standard dorsal scan [28, 29]. Gouty erosions are characteristically described on conventional radiography as well-defined, punched-out lesions with overhanging edges [30]. Ultrasound has been found to be

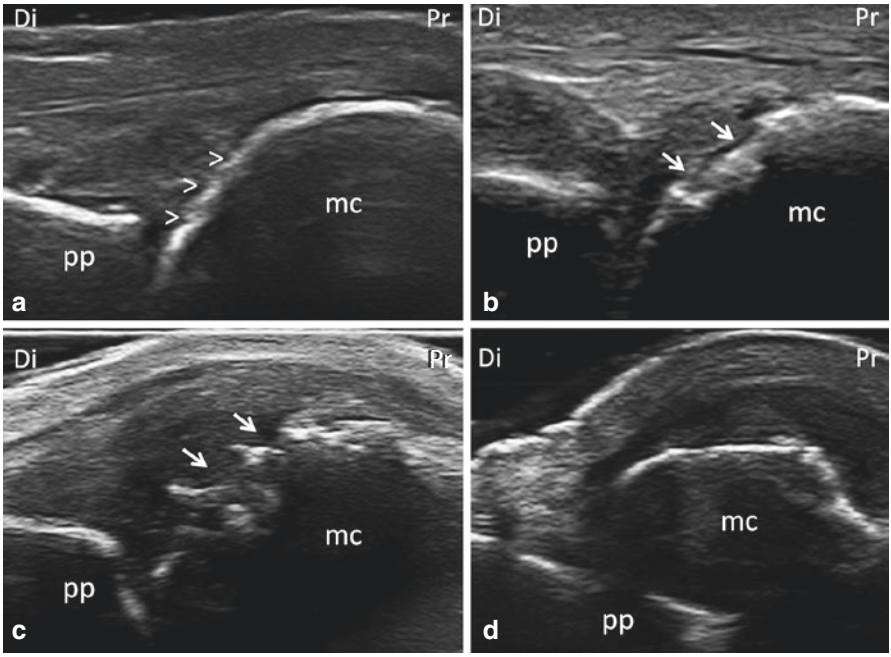

Fig. 7.17 Dorsal longitudinal scan of a metacarpophalangeal joint. Different grades of joint damage. (**a**) Complete cartilage reabsorption with initial subchondral irregularities (arrowheads); (**b**) Subchondral erosion (arrows); (**c**) Extensive subchondral erosions (arrows); (**d**) Dorsal dislocation of the metacarpal head. *et* finger extensor tendon, *mc* metacarpal head, *pp* proximal phalanx, *Di* distal, *Pr* proximal

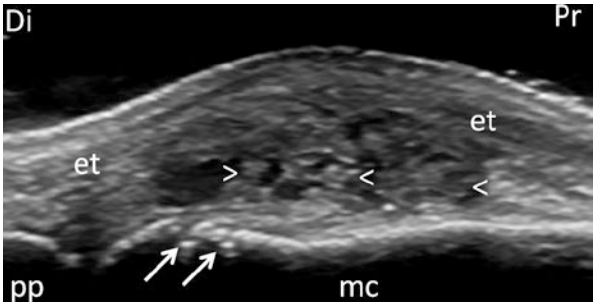

Fig. 7.18 Dorsal longitudinal scan of a metacarpophalangeal joint. Proliferative synovitis in established rheumatoid arthritis. Joint cavity enlargement mainly due to synovial hyperplasia (arrowheads). The arrows indicate very small breaks of the cortical bone which represent early signs of bone erosions. *et* finger extensor tendon, *mc* metacarpal bone, *pp* proximal phalanx, *Di* distal, *Pr* proximal

more sensitive than conventional radiography for the detection of erosions in gout [31] which are commonly found on the medial aspect of the first metatarsal head and MCP joints. Erosions in gout are commonly multifocal and may occur extra-articularly [30]. While erosions appear similar in psoriatic arthritis (PsA) and RA, larger

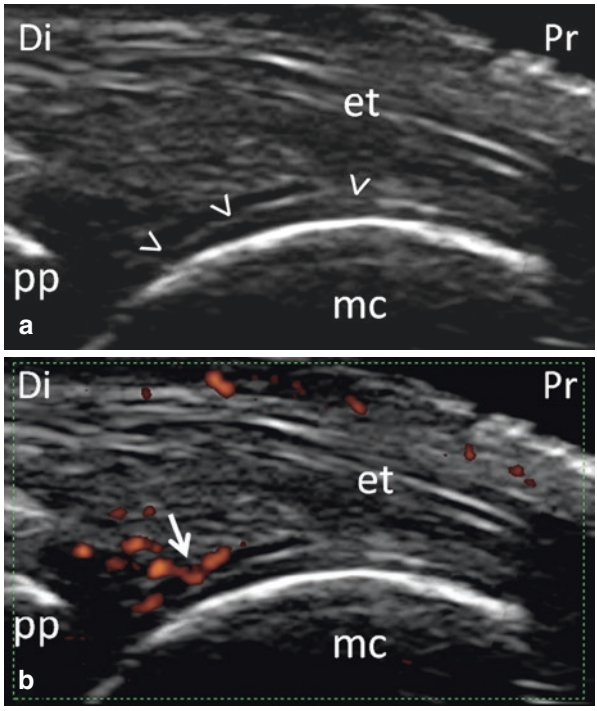

Fig. 7.19 Dorsal longitudinal scan of a metacarpophalangeal joint. Rheumatoid arthritis. Grayscale (**a**) and power Doppler (**b**) images. The arrowheads indicate breaks of the chondro-synovial margin. The arrow indicates inflamed synovial tissue attached to the cartilage surface. *et* finger extensor tendon, *mc* metacarpal head, *pp* proximal phalanx, *Di* distal, *Pr* proximal, *Ra* radial, *Ul* ulnar

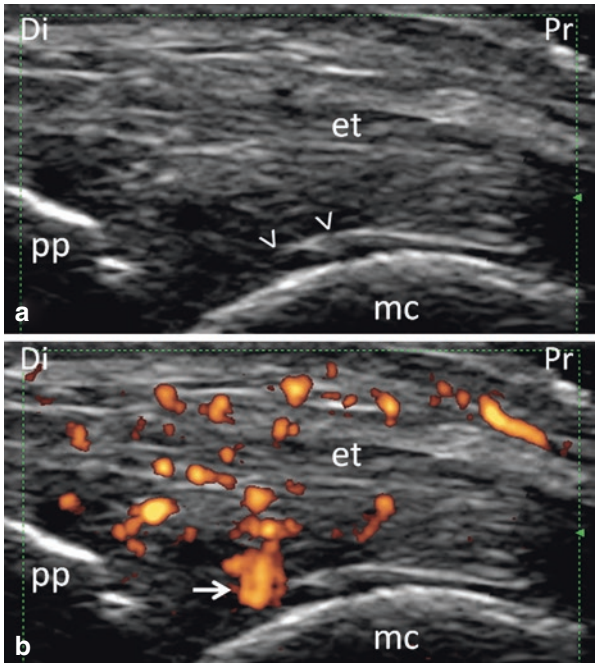

Fig. 7.20 Dorsal longitudinal scan of a metacarpophalangeal joint. Rheumatoid arthritis. Grayscale (**a**) and power Doppler (**b**) images. The arrowheads indicate breaks of the chondro-synovial margin. The arrow indicates inflamed pannus damaging the hyaline cartilage of the metacarpal head. *et* finger extensor tendon, *mc* metacarpal head, *pp* proximal phalanx, *Di* distal, *Pr* proximal, *Ra* radial, *Ul* ulnar

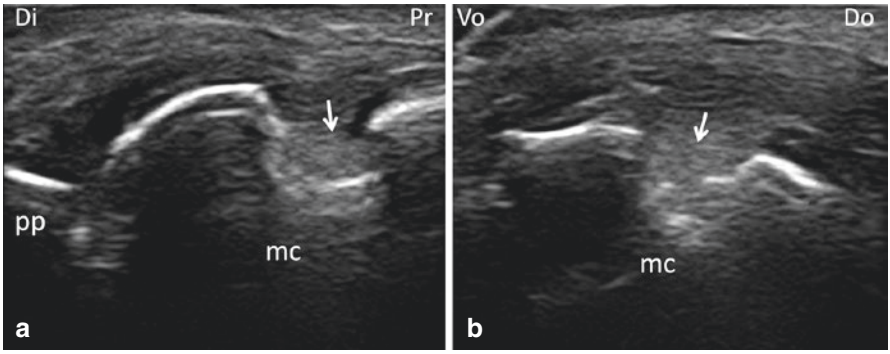

Fig. 7.21 Lateral longitudinal (**a**) and transverse (**b**) scans of a metacarpophalangeal joint. Rheumatoid arthritis. The arrows indicate a fibrous rheumatoid pannus within a bone erosion of the lateral aspect of the metacarpal head. *mc* metacarpal head, *pp* proximal phalanx, *Di* distal, *Pr* proximal, *Do* dorsal, *Vo* volar

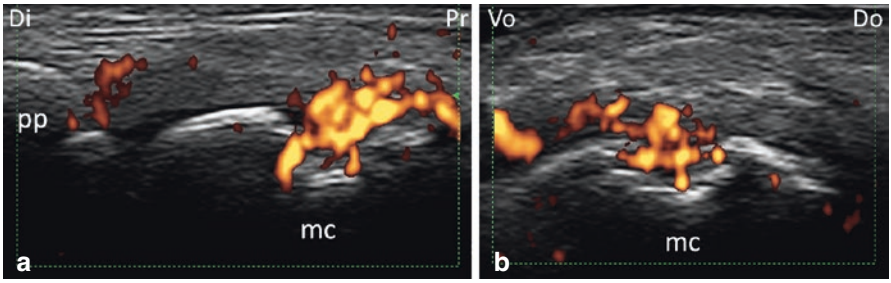

Fig. 7.22 Lateral longitudinal (**a**) and transverse (**b**) scans of a metacarpophalangeal joint. The power Doppler signal shows inflamed pannus invading the lateral aspect of the metacarpal head in rheumatoid arthritis. *mc* metacarpal head, *pp* proximal phalanx, *Di* distal, *Pr* proximal, *Do* dorsal, *Vo* volar

erosions in selected joints, especially the second and fifth MCP, fifth MTP joints, and distal ulna, were highly specific for and predictive of RA in a comparative study [32]. PsA erosions are located mainly at the entheseal insertion. Appearance resembling mouse ears and central erosions are typical. End-stage pencil-in-cup joint destruction involving the two edges of bones, and DIP mutilation may occur in later stages. Bone irregularities due to periostitis and enthesitis are more frequent in PsA than other arthritis [33]. Joint damage in RA eventually may lead to joint malalignment, including subluxations and classical deformities, such as swan neck and boutonniere deformity (Fig. 7.23).

The small joints of the hand, in particular the PIP and DIP joints and, to lesser extent, the MCP joints, are frequently evaluated in hand osteoarthritis (HOA). HOA features a number of characteristic pathological signs, including synovial, cartilage, and bony changes. Synovial changes are similar to those seen in RA or PsA (Fig. 7.24). Bony changes may include bone erosions (e.g., classical seagull

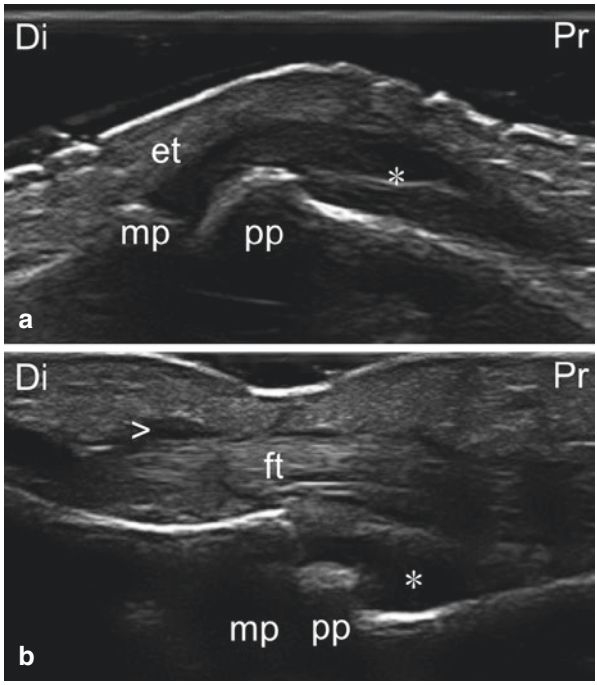

Fig. 7.23 Dorsal (**a**) and volar (**b**) longitudinal scans of a proximal interphalangeal joint. Swan neck deformity in rheumatoid arthritis. Joint cavity enlargement mainly due to synovial fluid with synovial hyperplasia (asterisk). Tenosynovitis of the finger flexor tendons (arrowhead). *et* finger extensor tendon, *ft* finger flexor tendon, *mp* middle phalanx, *pp* proximal phalanx, *Di* distal, *Pr* proximal

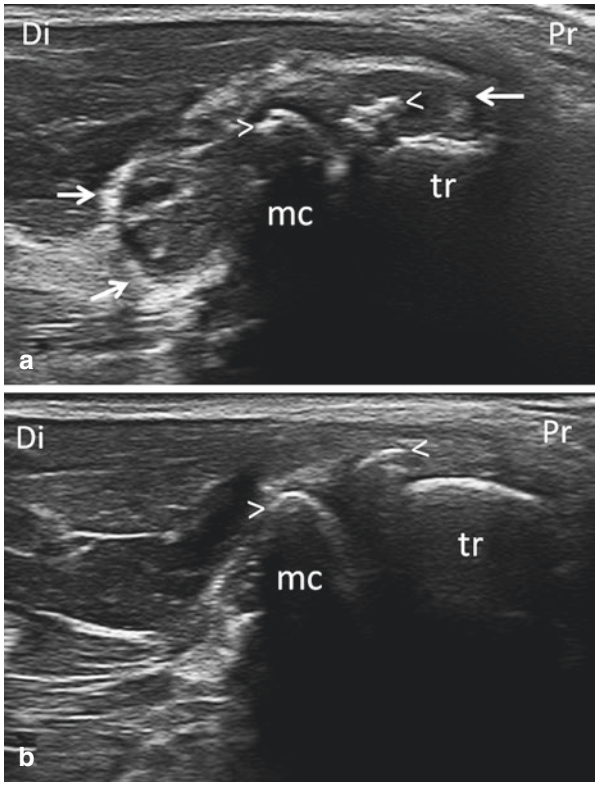

Fig. 7.24 Volar longitudinal scan of the thenar eminence. Right (**a**) left (**b**) comparison. Carpometacarpal joint osteoarthritis. The arrowheads indicate the osteophytes. (**a**) Image taken at the dominant side showing marked joint cavity widening (the arrows indicate the distal and proximal cul-de-sacs); (**b**) Contralateral asymptomatic side. *mc* metacarpal head, *tr* trapezium, *Di* distal, *Pr* proximal

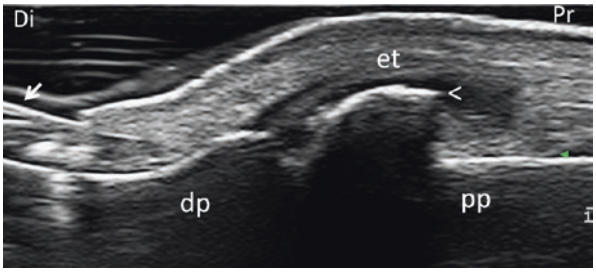

Fig. 7.25 Dorsal longitudinal scan of the interphalangeal joint of the thumb. Osteoarthritis. The arrowhead indicates an evident osteophyte on the head of the proximal phalanx. The arrow indicates the nail plate. *dp* distal phalanx, *et* finger extensor tendon, *pp* proximal phalanx, *Di* distal, *Pr* proximal

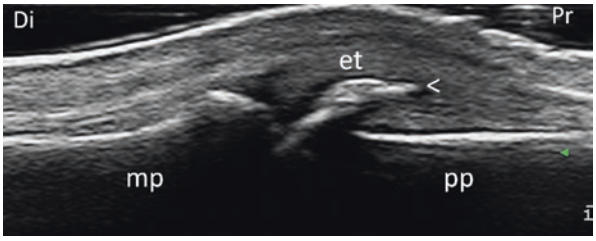

Fig. 7.26 Dorsal longitudinal scan of a proximal interphalangeal joint. Osteoarthritis. The arrowhead indicates an evident osteophyte on the head of the proximal phalanx. *et* finger extensor tendon, *mp* middle phalanx, *pp* proximal phalanx, *Di* distal, *Pr* proximal

or gull-wing central erosion) and in particular osteophytes, which are a hallmark of HOA (Figs. 7.25 and 7.26) [33]. Increased sensitivity in detecting bone erosions as compared to radiography would suggest that US could be helpful in differentiating between erosive and nonerosive OA. Due to feasibility problems of evaluating erosions in the presence of osteophytes as well as to conflicting results, the preliminary OA US scoring system does not include erosions [34]. Cartilage changes include the asymmetrical thinning of articular cartilage, loss of normal anechoic echostructure, and blurring or loss of clarity of margins. The use of US for the evaluation of cartilage in HOA is currently not recommended due to low reliability [35].

Crystal Deposition and Tophi

Crystal-induced arthropathies, e.g., gout, calcium pyrophosphate deposition disease (CPPD), and hydroxyapatite deposition disease, are also characterized by synovial, cartilage, and bony and soft tissue changes [36]. Synovitis seen in gout typically features small echogenic particles, representing monosodium urate crystal deposits, both in areas of synovial hyperplasia and in synovial fluid itself

Fig. 7.27 Dorsal longitudinal scan of a metacarpophalangeal joint. Gout. The arrows indicate tophaceous deposits which impair the visualization of the finger extensor tendon and of the underlying metacarpal bone. The arrowheads indicate the hyperechoic enhancement of the chondro-synovial interface also known as the double contour sign which is due to urate deposits on the cartilage surface. *et* finger extensor tendon, *mc* metacarpal head, *pp* proximal phalanx, *Di* distal, *Pr* proximal

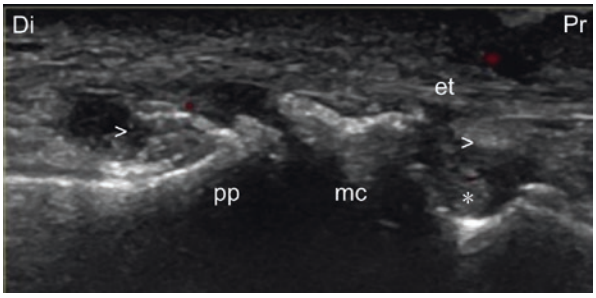

Fig. 7.28 Dorsal longitudinal scan of a metacarpophalangeal joint. Gout. The arrowheads indicate tophaceous deposits which impair the visualization of the finger extensor tendon. The asterisk indicates a large erosion. *et* finger extensor tendon, *mc* metacarpal head, *pp* proximal phalanx, *Di* distal, *Pr* proximal

(Fig. 7.3). In time tophi develop, which appear as a heterogeneous, hypo- to hyperechogenic periarticular material, often surrounded by a small anechoic rim with surrounding edematous, hypervascularized surrounding soft tissue (Figs. 7.27 and 7.28). Tophi may be commonly seen extra-articularly, particularly within and in the vicinity of tendons (Fig. 7.29). The double contour sign, a distinct hyperechoic enhancement of the chondro-synovial margin of the hyaline cartilage, has been suggested by several studies to be a highly specific sign of gout (Fig. 7.30). This sign should be distinguished from the cartilage interface artifact, since it only appears when the cartilage is insonated perpendicularly and therefore disappears when the transducer is moved along the bony contour during dynamic examination (Fig. 7.31) [37].

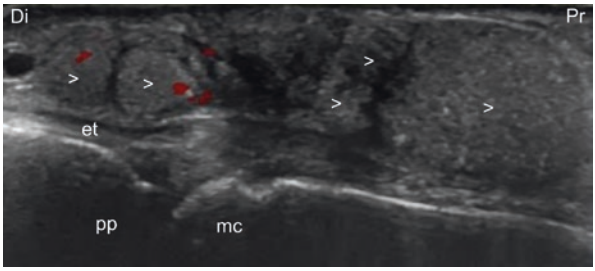

Fig. 7.29 Dorsal longitudinal scan of a metacarpophalangeal joint. Secondary gout in macrophage activation syndrome. The arrowheads indicate large tophaceous deposits overlying the finger extensor tendon. *et* finger extensor tendon, *mc* metacarpal head, *pp* proximal phalanx, *Di* distal, *Pr* proximal

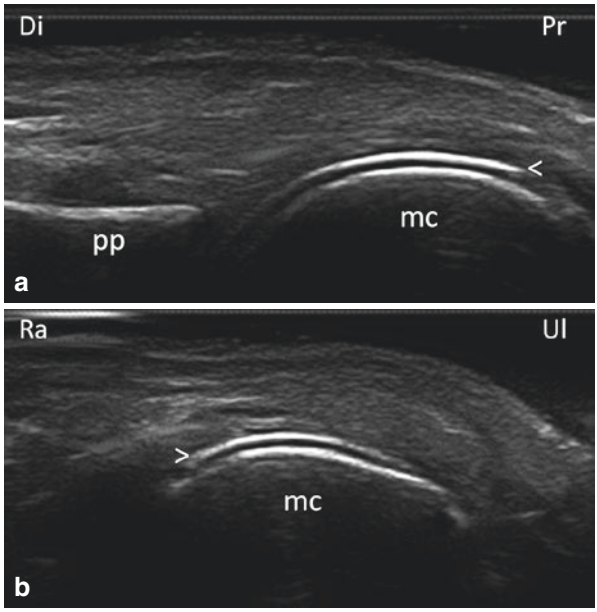

Fig. 7.30 Dorsal longitudinal (**a**) and transverse (**b**) scans of a metacarpophalangeal joint. Gout. The arrowheads indicate the hyperechoic enhancement of the chondro-synovial interface: the double contour sign which is due to monosodium urate deposits on the cartilage surface. *mc* metacarpal head, *pp* proximal phalanx, *Di* distal, *Pr* proximal, *Ra* radial, *Ul* ulnar

In CPPD, calcium pyrophosphate crystal deposits appear as either thin hyperechoic bands, parallel to the surface of the hyaline cartilage; as thin hyperechoic spots, more common in fibrous cartilage and in tendons; or as homogeneous hyperechoic nodular or oval deposits localized in bursae and articular recesses on US [38] (Figs. 7.4 and 7.32). In the wrist, crystal deposits can also be commonly detected in the triangular fibrocartilage complex (TFCC). They can also be detected on conventional radiography or in the vicinity of the extensor carpi ulnaris tendon (Figs. 7.33 and 7.34).

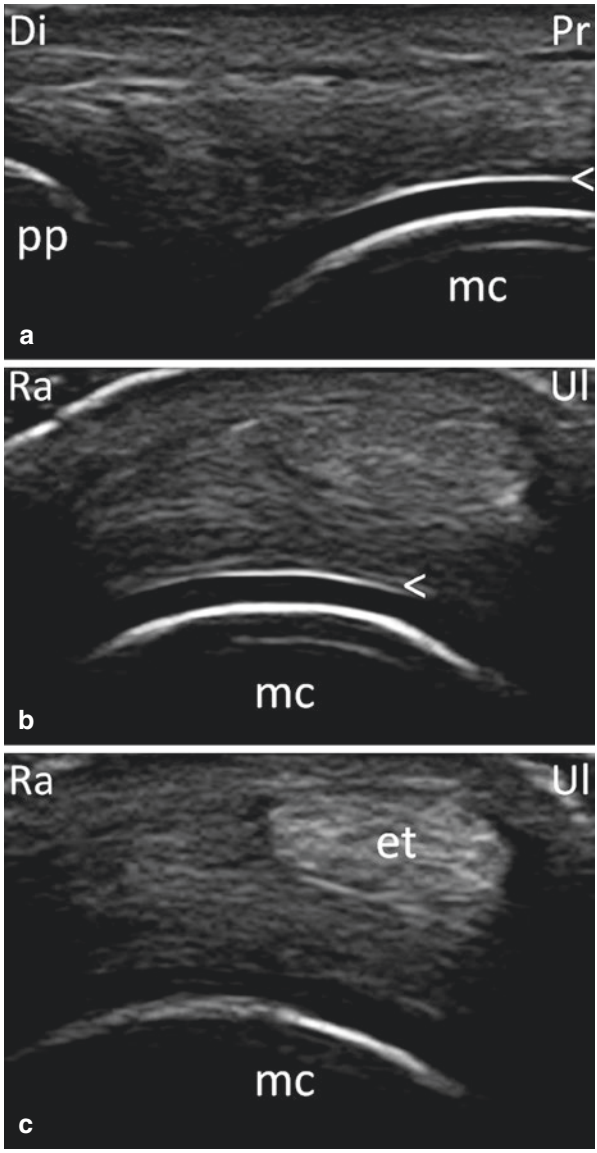

Fig. 7.31 Dorsal longitudinal (**a**) and transverse (**b**, **c**) scans of a metacarpophalangeal joint obtained using a 22 MHz linear probe in a healthy subject. The chondro-synovial interface (arrowhead) is visible only if insonated perpendicularly in **a** and **b** but not in **c**. *et* finger extensor tendon, *mc* metacarpal head, *pp* proximal phalanx, *Di* distal, *Pr* proximal, *Ra* radial, *Ul* ulnar

Carpal-Tunnel Syndrome

Carpal tunnel syndrome (CTS) is the most common form of peripheral nerve entrapment and is also one of the most frequent extra-articular manifestations of RA [39]. The utility of US for both diagnosis and guided injection in CTS was assessed by a large number of studies and has been found to be an ideal tool for both diagnosis and

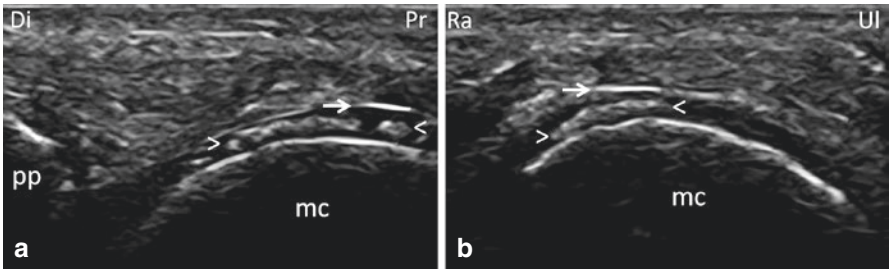

Fig. 7.32 Dorsal longitudinal (**a**) and transverse (**b**) scans of a metacarpophalangeal joint. Calcium pyrophosphate deposition disease. The arrowheads indicate crystal deposits within the hyaline cartilage of the metacarpal head. The arrows indicate the chondro-synovial margin where the incident ultrasound beam was perpendicular to the cartilage surface. *mc* metacarpal head, *pp* proximal phalanx, *Di* distal, *Pr* proximal, *Ra* radial, *Ul* ulnar

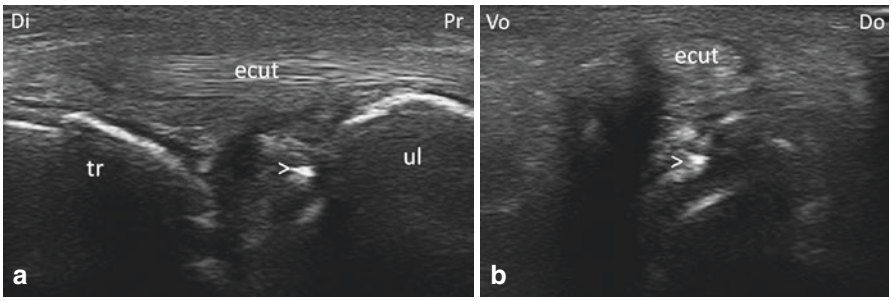

Fig. 7.33 Ulnar longitudinal (**a**) and transverse (**b**) scans of the triangular fibrocartilage of the wrist. Calcium pyrophosphate deposition disease. The arrowheads indicate crystal deposits within the fibrocartilage. *ecut* extensor carpi ulnaris tendon, *tr* triquetrum, *ul* ulna, *Di* distal, *Do* dorsal, *Pr* proximal, *Vo* volar

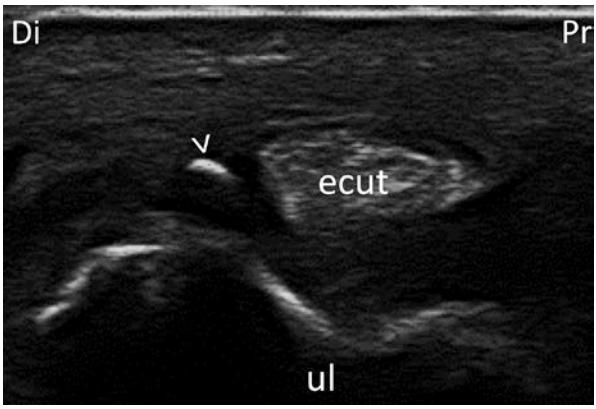

Fig. 7.34 Transverse scan of the ulnar wrist. Hydroxyapatite deposition disease. The arrowhead indicates a crystal deposit within the tendons sheath which casts an acoustic shadow on the underlying ulna. *ecut* extensor carpi ulnaris tendon, *ul* ulna, *Di* distal, *Pr* proximal

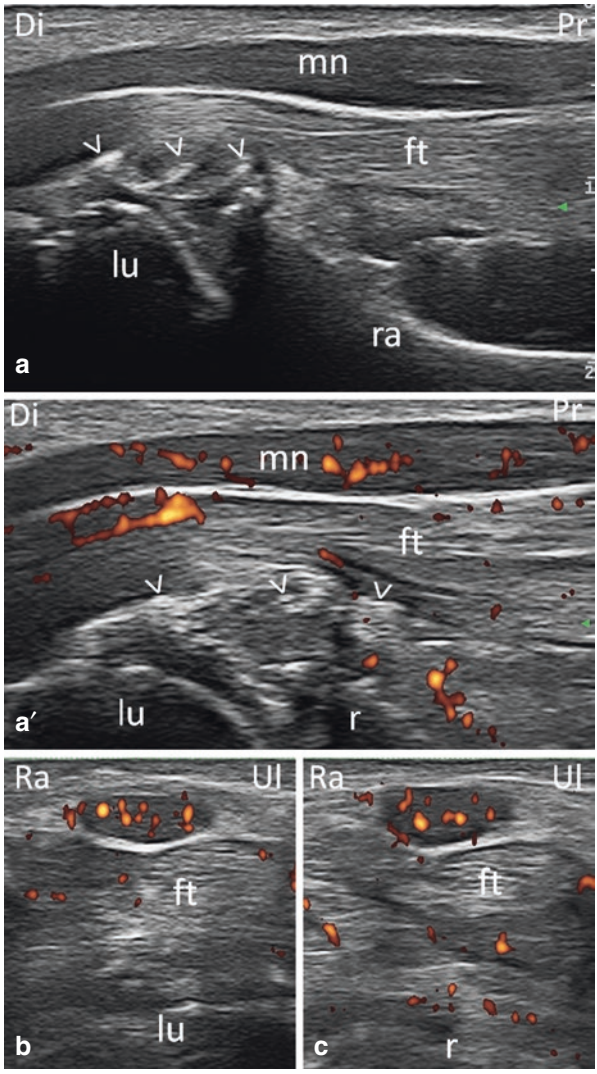

Fig. 7.35 Volar longitudinal (**a**, **a′**) and transverse (**b**, **c**) scans of the carpal tunnel in calcium pyrophosphate deposition disease and carpal tunnel syndrome. Grayscale (**a**) and power Doppler (**a′**, **b**, **c**) images. The arrowheads indicate pyrophosphate deposits which compress the median nerve that appears swollen in the proximal part of the carpal tunnel. The power Doppler technique allowed the detection of signal within the median nerve and surrounding the finger flexor tendons at the level of the carpal tunnel. *ft* finger flexor tendons, *lu* lunate bone, *mn* median nerve, *r* radius, *Di* distal, *Pr* proximal, *Ra* radial, *Ul* ulnar

management [40]. The most relevant pathological finding relating to the median nerve is the change of its cross-sectional area. Ultrasound criteria for median nerve compression include the classic triad of prestenotic swelling, stenotic and poststenotic flattening, and volar bowing or bulging of the flexor retinaculum. Other less commonly used measures include the nerve perimeter and the ratio between the transverse and the anteroposterior diameter [41–43]. An increment of the transverse area of the nerve at the proximal entrance to the carpal tunnel is the most frequent and nonspecific sign of increased pressure within the tunnel (Fig. 7.35). A consequence of CTS, i.e., thenar atrophy, may also be evaluated by US, especially in unilateral cases when comparisons can be made between the two sides (Fig. 7.36).

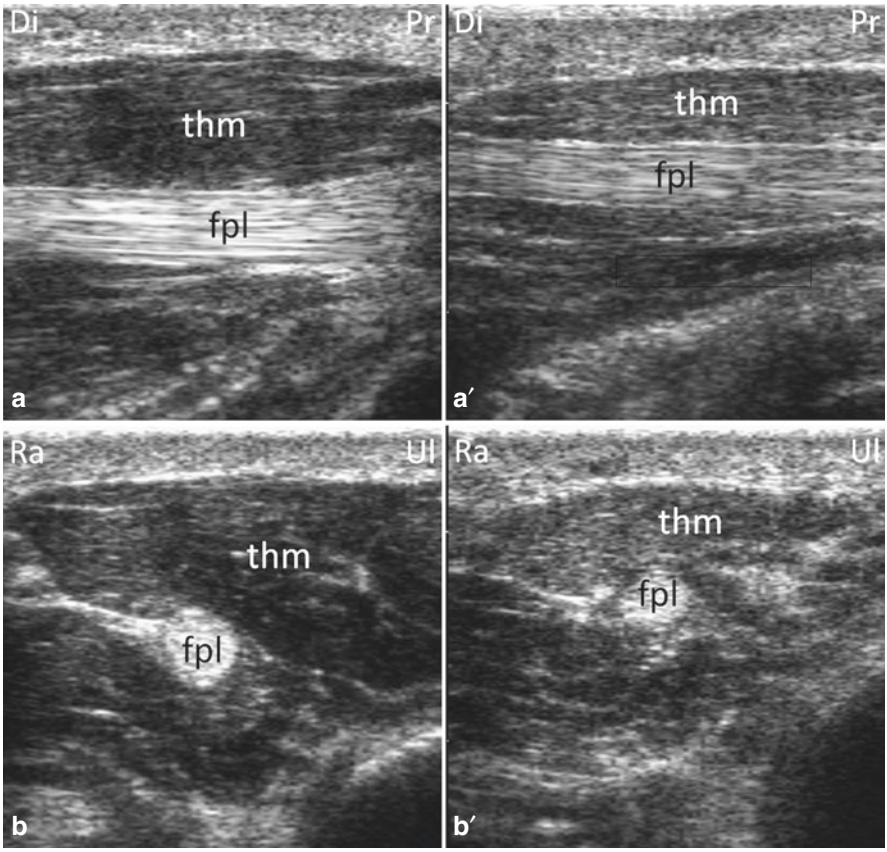

Fig. 7.36 Volar longitudinal (**a**, **a′**) and transverse (**b**, **b′**) scans of the thenar eminence. Right (**a**, **b**) left (**a′**, **b′**) comparison showing hypotrophy of the thenar eminence muscles in carpal tunnel syndrome. *fpl* flexor pollicis longus tendon, *thm* thenar eminence muscles, *Di* distal, *Pr* proximal, *Ra* radial, *Ul* ulnar

Ultrasound also allows the evaluation of distinct median nerve and carpal tunnel pathologies, including a bifid median nerve, persistent median artery, tenosynovitis of the flexor tendons, radiocarpal or intercarpal synovitis, urate, CPPD or amyloidosis deposits, arthrogenic cysts, aberrant muscles, or other space-occupying structures (Figs. 7.35, 7.37, and 7.38). A focal thinning of the median nerve (notch sign) is also a morphological change indicative of a secondary cause of CTS.

Connective Tissue Diseases

Ultrasound of the hand and wrist may also be used for the evaluation of connective tissue diseases. In remitting seronegative symmetrical synovitis with pitting edema, US may reveal tenosynovitis of extensor and flexor tendons at the wrist and the

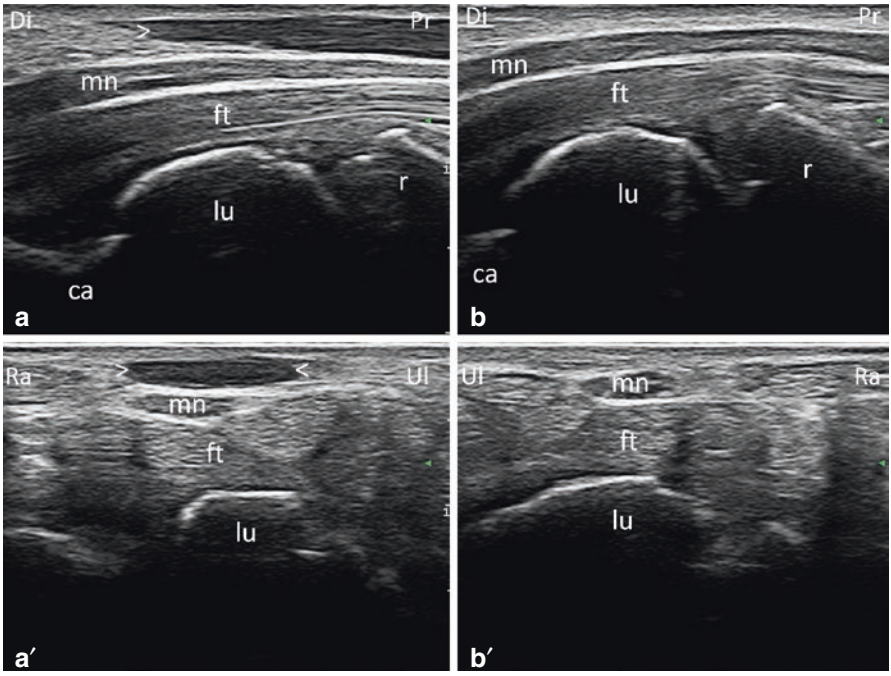

Fig. 7.37 Volar longitudinal (**a**, **b**) and transverse (**a′**, **b′**) scans of the carpal tunnel. Right (**a**, **a′**) left (**b**, **b′**) comparison. The arrowheads indicate the abnormal muscle which compresses the median nerve. *ca* capitate, *ft* finger flexor tendons, *lu* lunate, *mn* median nerve, *r* radius, *Di* distal, *Pr* proximal, *Ra* radial, *Ul* ulnar

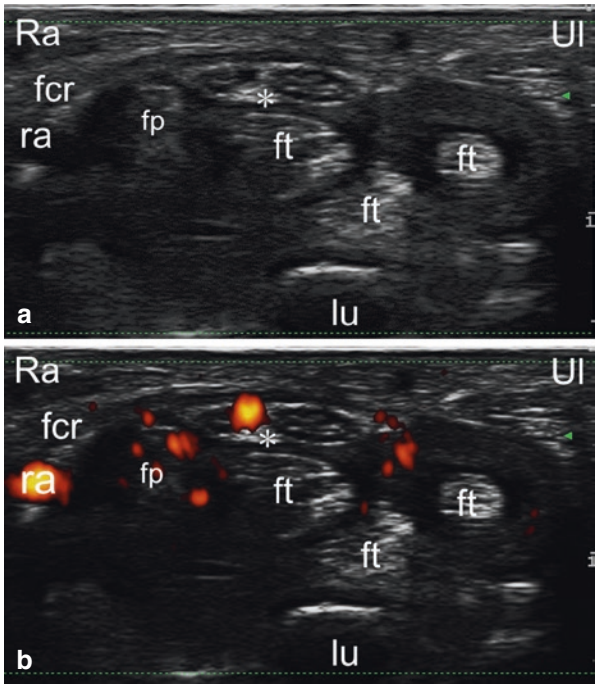

Fig. 7.38 Volar transverse scan (**a**, **b**) of the carpal tunnel. The asterisk indicates a bifid median nerve (**a**, **b**) and persistent median artery (**b**). *fcr* flexor carpi radialis tendon, *fp* flexor pollicis tendon, *ft* finger flexor tendons, *lu* lunate, *ra* radial artery, *Ra* radial, *Ul* ulnar

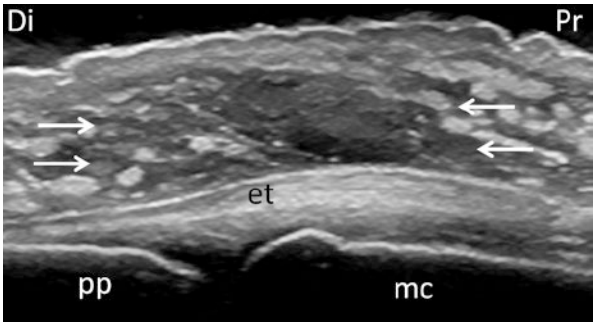

Fig. 7.39 Dorsal longitudinal scan of a metacarpophalangeal joint. Periarticular edema, marked thickening of the periarticular subcutaneous tissue (arrows) in remitting seronegative symmetrical synovitis with pitting edema (RS3PE) syndrome. *et* finger extensor tendon, *mc* metacarpal head, *pp* proximal phalanx, *Di* distal, *Pr* proximal

Fig. 7.40 Dorsal longitudinal scan of a metacarpophalangeal joint. Subluxation of the proximal phalangeal base in relation to the metacarpal head in Jaccoud arthropathy. *et* finger extensor tendon, *mc* metacarpal head, *pp* proximal phalanx, *Di* distal, *Pr* proximal

metacarpal heads as well as thickening of periarticular subcutaneous tissue (Fig. 7.39). Ultrasound examination of the hand in patients with systemic lupus erythematosus (SLE) also revealed a high prevalence of findings, although rates of abnormality were highly variable [44]. Jaccoud arthropathy is a chronic joint disorder which frequently accompanies SLE and other connective tissue diseases and commonly leads to subluxation of the MCP joints [45] (Fig. 7.40).

Miscellaneous Disorders

High-frequency US may also be useful for diagnosing osseous, injury- or overuse-related disorders of the wrist and hand, such as occult scaphoid fractures and scapholunate ligament tear and/or advanced collapse. Carpal boss, also known as hunchback carpal bone, indicates a commonly overlooked bony prominence on the dorsal aspect of the second and/or third carpometacarpal joint yet another condition where US may help in confirming the clinical diagnosis (Fig. 7.41).

Ganglion cysts represent the most common benign soft tissue tumors of the hand and wrist, appearing as oval or round, unilobulated or more commonly multilobulated, fluid-filled, anechoic or hypoechoic sacs on US, in conjunction with either a joint (e.g., scapholunate) or a tendon sheath (e.g. extensor tendons) (Fig. 7.42) [46]. Care should be taken to differentiate these benign tumors from

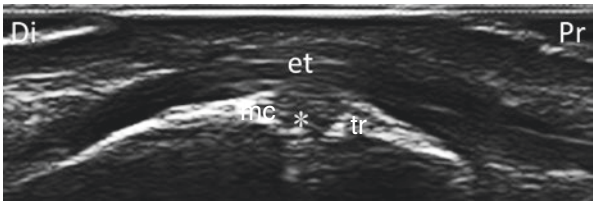

Fig. 7.41 Dorsal longitudinal scan of the second carpometacarpal joint. Carpal boss. Dorsal protuberance and disintegration of the joint (asterisk), featuring osteophytes at the bone endings and complete loss of cartilage. *et* finger extensor tendon, *mc* metacarpal, *tr* trapezoid, *Di* distal, *Pr* proximal

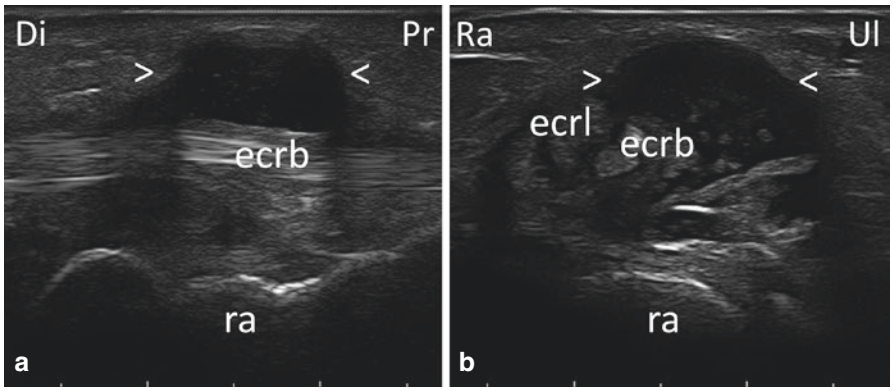

Fig. 7.42 Dorsal longitudinal (**a**) and transverse (**b**) scan of the radiocarpal joint. Arrowheads indicate a ganglion cyst of the extensor carpi radialis brevis tendon. *ecrb* extensor carpi radialis brevis tendon, *ecrl* extensor carpi radialis longus tendon, *ra* radius, *Di* distal, *Pr* proximal, *Ra* radial, *Ul* ulnar

rare neoplasms of the hand and wrist. Vascularization, as assessed by Doppler flow, presence or absence of capsule, echogenicity, and echostructure of the lesion as well as follow-up through time, may aid the differentiation of neoplasms; however, it is advised to perform further diagnostic tests. Ganglion cysts must also be differentiated from intra-articular synovial fluid, although there may be communication between the ganglion cyst and the joint. Similarly, ganglion cysts should also be differentiated from tenosynovitis in cases when such cysts originate from the tendon sheath.

The ulnar collateral ligament of the thumb which runs at an oblique angle from the ulnar side of the first metacarpal bone to the lateral tubercle of the proximal phalanx of the thumb can be visualized by performing a longitudinal scan of the ulnar aspect of the first MCP joint, followed by a transverse scan of the ligament (Fig. 7.43). The acute tear of this convex hypoechoic ligament is known as gamekeeper or skier thumb, while a chronic tear is known as Stener

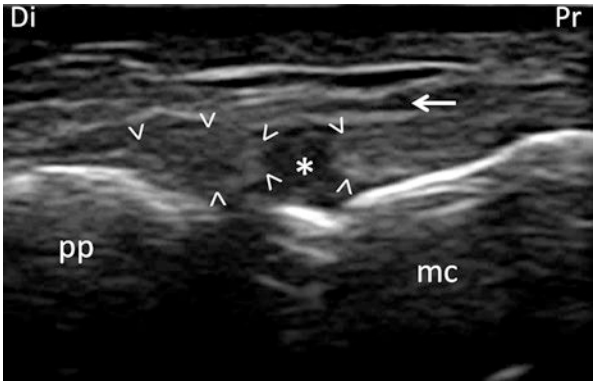

Fig. 7.43 Longitudinal lateral scan of the first metacarpophalangeal joint using a 22 MHz linear probe. Rupture of the ulnar collateral ligament. Metacarpophalangeal joint of the thumb. The arrowheads delimit the two stumps of the ulnar collateral ligament. The asterisk indicates the gap between the two stumps. The arrow indicates the overlying aponeurosis of the adductor pollicis longus which moves during flexion-extension movements of the interphalangeal joint of the thumb. The proximal stump is under the aponeurosis. *mc* metacarpal bone, *pp* proximal phalanx, *Di* distal, *Pr* proximal

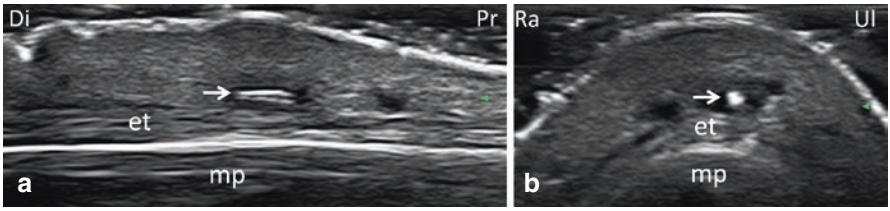

Fig. 7.44 Dorsal longitudinal (**a**) and transverse (**b**) scans of a finger. The arrow indicates a foreign body, a palm thorn in the subcutaneous tissue appearing as a hyperechoic band and spot respectively in longitudinal and transverse view. *et* finger extensor tendon, *mp* middle phalanx, *Di* distal, *Pr* proximal, *Ra* radial, *Ul* ulnar

lesion, in which there is significant retraction of the proximal fragment, which then dislocates superficial to the adductor aponeurosis, which normally runs superior to the ligament [47].

The hand is prone to injury, including injury due to foreign bodies, which can be detected by US (Fig. 7.44). In Dupuytren's contracture, US depicts fibrous nodules and adhesions as hypoechogenic masses on US (Fig. 7.45) [48].

Interventional procedures, including both diagnostic (e.g., arthrocentesis, synovial, tenosynovial, soft tissue biopsies, etc.) and therapeutic procedures (e.g., intra-articular and extra-articular injections/infiltrations, aspirations, carpal tunnel release, etc.) of the hand and wrist, have an important role in the diagnosis and treatment of a wide variety of disorders [49–53] (Fig. 7.46).

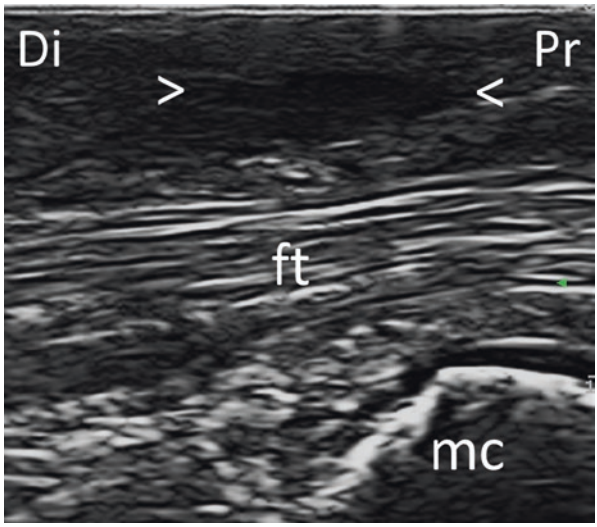

Fig. 7.45 Volar longitudinal scan of a metacarpophalangeal joint. Arrowheads indicate a thickened fibrotic and edematous palmar aponeurosis in Dupuytren's contracture. *ft* finger flexor tendon, *mc* metacarpal head, *Di* distal, *Pr* proximal

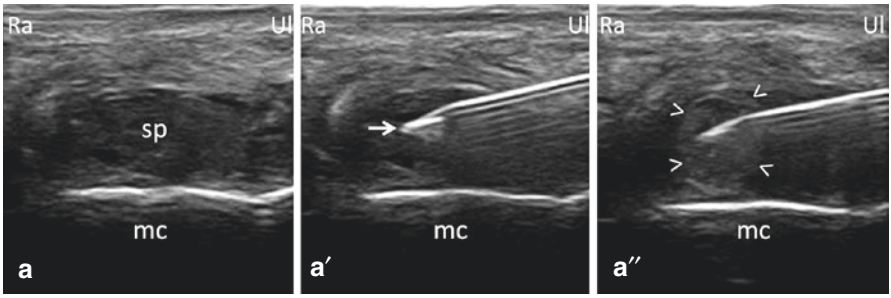

Fig. 7.46 Dorsal transverse scan of the proximal cul-de-sac of an inflamed metacarpophalangeal joint in established rheumatoid arthritis. (**a**) Definition of the probe positioning to guide the injection. (**a**′) Correct placement of the tip of the needle (arrow). (**a**″) Injection of the steroid spreading within the joint cavity (arrowheads). *mc* metacarpal, *sp* synovial proliferation, *Ra* radial, *Ul* ulnar

References

1. Mandl P, Naredo E, Wakefield RJ, Conaghan PG, D'Agostino MA, OMERACT Ultrasound Task Force. A systematic literature review analysis of ultrasound joint count and scoring systems to assess synovitis in rheumatoid arthritis according to the OMERACT filter. J Rheumatol. 2011;38:2055–62.
2. Filer A, de Pablo P, Allen G, Nightingale P, Jordan A, Jobanputra P, Bowman S, Buckley CD, Raza K. Utility of ultrasound joint counts in the prediction of rheumatoid arthritis in patients with very early synovitis. Ann Rheum Dis. 2011;70:500–7.
3. Scheel AK, Hermann KG, Kahler E, Pasewaldt D, Fritz J, Hamm B, Brunner E, Müller GA, Burmester GR, Backhaus M. A novel ultrasonographic synovitis scoring system suitable for analyzing finger joint inflammation in rheumatoid arthritis. Arthritis Rheum. 2005;52:733–43.

4. Hau M, Schultz H, Tony HP, Keberle M, Jahns R, Haerten R, Jenett M. Evaluation of pannus and vascularization of the metacarpophalangeal and proximal interphalangeal joints in rheumatoid arthritis by high-resolution ultrasound (multidimensional linear array). Arthritis Rheum. 1999;42:2303–8.
5. De Flaviis L, Scaglione P, Nessi R, Ventura R, Calori G. Ultrasonography of the hand in rheumatoid arthritis. Acta Radiol. 1988;29:457–60.
6. Witt MN, Mueller F, Weinert P, Nigg AP, Reindl CS, Proft F, Schulze-Koops H, Grunke M. Ultrasound of synovitis in rheumatoid arthritis: advantages of the dorsal over the palmar approach to finger joints. J Rheumatol. 2014;41:422–8.
7. Cardinal E, Lafortune M, Burns P. Power Doppler US in synovitis: reality or artifact? Radiology. 1996;200:868–9.
8. Klauser A, Frauscher F, Schirmer M, Halpern E, Pallwein L, Herold M, Helweg G, ZurNedden D. The value of contrast-enhanced color Doppler ultrasound in the detection of vascularization of finger joints in patients with rheumatoid arthritis. Arthritis Rheum. 2002;46:647–53.
9. Terslev L, Torp-Pedersen S, Qvistgaard E, von der Recke P, Bliddal H. Doppler ultrasound findings in healthy wrists and finger joints. Ann Rheum Dis. 2004;63:644–8.
10. Albrecht K, Grob K, Lange U, Müller-Ladner U, Strunk J. Reliability of different Doppler ultrasound quantification methods and devices in the assessment of therapeutic response in arthritis. Rheumatology. 2008;47:1521–6.
11. Torp-Pedersen S, Christensen R, Szkudlarek M, Ellegaard K, D'Agostino MA, Iagnocco A, Naredo E, Balint P, Wakefield RJ, Torp-Pedersen A, Terslev L. Power and color Doppler ultrasound settings for inflammatory flow: impact on scoring of disease activity in patients with rheumatoid arthritis. Arthritis Rheumatol. 2015;67:386–95.
12. Rezaei H, Af Klint E, Hammer HB, Terslev L, D'Agostino MA, Kisten Y, Arnaud L. Analysis of correlation and causes for discrepancy between quantitative and semi-quantitative Doppler scores in synovitis in rheumatoid arthritis. Rheumatology. 2017;56:255–62.
13. Wakefield RJ, Balint PV, Szkudlarek M, Filippucci E, Backhaus M, D'Agostino MA, Sanchez EN, Iagnocco A, Schmidt WA, Bruyn GA, Kane D, O'Connor PJ, Manger B, Joshua F, Koski J, Grassi W, Lassere MN, Swen N, Kainberger F, Klauser A, Ostergaard M, Brown AK, Machold KP, Conaghan PG; OMERACT 7 Special Interest Group. Musculoskeletal ultrasound including definitions for ultrasonographic pathology. J Rheumatol. 2005;32:2485–7.
14. Filippucci E, Gabba A, Di Geso L, Girolimetti R, Salaffi F, Grass W. Hand tendon involvement in rheumatoid arthritis: an ultrasound study. Semin Arthritis Rheum. 2012;41:752–60.
15. Østergaard M, Eder L, Christiansen SN, Kaeley GS. Imaging in the diagnosis and management of peripheral psoriatic arthritis-the clinical utility of magnetic resonance imaging and ultrasonography. Best Pract Res Clin Rheumatol. 2016;30:624–37.
16. Kim HR, Lee SH. Ultrasonographic assessment of clinically diagnosed trigger fingers. Rheumatol Int. 2010;30:1455–8.
17. Guerini H, Pessis E, Theumann N, Le Quintrec JS, Campagna R, Chevrot A, Feydy A, Drapé JL. Sonographic appearance of trigger fingers. J Ultrasound Med. 2008;27:1407–13.
18. Bakewell CJ, Olivieri I, Aydin SZ, Dejaco C, Ikeda K, Gutierrez M, Terslev L, Thiele R, D'Agostino MA, Kaeley GS, OMERACT Ultrasound Task Force. Ultrasound and magnetic resonance imaging in the evaluation of psoriatic dactylitis: status and perspectives. J Rheumatol. 2013;40:1951–7.
19. McGonagle D, Gibbon W, O'Connor P, Green M, Pease C, Emery P. Characteristic magnetic resonance imaging entheseal changes of knee synovitis in spondylarthropathy. Arthritis Rheum. 1998;41:694–700.
20. McGonagle D, Gibbon W, Emery P. Classification of inflammatory arthritis by enthesitis. Lancet. 1998;352:1137–40.
21. McGonagle D, Pease C, Marzo-Ortega H, O'Connor P, Emery P. The case for classification of polymyalgia rheumatica and remitting seronegative symmetrical synovitis with pitting edema as primarily capsular/entheseal based pathologies. J Rheumatol. 2000;27:837–40.

22. Tan AL, Benjamin M, Toumi H, Grainger AJ, Tanner SF, Emery P, McGonagle D. The relationship between the extensor tendon enthesis and the nail in distal interphalangeal joint disease in psoriatic arthritis–a high-resolution MRI and histological study. Rheumatology. 2007;46:253–6.
23. McGonagle D, Tan AL, Benjamin M. The nail as a musculoskeletal appendage-implications for an improved understanding of the link between psoriasis and arthritis. Dermatology. 2009;218:97–102.
24. Filippucci E, da Luz KR, Di Geso L, Salaffi F, Tardella M, Carotti M, Natour J, Grassi W. Interobserver reliability of ultrasonography in the assessment of cartilage damage in rheumatoid arthritis. Ann Rheum Dis. 2010;69:1845–8.
25. Mandl P, Supp G, Baksa G, Radner H, Studenic P, Gyebnar J, Kurucz R, Niedermayer D, Aletaha D, Balint PV, Smolen JS. Relationship between radiographic joint space narrowing, sonographic cartilage thickness and anatomy in rheumatoid arthritis and control joints. Ann Rheum Dis. 2015;74:2022–7.
26. Filippucci E, Meenagh G, Delle Sedie A, Salaffi F, Riente L, Iagnocco A, Scirè CA, Montecucco C, Bombardieri S, Valesini G, Grassi W. Ultrasound imaging for the rheumatologist. XX. Sonographic assessment of hand and wrist joint involvement in rheumatoid arthritis: comparison between two- and three-dimensional ultrasonography. Clin Exp Rheumatol. 2009;27:197–200.
27. Tămaş MM, Filippucci E, Becciolini A, Gutierrez M, Di Geso L, Bonfiglioli K, Voulgari PV, Salaffi F, Grassi W. Bone erosions in rheumatoid arthritis: ultrasound findings in the early stage of the disease. Rheumatology. 2014;53:1100–7.
28. Grassi W, Filippucci E, Farina A, Salaffi F, Cervini C. Ultrasonography in the evaluation of bone erosions. Ann Rheum Dis. 2001;60:98–103.
29. Tan AL, Tanner SF, Conaghan PG, Radjenovic A, O'Connor P, Brown AK, Emery P, McGonagle D. Role of metacarpophalangeal joint anatomic factors in the distribution of synovitis and bone erosion in early rheumatoid arthritis. Arthritis Rheum. 2003;48:1214–22.
30. Chowalloor PV, Siew TK, Keen HI. Imaging in gout: a review of the recent developments. Ther Adv Musculoskelet Dis. 2014;6:131–43.
31. Wright SA, Filippucci E, McVeigh C, Grey A, McCarron M, Grassi W, Wright GD, Taggart AJ. High-resolution ultrasonography of the first metatarsal phalangeal joint in gout: a controlled study. Ann Rheum Dis. 2007;66:859–64.
32. Zayat AS, Ellegaard K, Conaghan PG, Terslev L, Hensor EM, Freeston JE, Emery P, Wakefield RJ. The specificity of ultrasound-detected bone erosions for rheumatoid arthritis. Ann Rheum Dis. 2015;74:897–903.
33. Martel W, Stuck KJ, Dworin AM, Hylland RG. Erosive osteoarthritis and psoriatic arthritis: a radiologic comparison in the hand, wrist, and foot. Am J Roentgenol. 1980;134:125–35.
34. Keen HI, Lavie F, Wakefield RJ, D'Agostino MA, Berner-Hammer H, Hensor EMA, Pendleton A, Kane D, Guerini H, Schueller-Weidekamm C, Kortekaas MC, Birrel F, Kloppenburg M, Stamm T, Watt I, Smolen JS, Maheu E, Dougados M, Conaghan PG. The development of a preliminary ultrasonographic scoring system for features of hand osteoarthritis. Ann Rheum Dis. 2008;67:651–5.
35. Hammer HB, Iagnocco A, Mathiessen A, Filippucci E, Gandjbakhch F, Kortekaas MC, Möller I, Naredo E, Wakefield RJ, Aegerter P, D'Agostino MA. Global ultrasound assessment of structural lesions in osteoarthritis: a reliability study by the OMERACT ultrasonography group on scoring cartilage and osteophytes in finger joints. Ann Rheum Dis. 2016;75:402–7.
36. Filippucci E, Di Geso L, Girolimetti R, Grassi W. Ultrasound in crystal-related arthritis. Clin Exp Rheumatol. 2014;32:S42–7.
37. Irsay L, Mandl P, Balint PV. Chapter 3: pitfalls of gray-scale artifacts. In: D'Agostino MA, Wakefield RJ, editors. Essential applications of ultrasound in rheumatology. Philadelphia: Elsevier; 2010. p. 29–43.
38. Frediani B, Filippou G, Falsetti P, Lorenzini S, Baldi F, Acciai C, Siagkri C, Marotto D, Galeazzi M, Marcolongo R. Diagnosis of calcium pyrophosphate dihydrate crystal deposition disease: ultrasonographic criteria proposed. Ann Rheum Dis. 2005;64:638–40.

39. Carmona L, González-Alvaro I, Balsa A, Angel Belmonte M, Tena X, Sanmartí R. Rheumatoid arthritis in Spain: occurrence of extra-articular manifestations and estimates of disease severity. Ann Rheum Dis. 2003;62:897–900.
40. McDonagh C, Alexander M, Kane D. The role of ultrasound in the diagnosis and management of carpal tunnel syndrome: a new paradigm. Rheumatology. 2015;54:9–19.
41. Buchberger W, Schon G, Strasser K, Jungwirth W. High-resolution ultrasonography of the carpal tunnel. J Ultrasound Med. 1991;10:531–7.
42. Martinoli C, Bianchi S, Gandolfo N, Valle M, Simonetti S, Derchi LE. US of nerve entrapments in osteofibrous tunnels of the upper and lower limbs. Radiographics. 2000;20:S199–213.
43. Kamolz LP, Schrögendorfer KF, Rab M, Girsch W, Gruber H, Frey M. The precision of ultrasound imaging and its relevance for carpal tunnel syndrome. Surg Radiol Anat. 2001;23:117–21.
44. Zayat AS, Md Yusof MY, Wakefield RJ, Conaghan PG, Emery P, Vital EM. The role of ultrasound in assessing musculoskeletal symptoms of systemic lupus erythematosus: a systematic literature review. Rheumatology. 2016;55:485–94.
45. Saketkoo LA, Quinet R. Revisiting Jaccoud arthropathy as an ultrasound diagnosed erosive arthropathy in systemic lupus erythematosus. J Clin Rheumatol. 2007;13:322–7.
46. Bianchi S, Abdelwahab IF, Zwass A, Giacomello P. Ultrasonographic evaluation of wrist ganglia. Skelet Radiol. 1994;23:201–3.
47. Ebrahim FS, De Maeseneer M, Jager T, Marcelis S, Jamadar DA, Jacobson JA. US diagnosis of UCL tears of the thumb and Stener lesions: technique, pattern-based approach, and differential diagnosis. Radiographics. 2006;26:1007–20.
48. Markham DE, Wood MR. Ultrasound for Dupuytren's contracture. Physiotherapy. 1980;66:55–8.
49. Teh J, Vlychou M. Ultrasound-guided interventional procedures of the wrist and hand. Eur Radiol. 2009;19:1002–10.
50. Colio SW, Smith J, Pourcho AM. Ultrasound-guided interventional procedures of the wrist and hand: anatomy, indications, and techniques. Phys Med Rehabil Clin N Am. 2016;27:589–605.
51. Rojo-Manaute JM, Capa-Grasa A, Chana-Rodríguez F, Perez-Mañanes R, Rodriguez-Maruri G, Sanz-Ruiz P, Muñoz-Ledesma J, Aburto-Bernardo M, Esparragoza-Cabrera L, Cerro-Gutiérrez MD, Vaquero-Martín J. Ultra-minimally invasive ultrasound-guided carpal tunnel release: a randomized clinical trial. J Ultrasound Med. 2016;35:1149–57.
52. Kelly S, Humby F, Filer A, Ng N, Di Cicco M, Hands RE, Rocher V, Bombardieri M, D'Agostino MA, McInnes IB, Buckley CD, Taylor PC, Pitzalis C. Ultrasound-guided synovial biopsy: a safe, well-tolerated and reliable technique for obtaining high-quality synovial tissue from both large and small joints in early arthritis patients. Ann Rheum Dis. 2015;74:611–7.
53. Balint PV, Mandl P. Chapter 23: interventional musculoskeletal ultrasound. In: D'Agostino MA, Wakefield RJ, editors. Essential applications of ultrasound in rheumatology. Philadelphia: Elsevier; 2010. p. 292–314.

Index

P. V. Balint, P. Mandl (eds.), *Ultrasonography of the Hand in Rheumatology*,
https://doi.org/10.1007/978-3-319-74207-6